UC Berkeley
UC Berkeley Electronic Theses and Dissertations

Title

Development of quantitative models of nonphotochemical quenching regulatory dynamics in Arabidopsis thaliana through the use of multi-period actinic light exposure measurements of chlorophyll fluorescence

Permalink

Author

Morris, Jonathan Michael

Publication Date

2019

Peer reviewed|Thesis/dissertation

Development of quantitative models of nonphotochemical quenching regulatory dynamics in *Arabidopsis thaliana* through the use of multi-period actinic light exposure measurements of chlorophyll fluorescence

By

Jonathan Michael Morris

A dissertation submitted in partial satisfaction of the

requirements for the degree of

Doctor of Philosophy

in

Engineering – Applied Science & Technology

in the

Graduate Division

of the

University of California, Berkeley

Committee in charge:

Professor Graham R. Fleming, Chair
Professor David T. Attwood
Professor Krishna K. Niyogi

Summer 2019

Abstract

Development of quantitative models of nonphotochemical quenching regulatory
dynamics in *Arabidopsis thaliana* through the use of multi-period actinic light exposure
measurements of chlorophyll fluorescence

by

Jonathan Michael Morris

Doctor of Philosophy in Engineering – Applied Science & Technology

University of California, Berkeley

Professor Graham R. Fleming, Chair

In photosynthesis, solar energy is absorbed and converted into chemical energy. Chlorophyll embedded in proteins absorb light and transfer excitation energy to reaction centers where charge separation occurs. However, the solar flux incident on photosynthetic organisms is highly variable, requiring complex feedback systems to regulate the excitation pressure on reaction centers and prevent excess absorbed energy from causing damage. Upon exposure to transient high intensity light, processes to dissipate excess absorbed energy are activated. This is routinely observed upon exposure of a photosynthetic sample to actinic light as the quenching of chlorophyll fluorescence, and often broadly referred to as non-photochemical quenching (NPQ). Understanding NPQ and its regulation at a quantitative and mechanistic level is an important challenge for optimizing crop yields and design of biomimetic solar devices for energy harvesting.

The regulation of NPQ allows for photosynthetic organisms to responds to changes in light intensity that occur on multiple timescales, from as little as a few seconds due to e.g. changes in shading of a leaf, to daily oscillations due to the position of the sun in the sky, and even seasonal oscillations. Various biochemical regulators of NPQ have been identified from measurements of the chlorophyll fluorescence of model organisms upon chemical and genetic manipulation. In vascular plants such as *Arabidopsis thaliana*, the rapidest regulation of NPQ is triggered by a pH gradient across the thylakoid membrane (ΔpH) that is mediated by the PsbS protein. ΔpH simultaneously regulates the concentration of various xanthophylls, that are thought to influence direct photochemical mechanisms of quenching via the chemical composition of pigment-protein complexes and structural aspects of pigment-protein complex fluctuations and membrane organizations. However, the various regulatory responses often depend on shared biochemical regulatory components, such as the accumulation of the carotenoid zeaxanthin or the presence of the pH-sensitive PsbS protein. This makes distinguishing contributions of different regulatory responses to the overall response a challenging problem.

1

The biochemical regulation of NPQ ultimately activates photochemical mechanisms of energy dissipation, where excess solar energy absorbed by chromophores is dissipated via a non-radiative process to prevent photodamage. Proposed mechanisms include the nonradiative decay of an excited state of xanthophylls, a xanthophyll radical cation formation and recombination, and chlorophyll-chlorophyll charge separation and recombination. However, the electronic states of the chromophores proposed to be involved in energy dissipation indicate that even small fluctuations in the protein environment could preference which mechanisms are most favorable for any particular chromophore and therefore suggests that the quenching process is heterogeneous and dependent on a number of factors including protein conformation and membrane organization. Therefore, understanding the mechanisms through which photosynthetic systems dissipate excess energy and regulate excitation pressure in response to variable light conditions requires extensive quantitative measurements and modeling of the photosynthetic system and energy dissipation.

Developing a comprehensive understanding of the regulation of NPQ and the underlying photochemical mechanisms of energy dissipation is an challenging question in the study of NPQ and photosynthesis. Although numerous elements of the regulatory response of NPQ have been identified, each of the elements of the regulatory response occur on various timescales that contribute to the overall response. What are the timescales of these regulatory responses? What are the mechanisms of energy dissipation and which do various regulatory processes activate? How much do these mechanisms contribute to the overall quenching response? This work describes attempts to address these questions through the use of time correlated single photon counting (TCSPC) measurements of the chlorophyll fluorescence of *Arabidopsis thaliana* over multiple periods of exposure to high intensity actinic light and subsequent dark recovery to inform kinetic modeling of the regulation in order to attempt to distinguish features of the regulatory processes and connect the regulatory processes to proposed photochemical mechanisms of energy dissipation in a quantitative manner. The work makes important steps toward the ability to incorporate energy dissipation into first principles models of the photosynthetic system that relate membrane scale models of energy transfer to experimental observations, and establishing predictive models of how modifications of the regulatory systems will influence the resulting quenching and yields of photosynthesis for the optimization of crop yields.

Chapter 1 contains a review discussing efforts to model energy dissipation, or quenching, in *Arabidopsis thaliana* and their connections to models of regulatory systems that control quenching. First, theory used to describe energy transfer and experimental data obtained to construct energy transfer models of the photosynthetic antenna system that underlie the interpretation of chlorophyll fluorescence quenching is reviewed. Second, experimental evidence leading to proposed molecular mechanisms of quenching and the implications for modeling are discussed. The initial incorporation of depictions of proposed mechanisms into quantitative energy transfer models is reviewed. Finally, the necessity of connecting energy transfer models that include molecular models of quenching mechanisms with regulatory models is discussed.

Chapter 2 discusses experimental TCSPC measurements were performed on *Arabidopsis thaliana* to quantify the dependence of the response of NPQ to changes in light intensity on the presence and accumulation of zeaxanthin and lutein. Measurements were performed on wild type and mutant plants deficient in one or both of the xanthophylls, as well as a transgenic line that accumulates lutein via an engineered lutein epoxide cycle. Changes in the response of NPQ to light acclimation in wild type and mutant plants were observed between two successive light acclimation cycles, suggesting that the character of the rapid and reversible response of NPQ in fully dark-acclimated plants is substantially different than in conditions plants are likely to experience due to changes in light intensity during daylight. Mathematical models of the response of zeaxanthin- and lutein-dependent reversible NPQ were constructed that accurately describe the observed differences between the light acclimation periods. Finally, the wild-type response of NPQ was reconstructed from isolated components present in mutant plants with a single common scaling factor, which enabled deconvolution of the relative contributions of zeaxanthin- and lutein-dependent NPQ.

Chapter 3 discusses measurements undertaken In order to simultaneously resolve timescales of regulatory processes operating on different timescales, but with shared biochemical regulators, TCSPC measurements were performed on several *Arabidopsis thaliana* mutants during periodic actinic light exposure. Over successive periods of actinic light, TCSPC measurements show distinct intra-period and inter-period dynamics and demonstrate complex roles of the biochemical regulators PsbS and zeaxanthin in both fast and slow timescale responses of NPQ. Comparison between mutant lines suggests evidence of a role of PsbS in the longer timescale quenching response not previously emphasized. Finally, a mathematical model was constructed demonstrating how short timescale, rapidly reversible quenching processes and longer timescale quenching processes combine to produce the overall quenching response.

Chapter 4 discusses aspects of analyzing and interpreting snapshot fluorescence lifetime data obtained from *in vivo* samples using complex actinic exposure patterns to probe and quantify aspects of the regulatory response of quenching. First, a technique involving interleaving data from measurements on separate leaves to achieve increased actinic timescale resolution is discussed, including the application of filters to remove artifacts of leaf-to-leave systematic variability that introduce high frequency oscillation in the data. Second, the application of singular value decomposition on complex data sets for validation and filtering is discussed.

Chapter 5 summarizes conclusions of this work and provides an outlook towards future steps necessary for the optimization of crop yields.

Table of Contents

Acknowledgements

I must also acknowledge Kris Niyogi, our group's key collaborator for all things biology. Without Kris and his postdocs and students, including Alizée Malnoë, Cindy Amstutz, and Masa Iwai, the messy and complicated world of plant biology would be very difficult to navigate: every protocol figured out, and made easy – even things that at first glance sound basic such as germinating seeds have their own tricks that separate it from being an impossible task to routine and reliable. They're real professionals at the benchwork needed to make our work possible.

Another big part of my time at Berkeley involves my work with the Graduate Assembly, the graduate student organization that tries to make life just that one bit easier for grad students that is the difference between success in lab and struggles just navigating all the parts of campus and life in Berkeley that have to be out of the way in order to get anything done. Although it has been immensely rewarding to contribute to science, it was there that I found what will be the next step for me. Housing in Berkeley is expensive, after downzoning in the 1970's and the ensuing 10-1 added jobs-housing ratio since then, but it's just a micro chasm of nationwide trends. It's just one part of the carbon intensive lifestyle that jeopardizes the global climate, mired in equity and social justice concerns. After several years advocating on housing issues on behalf of other grad students, it inspired deciding on more school – law school. Of course, again, the people I had the privilege of working with in the GA, including Aaron Smyth, Dax Vivid, Andy Schwartz, and Adam Orford deserve their own acknowledgement. Best of luck to Adam, picking up where I left off with the GA.

Of course, all this has also been supported by an outstanding group of friends. Those first Saturday morning surf sessions with Brandon Wood and Zack Phillips that were also AS&T students were life changing, providing an experience to get out of my own head and find moments of peace, instilling a love of the ocean that I suspect I'll have for life. Through Zack and Brandon, we found a truly core group of friends that made possible the surf trips, diving trips, backpacking trips, and all the parts of California that need to be experienced to do them justice: JB & Mike Chapman, Chris Lalau-Kelly, and Silas Wolff-Goodrich.

I also must acknowledge Liz Lawler, who has become a fantastic and supportive partner this past year. Although it seems like we are headed our different ways, I am hopeful our paths will cross again in some way.

Finally, I need to acknowledge my parents, Jeri and Michael, and my brother Andrew. Over the years, they provided the support, encouragement, and critique I needed to put myself in the position to have the opportunity to undertake a Ph.D. at Berkeley that I am incredibly thankful for.

Chapter 1: Quantitative modeling of energy dissipation in *Arabidopsis thaliana*

This chapter reproduces a review article entitled "Quantitative modeling of energy dissipation in Arabidopsis thaliana" by J.M. Morris and G.R. Fleming, appearing in *Environmental and Experimental Botany* 154:99-109 (2018).

This work introduces many important aspects of the study of nonphotochemical quenching (NPQ) that are necessary for current efforts to comprehensively and quantitatively model energy dissipation, or quenching, in *Arabidopsis thaliana* and the regulatory systems that control quenching.

Understanding the meaning of measurements of chlorophyll fluorescence relies on underlying theory of energy transfer in the photosynthetic membrane. Two historical limits are the "lake" and "puddle" models that describe the connectivity of the photosynthetic antenna that absorbs solar energy and the reaction centers where productive photochemistry occurs. In one limit, each reaction center is surrounded by its own antenna, disconnected from the antenna of other reaction centers, as if the photosynthetic membrane consisted of a set of "puddles." In the other limit, each reaction center is embedded in a "lake" and excitation absorbed in the antenna can reach a number of reaction centers. The choice of model therefore has important consequences for the interpretation of how quenching mechanisms result in the quenching.

Recent developments, relying on advancements in supercomputing, allow large scale models of energy transfer networks that can describe the photosynthetic membrane system quantitatively, improving upon these historical limits. The construction these models relies on experimental data of the structure of photosynthesis pigment protein complexes, the photosynthetic membrane, and energy transfer. These aspects are reviewed to provide context for the interpretation and analysis of experimental and modeling work performed in this work.

Within these models, quenching sites can be incorporated to describe the dissipation excess energy that results in the observed quenching of chlorophyll fluorescence. Experimental evidence leading to proposed molecular mechanisms of quenching and the implications for modeling are therefore discussed, providing a foundation for the connections between the observations of the regulatory dynamics of quenching and the construction of models in later chapters.

Finally, the initial incorporation of depictions of proposed mechanisms into quantitative energy transfer models is reviewed and the necessity of connecting energy transfer models that include molecular models of quenching mechanisms with regulatory models is discussed. This provides important context and motivation for the development of regulatory models, informed by understanding of the energy transfer networks, the structural dynamics of pigment-protein complex and membrane organization, mechanisms of quenching, and biochemical regulatory cycles that constitute the bulk of this work.

Abstract

In photosynthesis, solar energy is absorbed and converted into chemical energy. Chlorophyll embedded in proteins absorb light and transfer excitation energy to reaction centers where charge separation occurs. However, the solar flux incident on photosynthetic organisms is highly variable, requiring complex feedback systems to regulate the excitation pressure on reaction centers and prevent excess absorbed energy from causing damage. During periods of transient high light, excess absorbed energy is dissipated as heat. This is routinely observed as the quenching of chlorophyll fluorescence, and often broadly referred to as non-photochemical quenching (NPQ). Understanding the mechanisms through which photosynthetic systems dissipate excess energy and regulate excitation pressure in response to variable light conditions requires extensive quantitative modeling of the photosynthetic system and energy dissipation to interpret experimental observations. This review discusses efforts to model energy dissipation, or quenching, in *Arabidopsis thaliana* and their connections to models of regulatory systems that control quenching. We begin with a review of theory used to describe energy transfer and experimental data obtained to construct energy transfer models of the photosynthetic antenna system that underlie the interpretation of chlorophyll fluorescence quenching. Second, experimental evidence leading to proposed molecular mechanisms of quenching and the implications for modeling are discussed. The initial incorporation of depictions of proposed mechanisms into quantitative energy transfer models is reviewed. Finally, the necessity of connecting energy transfer models that include molecular models of quenching mechanisms with regulatory models is discussed.

1. Introduction

Photosynthesis is the process by which organisms absorb sunlight to drive electron transfer and energy storage, but excess sunlight can damage the organism (Blankenship, 2014). The natural fluctuations in light intensity experienced by plants require processes that dissipate energy absorbed in excess of what can be used productively, and that can be rapidly optimized to the light condition (Külheim et al., 2002). Of the two photosystems in higher plants, photoprotection in photosystem II (PSII) has been extensively studied. The suite of dissipative, or photoprotective, mechanisms that protect PSII collectively result in, and are referred to as, non-photochemical quenching (NPQ): the reduction in chlorophyll a fluorescence yield due to dissipation of excess excitation by mechanisms other than photochemistry (Demmig-Adams and Adams III, 1992; Niyogi, 1999; Ruban, 2016).

NPQ is a broad term encompassing several constituent components often separated into q_E, the rapidly reversible, energy-dependent (pH-dependent) quenching component, and q_I, the slowly reversible component associated with PSII photoinhibition (Krause and Weis, 1991; van Kooten and Snel, 1990; Wraight and Crofts, 1970). Although important in many photosynthetic systems, q_T, a component of NPQ associated with excitation balance between PSI and PSII by altering the relative antenna size, does not contribute significantly in vascular plants, such as *Arabidopsis thaliana*, exposed to high light (Niyogi, 1999). q_E and another related NPQ component termed q_Z (Nilkens et al., 2010) have been the subject of intense study. While there is little consensus surrounding the numerous proposed molecular mechanisms (Duffy and Ruban, 2015) underlying the quenching pathways intrinsic to NPQ in PSII, many elements of the regulation of photoprotection are widely agreed upon (Demmig-Adams et al., 2014). Modeling (Laisk et al., 2009) the proposed mechanisms in the context of the photosynthetic energy transfer network and in the context of the regulatory system provides a powerful way to evaluate whether, and in what way, proposed mechanisms play a role in dissipating energy to protect the photosynthetic solar collection apparatus.

One approach to modeling quenching in the photosynthetic system is to construct a model capable of predicting experimental measurements, including, e.g., of the fluorescence lifetimes of the *in vivo* system, from quantum and statistical mechanical first principles, structural and spectroscopic data of individual pigments and pigment protein complexes, and membrane imaging (Amarnath et al., 2016). A model must be capable of appropriate treatment of the absorption of light by antenna (Müh et al., 2010; Müh and Renger, 2012; Renger et al., 2011), the transfer of energy to reaction centers (Bennett et al., 2013), and the charge separation process (Novoderezhkin et al., 2011b) to provide a system in which various mechanisms of quenching can be evaluated. Absorption, energy transfer, and charge separation are fundamentally quantum mechanical in their nature. However, to provide a physically meaningful picture, a model must span length scales from angstroms to hundreds of nanometers. To do so requires multiscale modeling and course graining by making appropriate approximations to simplify much of the quantum dynamical calculations; treating the entire system quantum mechanically is impractical, even for modern supercomputers (Kreisbeck and Aspuru-Guzik, 2016). Fortunately, a number of approximations can be made to allow for a model that contains enough of the quantum mechanical features to adequately represent the system. Even so, an accurate model of the system must still integrate data from numerous areas of photosynthesis, making the building of accurate models challenging.

A second area of study that incorporates modeling is the regulatory function of the plant systems that controls the extent of quenching in the photosynthetic antenna (Zaks et al., 2012). The regulatory system operates on timescales from seconds to the lifespan of the plant, but the timescales of greatest interest for regulating the rapid response include changes in the chemical environment of the thylakoid membrane over timescales of seconds to minutes. Current knowledge indicates that a fundamental trigger for inducing quenching is the formation of a transthylakoid pH gradient that, in turn, activates various proteins that influence the actual quenching (Ruban et al., 2012). One of these is the enzyme violaxanthin de-epoxidase that converts violaxanthin to antheraxanthin and zeaxanthin on a timescale of a few minutes when intrathylakoid pH is low (Jahns et al., 2009). These xanthophylls are important players in the molecular mechanisms of quenching and play a number of roles in the pigment protein complexes that effect the ultrafast dynamics of energy transfer. Chemical regulatory models seek to describe quantitatively how the multiple components contribute to the plant system's regulatory response that controls the quenching.

Important open questions include the importance of various quenching mechanisms identified experimentally, and models of how the biochemical regulatory systems control the activation of potential quenching mechanisms. The dynamic nature of the light incident on plants (Külheim et al., 2002) may imply that various mechanisms could play important roles at different times of day or in different patterns of light variability, suggesting that integrated models of the quenching processes and the regulatory response are key for insight into the potential for optimization (Zhu et al., 2004) of various elements of the quenching mechanisms and regulatory system in order to increase crop yields (Kromdijk et al., 2016) or design biomimetic solar energy devices (Terazono et al., 2011). This review focuses on efforts to model energy dissipation mechanisms using multiscale models that integrate the understanding of structure and function of energy-transfer networks, quenching mechanisms, and chemical regulatory systems that are all necessary for developing the level of understanding and tools required to eventually begin engineering quenching systems.

2. Models of Energy Transfer for Evaluating Quenching Mechanisms

Upon absorption of a photon by a chlorophyll molecule in the photosynthetic system, the energy absorbed may be transferred to reaction centers where charge separation occurs that drives downstream chemical reactions. When reaction centers are unable to productively accept the energy absorbed by antenna chlorophyll, the photosynthetic system must dissipate the excess energy to prevent unwanted generation of reactive oxygen species.

Historically, the flow of energy through the system has been described using either "lake" or "puddle" models (Robinson, 1967) that describe transfer within the antenna and to the reaction centers. In a lake model, reaction centers sit embedded in a common pool of antenna; in a puddle model, each reaction center has its own antenna. Intermediate cases were described using a variety of connected unit (Lavorel and Joliot, 1972) and domain models (Den Hollander et al., 1983; Paillotin et al., 1979) to define or model transfer within and between antennas and reaction centers. These types of models still implicitly facilitate the interpretation of many studies of quenching behavior, and provide intuition about the photosynthetic system, but are unsuitable for

quantitatively evaluating molecular mechanisms and models of quenching as it is difficult to distinguish between these models with experimental data (Bernhardt and Trissl, 1999).

In order to accurately describe the energy transfer process in a quantitative model, appropriate theories to describe the processes involved as well as information about the parameters of the photosynthetic system are required. The theories and data necessary to develop the parameters have all been areas of intense study, spanning from electronic structure of chlorophyll molecules that serve as the primary molecule used to capture photons in individual pigment-protein complexes to the mesoscopic structure of the photosynthetic membrane. These elements can be integrated into a mathematical description of the energy-transfer network that allows for a quantitative prediction of the behavior of absorbed photons and, in turn, predictions of experimental observables such as the fluorescence lifetimes of a photosynthetic system under varying conditions. The most recent efforts build upon many years of work.

2.1 Models of Energy Transfer Processes

For very simple quantum mechanical systems, such as an isolated atom, all the information necessary to describe the time evolution of the system can be contained in a mathematical operator called the Hamiltonian (Atkins and Friedman, 2011). However, even for systems as simple as a single molecule in solution, much of the information in the Hamiltonian cannot be specified exactly, and therefore describing the time evolution requires a statistical approach. A common approach is to partition the complete description into a system of interest and average over the remaining environment (Mukamel, 1995). To describe energy transfer in pigment-protein complexes of the photosynthetic system, the system of interest commonly includes chlorophyll molecules, or chromophores, where energy in the system is absorbed and can flow towards where charge separation occurs. The environment usually consists of the protein matrix that holds the chromophores and surrounding solvent (van Amerongen et al., 2000).

A fundamental concept used to describe electronic excitations is the exciton, a term describing excitation that may be delocalized, or spread, across more than one molecule due to electronic coupling between the molecules (Scholes and Rumbles, 2006). Although this is applicable to a wide range of semiconductor and molecular systems, excitons in photosynthetic systems delocalize over one or a few chromophores due to differences in the strength of electronic interactions within a chromophore and those between neighboring chromophores. This allows for the construction of a relatively simple quantum mechanical model that treats each chromophore as a "site" where a share of the exciton can be located (Fassioli et al., 2014).

The energy gap between the ground and excited electronic state in a specific sites is referred to as the site energy (Cheng and Fleming, 2009; Hu et al., 2002; Mirkovic et al., 2017; Renger et al., 2001). In an ensemble, similar sites generally exhibit a distribution of energy gaps. When a site is excited, energy is stored in the system. The transfer of excitation between sites can then be described quantitatively using an appropriate mathematical treatment. Two essential parameters for determining the appropriate model are the electronic coupling, or interaction energy, between chromophores and the coupling to the surrounding protein and solvent environment, or reorganization energy. Together, the site energies and the interaction energies between sites comprise the system Hamiltonian, while the reorganization energy describing the coupling to the environment is contained in the system-environment Hamiltonian. Large and small values of the

ratio between the interaction energy and the reorganization energy define two limits of a more complete theory of energy transfer.

In one limit, that of weak interaction energy between chromophores relative to the reorganization energy of the environment, the system can be described by the Förster theory of energy transfer (Förster, 1948) that underlies many measures of distance in biological applications. Förster theory is a perturbative treatment that exploits that the ratio of the interaction energy to the reorganization energy is small and results in a well-defined rate constant to describe the energy transfer. In the opposite limit, with a large interaction energy relative to the reorganization energy, the wave-like quantum nature of energy transfer must be accounted for, as energy moves freely through the system with wave-like coherence. In wave-like transfer, constructive interference of multiple waves determines the location of the energy. As the wave-like coherence decays, the energy stops flowing through the system, transferring the energy from one location to another. In this limit, another perturbative treatment called Redfield theory (Redfield, 1957) can be used to describe the energy transfer and results in a quantum master equation that accounts for the wavelike nature of the energy transfer.

However, in practice, the photosynthetic system is not well described be either limit individually (Ishizaki and Fleming, 2009a) due to the varying distances and energy scales involved. One example is in the simple model photosynthesis pigment protein complex, the Fenna-Matthews-Olson (FMO) complex (Fenna and Matthews, 1975), that has been found to have similar electronic couplings and reorganization energies using a variety of spectroscopic (Brixner et al., 2005; Cho et al., 2005) and structural (Vulto et al., 1998) information. Various methods exist to improve upon the perturbative treatments and extend the quantitative accuracy of the results further from the original cases of the limits and describe multichromophoric systems (Jang et al., 2004, 2002; Scholes et al., 2001; Sumi, 1999; Yang and Fleming, 2002; Zhang et al., 1998). A non-perturbative method that is valid over the full range of values of the parameters is the hierarchy equations of motion (Ishizaki and Fleming, 2009b). Nonperturbative techniques have been successfully applied to small photosynthetic systems (Ishizaki and Fleming, 2009c; Wilkins and Dattani, 2015), but it is not feasible to describe a system large enough to represent the photosynthetic membrane using non-perturbative methods (Strümpfer and Schulten, 2012). A simpler model based firmly on accurate microscopic theory is necessary for understanding the design principles of the photosynthetic system.

A viable approach is to use multiscale modeling to apply appropriate extensions of the perturbative techniques at different length scales. This allows not only for the employment of a tractable computational treatment of the photosynthetic system, but also for an intuitive understanding of the system. Of these extensions of the original Förster and Redfield theories, two are most important for developing models practicable at length scales required to realistically describe the photosynthetic system. These extension are the generalized Förster theory, which accounts for delocalization of the exciton (Jang et al., 2004; Scholes et al., 2001; Sumi, 1999), and modified Redfield theory, which treats only a subset of the couplings to the environment fluctuations perturbative to extend the range of validity (Yang and Fleming, 2002; Zhang et al., 1998). These extensions have been successfully combined in course-grained domain modes of individual higher plant pigment protein complexes (Novoderezhkin et al., 2011a) and supercomplexes (Bennett et al., 2013; Raszewski and Renger, 2008) to predict observed spectra. Coarse graining into domains

serves to average over the fast dynamics that require sophisticated treatments to describe accurately and results in a classical rate matrix that accurately describes the longer timescale dynamics most relevant to the fluorescence lifetimes used to study quenching. The latter approach has been validated against non-perturbative methods used to describe portions of the PSII supercomplex (Kreisbeck and Aspuru-Guzik, 2016; Roden et al., 2016). The course-grained model has been extended to the mesoscopic size necessary to realistically describe the observable fluorescence lifetimes of thylakoid membranes or intact leaves used to study quenching (Amarnath et al., 2016). A schematic of the relevant time and length scales of energy transfer processes and decay processes described by the various levels of theory is provided in Figure 1.
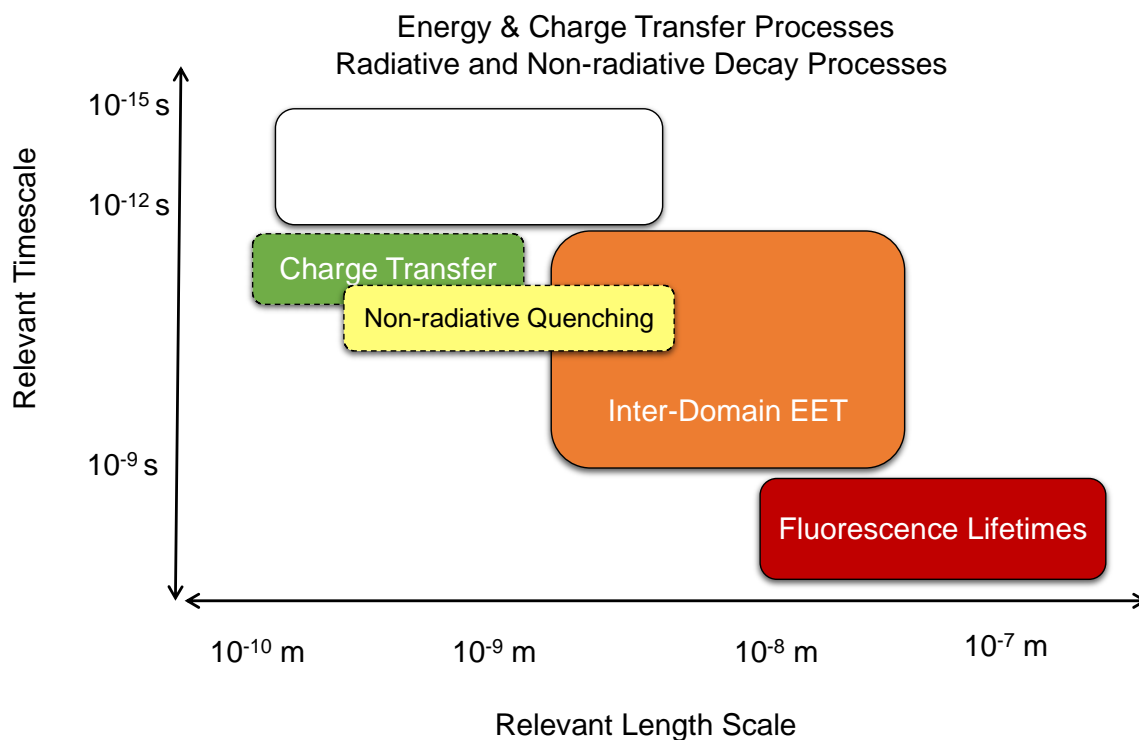
Figure 1. Semi-quantitative schematic depiction of time and length scales associated with various processes of energy transfer, charge transfer, and decay processes. Overlapping timescales of energy transfer between chlorophylls span rapid intra-domain electronic energy transfer (EET) within domains of closely spaced chlorophylls to long range inter-domain EET between adjacent domains of chlorophylls. Fluorescence decay occurs on the nanosecond timescale, with energy often diffusing many nanometers before charge separation at the reaction center or fluorescence. When quenching sites are active, energy and charge transfer to non-radiative quenching sites are suggested to occur at similar distances from neighboring chlorophyll. Quenching sites dissipate energy through non-radiative decay on timescales much faster than chlorophyll fluorescence.

2.2 Spectroscopic and Structural Determination of Parameters for Energy Transfer Models

In order to employ a model of the energy-transfer process to quantitatively describe fluorescence lifetimes, a number of components are required. Broadly, these fit into two categories: first, composition and arrangement of the pigment-protein complexes in the photosynthetic membrane, and second, a combination of accurate structural models of individual pigment-protein complexes, the complementary system Hamiltonians, and the nature of the system-environment coupling. Membrane organization can be determined via either imaging or statistical mechanical descriptions of the interactions between the pigment-protein complexes in the membrane (Schneider and Geissler, 2013a, 2013b). For the parameters describing the parameters of individual pigment-protein complexes, close combination of the structure determined via either x-ray crystallography, single-particle cryo-electron microscopy, spectroscopic data, and theory are required to determine the full set of parameters. These methods have been co-developed, with each improved iteration of one contribution informing the other's interpretation and analysis.

An example of studies that have focused on the structure-function relationship of an individual pigment-protein complex to inform models applicable to plants such as *A. thaliana* is the light harvesting complex II (LHCII) antenna that has been studied extensively via structural studies (Kühlbrandt, 1988; Kühlbrandt et al., 1994; Kühlbrandt and Wang, 1991; Liu et al., 2004; Standfuss et al., 2005), spectroscopic studies (Agarwal et al., 2000; Bittner et al., 1995, 1994; Calhoun et al., 2009; Connelly et al., 1997; Eads et al., 1989; Kleima et al., 1997; Kwa et al., 1992; Lewis et al., 2016; Remelli et al., 1999; Rogl and Kühlbrandt, 1999; Salverda et al., 2003; Schlau-Cohen et al., 2009; Visser et al., 1996; Yang et al., 1999), and theoretical treatments (Gradinaru et al., 1998; Gülen et al., 1997; İşeri and Gülen, 2001; Novoderezhkin et al., 2005, 2004, 2003; Trinkunas et al., 1997), resulting in steadily improving determinations of the parameters of the Hamiltonian. Initially, structural determinations of LHCII did not have sufficient resolution to determine chlorophyll site assignments or chlorophyll orientation (Kühlbrandt, 1988; Kühlbrandt and Wang, 1991). Instead, the structures only revealed generic tetrapyrrole rings. Contemporary time-resolved spectroscopic studies demonstrated that various theoretical treatments that assumed only Förster-type energy transfer failed to predict the spectroscopic data from the structural data (Bittner et al., 1995, 1994; Eads et al., 1989; Kwa et al., 1992).

Subsequent crystallography experiments made tentative assignments (Kühlbrandt et al., 1994), and spectroscopic studies attempted to verify them via measurement of chlorophyll *a* to *b* transfer (Connelly et al., 1997; Kleima et al., 1997; Visser et al., 1996). Models attempted to refine assignments and dipole orientations in order to connect the structural and spectroscopic data employing Förster-type transfer with some complications of compartments (Gradinaru et al., 1998; Gülen et al., 1997; Trinkunas et al., 1997). Site directed mutagenesis (modifying individual amino acids near chlorophyll sites to disrupt chlorophyll binding) was used in an attempt to refine the assignments of chlorophyll *a* vs. *b* and the orientation of the Q_y transition dipoles (Remelli et al., 1999; Rogl and Kühlbrandt, 1999; Yang et al., 1999). These studies reported varying results and raised the possibility of mixed chlorophyll *a* or *b* binding sites. Subsequent high resolution crystal structures have largely resolved this controversy. The high resolution structures are able to resolve the C7-formyl group of chlorophyll *b* from the C7-methyl group of chlorophyll *a* and do not observe mixed binding sites (Liu et al., 2004).

Application of photon echo techniques to examine energy transfer in pigment protein complexes overcame significant inhomogeneous broadening, or disorder, and allowed accurate determination of energy transfer rates and evaluation of models (Agarwal et al., 2000; Salverda et al., 2003). Simultaneous fits incorporating these data were performed to evaluate models based on Redfield-type energy transfer (Novoderezhkin et al., 2004, 2003), which resulted in much better fits of the observed data than previous attempts and demonstrated the necessity of a proper treatment of the energy transfer mechanism. However, these efforts still relied on fitting using a mixed site assumption. Subsequent full two-dimensional electronic spectroscopy (Calhoun et al., 2009; Schlau-Cohen et al., 2009) were able to evaluate site energies and couplings directly. Quantum and electrostatic calculations (Novoderezhkin et al., 2005) based on the high resolution crystallographic structures (Liu et al., 2004) were able to resolve many of the inadequacies of previous modeling efforts and compared well to parameters determined from two-dimensional spectra. Continued efforts seek to directly measure energy transfer in space, without the need of a model, through connecting the electronic spectrum to spatial vibrational tags to independently verify the conclusions (Lewis et al., 2016).

In many cases, including LHCII, similarities between different species' pigment protein complexes are exploited to determine complete sets of parameters for the pigment protein complexes. Much of the work has focused on the complexes associated with PSII due to the importance of photoprotection of PSII. One example is the reaction center core, which is well conserved from cyanobacteria to higher plants, thus allowing use of a model determined from cyanobacteria's reaction center core (Raszewski et al., 2008, 2005). The reaction center core includes the reaction center chlorophylls, where charge separation occurs, and that serve as sinks for energy absorbed by and transferred from the antennae. The minor complexes, including CP43, CP47, and CP29, are also described by well-developed models, with spectroscopic and structural data obtained from complexes isolated from spinach (Müh et al., 2012; Pan et al., 2011; Raszewski and Renger, 2008).

3. Mechanistic Modeling of Quenching

With well-developed models of energy transfer and many of the individual pigment protein complexes parameterized, many of the tools necessary to evaluate mechanistic models of quenching exist. A number of potential mechanisms for the rapidly inducible quenching that protects PSII have been proposed, and it seems likely that no single mechanism dominates the quenching. Broadly, many of the proposed molecular mechanisms involve either interactions between a chlorophyll and a xanthophyll or interactions between a pair of chlorophylls. A current challenge is to incorporate these mechanisms into models of energy migration in pigment-protein complexes.

3.1 Proposed Quenching Mechanisms

Proposed mechanisms involving xanthophylls are promising due to the short lifetime of the S_1 excited state, which is similar in energy to the Q_y state of chlorophyll. This suggests that energy could be easily transferred from chlorophylls to the xanthophylls and rapidly dissipated. However, the strong coupling between a chlorophyll and xanthophyll can also result in a charge transfer state that is similar in energy to the Q_y state. This finding suggests that a charge transfer and

recombination process could also be a viable molecular mechanism for energy dissipation. Study of these mechanisms has resulted in several points of contention – over whether quenching occurs via an energy transfer mechanism, an electron transfer mechanism, or both, which types of xanthophylls are involved, and in which pigment-protein complexes the dissipation occurs. Many of these issues are reviewed by Duffy and Ruban (Duffy and Ruban, 2015) and Jahns and Holzwarth (Jahns and Holzwarth, 2012).

One of the xanthophylls proposed to be involved in the mechanism of quenching is zeaxanthin, which accumulates upon exposure to high light upon two sequential de-epoxidations from violaxanthin and antheraxanthin via the enzyme violaxanthin de-epoxidase. An early proposed mechanism was that de-epoxidation lowered the energy of the S_1 state from above to below chlorophylls' Q_y state, thereby making energy transfer to zeaxanthin favorable and explaining both the observed chemical regulatory behavior and the molecular mechanism (Frank et al., 1997; Frank and Cogdell, 1996). However, it was later found experimentally that the S_1 energies of violaxanthin, antheraxanthin, and zeaxanthin were all below that of chlorophyll, both in solution (Frank et al., 2000; Polívka et al., 1999) and in LHCII (Polívka et al., 2002), necessitating further study.

Calculations of the excited-state energies of a chlorophyll-zeaxanthin dimer and a chlorophyll-violaxanthin dimer using a hybrid of time-dependent density functional theory (TD-DFT) (Runge and Gross, 1984) under the Tamm-Dancoff Approximation (TDA) (Hirata and Head-Gordon, 1999) and the configuration interaction singles (CIS) method (Foresman et al., 1992) suggest that the S_1 state and charge transfer state are both similar in energy to the chlorophyll Q_y state for the zeaxanthin complex, but that only the charge transfer state is similar in energy for the violaxanthin complex (Dreuw et al., 2005, 2003a, 2003b). The relative energies calculated for a single orientation are distance dependent, suggesting that some combination of the proposed mechanisms is possible, depending on details of the protein conformation and fluctuations in the protein matrix. A plot of the energies of zeaxanthin-chlorophyll charge transfer, zeaxanthin S_1, S_2, and chlorophyll a Q_y state as a function of separation distance between the chromophores is shown in Figure 2. Experimental evidence for both possibilities has been reported: The presence of a zeaxanthin radical cation signal was detected experimentally via transient absorption studies and localized to the minor antenna complexes (Ahn et al., 2008; Avenson et al., 2008; Holt et al., 2005), while direct two photon excitation of the forbidden S_1 state of zeaxanthin indicates excitonic energy transfer between zeaxanthin and chlorophyll molecules (Bode et al., 2009; Holleboom and Walla, 2014).
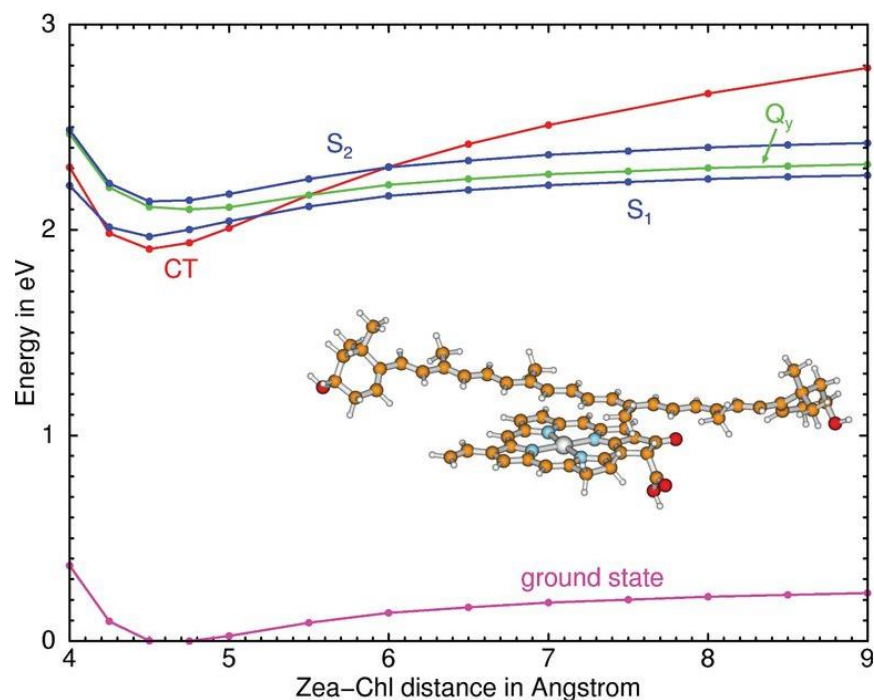
Figure 2. Potential energies of ground (magenta) and excited states (red, charge transfer states; green chlorophyll a excitonic states; blue, zeaxanthin excitonic states) of the zeaxanthin-chlorophyll dimer as a function of separation distances. This figure was originally published in A. Dreuw, G.R. Fleming and M. Head-Gordon, Biochem. Soc. Trans. 33(4):858-862 (2005).

A second proposed mechanism involves the xanthophyll lutein. Beginning with studies on zeaxanthin-deficient mutants, it has long been proposed that lutein can either play a direct role in the quenching process (Niyogi et al., 1997), or may indirectly contribute to the efficacy of another direct quenching mechanism (Pogson et al., 1998), possibly through a role in the structural organization of LHCII and the PSII antenna size (Lokstein et al., 2002). In isolated LHCII lacking zeaxanthin, the comparison of the kinetics of transient absorption measurements between the quenched and unquenched states support an energy transfer process to a carotenoid S_1 state, similar to the two photon excitation experiments, but since zeaxanthin is not present, the S_1 state is attributed to lutein due to a correspondence between the maximum bleach in the carotenoid triplet spectrum and lutein (Ruban et al., 2007). Additional experiments support the proposal that this is due to a conformational change in LHCII (Ilioaia et al., 2008) that could be moderated by the conversion of violaxanthin to zeaxanthin (Horton et al., 1991; Pascal et al., 2005; Ruban and Johnson, 2010).

In addition to the proposed energy transfer mechanism involving lutein, evidence has also been found for a lutein radical cation signal in mutants of *A. thaliana* lacking zeaxanthin, but overexpressing lutein (Li et al., 2009), as well as in reconstituted minor antenna complexes when zeaxanthin is present (Avenson et al., 2009). This suggests that either lutein can replace zeaxanthin in this radical cation mechanism, that both quenching mechanisms could contribute

11

simultaneously, or that zeaxanthin functions as an allosteric regulator for the lutein charge transfer quenching mechanisms. Evidence of both an energy transfer mechanism and a charge transfer mechanism indicate that lutein can play some role in the molecular mechanism of quenching.

In addition to the proposal that zeaxanthin modulates quenching, first hypothesized to occur via dimer formation and later as a charge transfer and recombination process (Horton et al., 1999), yet another proposed mechanism of quenching involves chlorophyll-chlorophyll interactions in LHCII. Transient absorption data subjected to global target analysis (van Stokkum et al., 2004) found species-associated spectra that do not support energy transfer to a carotenoid such as lutein in quenched LHCII oligomers deficient in zeaxanthin under annihilation-free experimental conditions (Müller et al., 2010). Instead, species-associated spectra are attributed to quenching via a chlorophyll-chlorophyll charge transfer state, in view of enhancement in the far-red portion of the spectra (Miloslavina et al., 2008). Recent work suggests that considering exciton-exciton annihilation, a process by which two excitons combine and then rapidly decay, may be necessary to explain the discrepancies between work that demonstrates chlorophyll-xanthophyll and chlorophyll-chlorophyll interactions as potential quenching mechanisms (van Oort et al., 2018).

Much of the work demonstrating potential molecular mechanisms acknowledges that multiple mechanisms may be present and work in parallel in the intact plant system. Single-molecule experiments provide a way to observe the function of pigment-protein complexes without the heterogeneity inherent to ensemble measurements (Kondo et al., 2017a). Under variable light, algae and mosses possess a pigment-protein complex that is well suited for single molecule fluorescence lifetime experiments called LHCSR (Peers et al., 2009). LHCSR is essential for the quenching response and performs both the regulatory function of sensing pH and the quenching itself (Liguori et al., 2016, 2013). In plants, these functions are distributed between several proteins, making it difficult to ensure that single molecule fluorescence lifetime studies observing two quenching states of LHCII monomers (Schlau-Cohen et al., 2015) are representative of *in vivo* conditions. Single-molecule fluorescence lifetime studies indicate that two distinct quenched states of LHCSR1 exist, with the probability of finding the protein in each state and the transition rate (up to 3.4 s^{-1}) influenced independently by the regulatory factors pH and presence of zeaxanthin (Kondo et al., 2017b). A representative schematic of the potential energy surface along two coordinates showing a change in barrier height that would result in an increased transition rate and a change in preferred conformation subject to control by xanthophyll content and pH is shown in Figure 3.
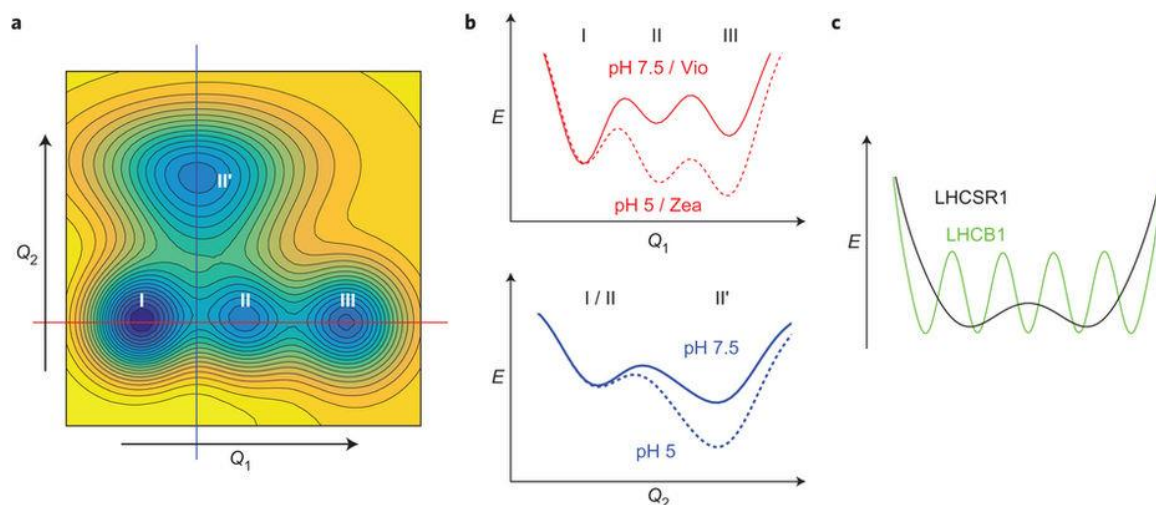
Figure 3. Representative illustration of the free-energy landscape of LHCSR1, a single protein pH sensor and quenching pigment-protein complex. (a) Contour plot showing three minima as a function of two nuclear coordinates. (b) Cuts along each coordinate displaying the change in surface due to changes in xanthophyll and pH that result in smaller barriers between states and a change in the lowest energy conformation. (c) comparison of barrier heights between conformational states of a non-quenching pigment-protein complex LHCB1. Reprinted by permission of Springer Nature: T. Kondo et al. Nature Chemistry 9(8):772-778 (2017).

The rapid rates of transition suggest that the various states are energetically similar and arise from only small conformational changes. Even small changes in orientation and distance could modulate the couplings and energies of different energetically similar excited and charge transfer states in chlorophylls or carotenoids (Dreuw et al., 2005, 2003a, 2003b). Subsequent evidence from similar studies on LHCIIs extracted from various mutant plants emphasizes that the transition rate is influenced by which carotenoid is present in LHCIIs, but the character of the quenched states observed are independent of the carotenoid present (Tutkus et al., 2017), further suggesting that quenching occurs heterogeneously and in agreement with single molecule fluorescence intensity measurements (Krüger et al., 2012). In ensemble measurements, the presence of a particular signal (such as the carotenoid radical cation, carotenoid S_1 excited state absorption, or far-red chlorophyll-chlorophyll charge transfer signals) may indicate that all of these mechanisms are involved in some way. However, addressing the roles they play in the overall plant photosynthetic system – inaccessible to a single molecule experiment – requires integrating information into a quantitative model to effectively evaluate the roles of mechanisms proposed upon observation of characteristic signals.

3.2 Incorporating Quenching Mechanisms into Energy Transfer Models

Incorporating the mechanisms described in Section 3.1 into energy transfer models of the photosynthetic antenna system and membrane allows an evaluation of how well the proposed mechanism, and the parameters identified from multiple experiments on isolated elements, can reproduce the experimentally observable decrease in fluorescence of the intact photosynthetic membrane. A first step is to accurately determine energies of the S_1 or dimer charge transfer states and their electronic couplings to neighboring chromophores that reflect the molecular

configuration and environment within the pigment-protein complex. The rates at which excitons are transferred into a dissipative state can then be calculated.

Although the energies of the excited states of carotenoids can be calculated reasonably accurately with common methods for electronic structure calculations (Dreuw et al., 2005, 2003a, 2003b), likely to a fortuitous cancellation of errors (Starcke et al., 2006), it is difficult to calculate the charge distributions of the excited states of the carotenoids accurately due to their two-electron character and the strong interactions between electrons (Macernis et al., 2012; Schulten et al., 1976; Starcke et al., 2006). As a result, determining the electronic couplings to neighboring chromophores is difficult. Semi-empirical calculations that take into account the effect of the electron interactions (Macernis et al., 2012) were used to calculate electronic couplings between a specific lutein and the closest adjacent chlorophylls in the structure of LHCII (Liu et al., 2004) and the resulting Förster energy transfer rates in a model of LHCII (Duffy et al., 2013). Figure 4 shows the lutein and adjacent chlorophylls embedded in the LHCII protein. With the energy of the S_1 state as a fit parameter, the model indicated that the most effective quenching occurred when the energy of the S_1 state was in agreement with the two-photon absorption spectrum (Walla et al., 2001). While an encouraging result, additional study is needed to understand the effects of heterogeneity in the position and orientation of lutein to evaluate the role this potential quenching mechanism plays in the plant system and how it might be regulated.
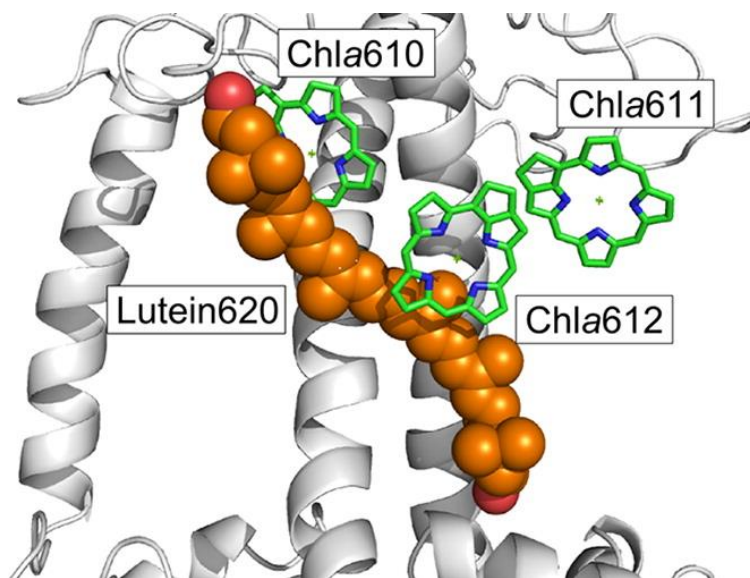
Figure 4. Structural depiction of a lutein quenching site associated with neighboring chlorophylls in LHCII. Reprinted with permission from Duffy C.D.P, Chmeliov, J, Macernis, M., Sulskus, J. Valkunas, L., Ruban, A.V., 2013, Modelling of Fluorescence Quenching by Lutein in the Plant Light-Harvesting Complex LHCII. J. Phys. Chem. B 117, 10974-10986. Copyright 2013 American Chemical Society.

To make predictions of quenched fluorescence lifetimes observed *in vivo*, the quantum mechanical descriptions of energy transfer to quenching sites must be incorporated into larger energy transfer models. The multiscale model of energy transfer at the membrane scale discussed in Section 2.1 (Amarnath et al., 2016) has been developed to include quenching sites located at

several of the suggested quenching sites in LHCII (Bennett et al., 2017) and can make predictions of fluorescence lifetimes given various quenching configurations. Changes in experimental fluorescence decay profiles of *A. thaliana* leaves (Sylak-Glassman et al., 2016) are accurately described by changes in a single effective quantity – the exciton diffusion length, L_D. L_D drops from about 50 nm in wild type plants at low light to around 25 nm in the maximally quenched system at high light levels. Conceptually, the L_D is a single variable that serves as the "tap" that controls light harvesting efficiency under conditions of excess light. L_D is a function of the intrinsic rate of quenching at a particular quenching site and the density of quenching sites. The functional dependence can be thought of, in the simplest approximation, as product of the two quantitates. Although different combinations of the intrinsic quenching rate and density of quenching sites can describe the fluorescence snapshot data, they all have the same L_D for a given quenched fluorescence lifetime (Bennett et al., 2017).

One proposed quenching mechanism the coarse grained model evaluates is the decay of the S_1 state of lutein near the terminal emitter of LHCII shown in Figure 4 (Duffy et al., 2013). The coarse grained model finds a 20 ps non-radiative decay constant for the domain predicts realistic quenched fluorescence lifetimes (Sylak-Glassman et al., 2016) with about 30% of the quenching sites active. On average, an exciton populates the domain for about 3 ps before either energy transfer to another domain or quenching occurs. These values agree with those suggested by semi-empirical calculations of couplings between lutein and adjacent chlorophylls (Duffy et al., 2013) and the probability of the LHCII adopting a quenched conformation determined from single molecule experiments (Krüger et al., 2012). In this parameter regime, the variety of proposed quenching mechanisms all operate in a "weak" limit, regardless of the specific details of the quenching mechanism. In the weak limit, an exciton does not spend much time within a domain before subsequent energy transfer, and therefore will visit multiple active quenching sites before it is likely to be dissipated.

To obtain L_D values that correspond to the highly quenched mutants, additional quenching sites in e.g. minor antenna complexes are required, suggesting that multiple quenching mechanisms work in parallel. Incorporating charge transfer states into exciton models of energy transfer presents another challenge. Exciton models assume that chromophores are locally excited, meaning that site energies and couplings can be calculated from quantum calculations of individual chromophores (Müh et al., 2010; Müh and Renger, 2012; Renger et al., 2011). When charge transfer occurs, this is no longer the case as electron density is transferred between chromophores as well (Dreuw et al., 2005, 2003a, 2003b). One extension of the exciton model uses calculations of the positive and negatively charged states of chromophores in addition to the usual calculations of local excited states to determine charge transfer states' energies and calculate the states' electronic couplings to locally excited states (Li et al., 2017). This method could be applied to begin to incorporate charge-transfer states into models of LHCII and minor antenna complexes to evaluate charge-transfer-based quenching mechanisms.

4. Chemical Regulation of Quenching

In comparison to the controversy surrounding the molecular mechanisms of quenching, there is relative consensus surrounding major components of the biochemical regulatory processes. It is generally accepted that the rapid induction of the quenching response in *A. thaliana* is triggered

by a trans-thylakoid pH gradient that forms in response to high light (Horton et al., 1996) as excitation pressure and charge separation outpace the ATP synthase (Kanazawa and Kramer, 2002). Excessively low pH in the thylakoid lumen protonates the non-pigment-binding PsbS (Li et al., 2004) and violaxanthin deepoxidase (VDE) that converts violaxanthin into zeaxanthin (Hager and Holocher, 1994; Jahns et al., 2009). Double mutants deficient in both PsbS and VDE lack all rapidly reversible q_E (Li et al., 2000). The presence of zeaxanthin, formed by VDE, and under certain conditions lutein (Ruban et al., 2007), allows the protonation-activated PsbS to act in the catalysis of rapid induction and relaxation of quenching (Sylak-Glassman et al., 2014). In addition, the presence of zeaxanthin is also associated with a longer timescale, non-pH-dependent quenching, called q_Z (Nilkens et al., 2010). Zeaxanthin levels and PSII light-harvesting efficiency are significantly and inversely correlated over time scales ranging from minutes to seasons (Adams III et al., 2008; Demmig-Adams et al., 2012). The many proposed molecular mechanisms of rapidly reversible quenching attempt to explain the quenching components identified by these regulatory dynamics (Duffy and Ruban, 2015; Jahns and Holzwarth, 2012).

Although there are numerous questions surrounding details of how each of the established components functions, including for example, the mechanism by which PsbS catalyzes the rapid induction of quenching (Daskalakis and Papadatos, 2017; Krishnan et al., 2017; Wilk et al., 2013), many aspects of their chemical kinetics have been measured (Jahns et al., 2009; Kalituho et al., 2007; Takizawa et al., 2007). The resulting kinetics of individual components have been incorporated into a quantitate kinetic model of the interior of the chloroplast with a simple model of the chemical regulation of quenching that predicts how fluorescence lifetimes change in response to changes in light intensity (Zaks et al., 2012). This model is an important tool for connecting the seconds to minutes timescale of the biochemical regulatory dynamics to the ultrafast timescales of energy transfer and quenching mechanisms: a major conclusion was that the pH gradient was insensitive to the presence of quenching. Therefore, subsequent and more sophisticated models of the regulation of quenching can approximate the pH gradient dynamics as an input, greatly simplifying the required details.

In a first attempt to develop a more sophisticated model of the regulation in *A. thaliana*, measurements of ultrafast fluorescence lifetime snapshots resolved on the regulatory timescale and matched to time resolved quantification of xanthophyll pigments were performed on intact leaves for a series of mutants deficient in either lutein or zeaxanthin (Leuenberger et al., 2017). In addition to addressing regulatory questions regarding memory effects of the xanthophyll cycle, the resulting kinetic model of regulation allowed the contributions of quenching controlled by different regulatory mechanisms to be quantified. A plot showing individual contributions to the wild type quenching response, formed from mutants deficient in either lutein or zeaxanthin, is shown in Figure 5. Within an individual mutant, it was found that zeaxanthin was a much more efficient quencher on a per molecule basis. Comparison of the individual components of quenching in wild type, which contains both lutein and zeaxanthin, indicated that the wild type quenching was more efficient on a per xanthophyll basis, than mutants containing just a single xanthophyll. Within an understanding of the exciton diffusion length, discussed in Section 3.2, it is difficult to assess either the origin of or the difference in quenching efficiency between lutein and zeaxanthin, or what results in the gain in efficiency of quenching when both are present: either the intrinsic quenching rate or the effective density of active quenching sites could change. Single molecule fluorescence lifetime studies indicate that multiple quenched states exist for LHCII could

all be present simultaneously with different non-radiative lifetimes (Krüger et al., 2012; Schlau-Cohen et al., 2015; Tutkus et al., 2017). Changes in the xanthophyll content could also change conformational behaviors of the pigment-protein complexes, reducing the density of quenching sites (Tutkus et al., 2017).
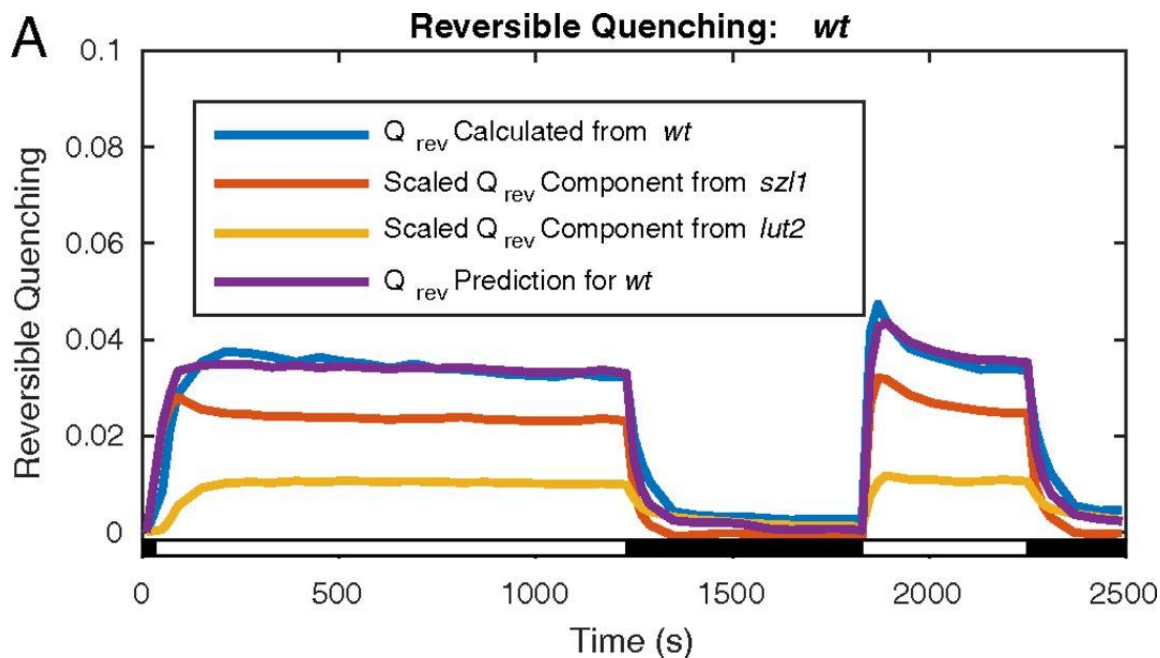
Figure 5. Analysis of quenching in response to two periods of light and dark acclimation into components isolating the contributions of lutein (red, from *szl1* mutant deficient in zeaxanthin) and zeaxanthin (yellow, from *lut2* mutant deficient in lutein) that require a single common scaling factor to obtain good agreement with wild type (blue, observed; purple, predicted from components). The scaling factor is greater than unity indicates that the wild type is more efficient on a per-molecule basis. Reprinted from Leuenberger et al. PNAS 114(33) E7009-E7017 (2017).

To quantitatively evaluate how the wild type realizes the observed efficiency gains, further work incorporating molecular models of quenching into models of the thylakoid membrane is necessary. Calculations of energy transfer rates to potential quenching states within single pigment-protein complexes (Duffy et al., 2013) upon substitution of xanthophylls as has been observed experimentally (Li et al., 2009; Lokstein et al., 2002) could indicate if substitution results in the observed discrepancy by changing the transfer or decay rate. However, recent single molecule experiments on monomeric LHCIIs from pigment deficient mutants suggest that xanthophyll deficiencies instead change pigment-protein complex conformational dynamics, and therefore the activation of quenching sites (Tutkus et al., 2017). Integrating these data into coarse grained membrane scale models (Amarnath et al., 2016; Bennett et al., 2017) would be useful for evaluating the effects of xanthophyll deficiency on molecular mechanisms of quenching in addition to the regulation of quenching.

Due to the complexity of the *in vivo* system, it is necessary to employ regulatory modeling to isolate the contributions of quenching with specific regulatory signatures that suggest distinct molecular mechanisms. For example, in the case of zeaxanthin, multiple quenching processes all depend on zeaxanthin and cannot be isolated with xanthophyll deficient mutants alone (Leuenberger et al., 2017). Upon isolation of the quenching attributable to a particular regulatory signature, the effect of a particular molecular mechanism of quenching on the L_D, and thus the change in fluorescence of an *in vivo* system evaluated with multiscale models, can be evaluated independently of the effect of the xanthophyll as a whole. As regulatory and molecular models of quenching converge, mechanistic connection between regulatory signatures and molecular mechanisms of energy dissipation itself could be achieved through analysis of minimal artificial systems or large scale molecular dynamics simulations.

Conclusion

This review discusses the quantitative modeling of energy dissipation, or quenching, in *A. thaliana*. Starting from energy transfer between individual chlorophyll molecules in the antenna, detailed quantum mechanical treatments are necessary at the fastest timescales. However, as time and length scales increase, much of quantum mechanical detail can be approximated into coarse grained models. These coarse-grained models are useful for evaluating proposed molecular mechanisms of quenching in a manner that can predict experimentally observable fluorescence lifetimes. Although evidence suggests a number of different mechanisms of quenching, that seem to occur simultaneously, combining molecular and mechanistic models with regulatory modeling that quantifies of the contributions of components with distinct regulatory signatures provides a path towards evaluating the roles and contributions of proposed mechanisms and to exploring optimization of the regulatory systems.

Acknowledgements

References

Adams III, W.W., Zarter, C.R., Mueh, K.E., Amiard, V., Demmig-Adams, B., 2008. Energy Dissipation and Photoinhibition: A Continuum of Photoprotection, in: Photoprotection, Photoinhibition, Gene Regulation, and Environment. Springer Netherlands, Dordrecht, pp. 49–64. https://doi.org/10.1007/1-4020-3579-9_5

Agarwal, R., Krueger, B.P., Scholes, G.D., Yang, M., Yom, J., Mets, L., Fleming, G.R., 2000. Ultrafast Energy Transfer in LHC-II Revealed by Three-Pulse Photon Echo Peak Shift Measurements. J. Phys. Chem. B 104, 2908–2918. https://doi.org/10.1021/JP9915578

Ahn, T.K., Avenson, T.J., Ballottari, M., Cheng, Y.-C., Niyogi, K.K., Bassi, R., Fleming, G.R., 2008. Architecture of a charge-transfer state regulating light harvesting in a plant antenna protein. Science 320, 794–7. https://doi.org/10.1126/science.1154800

Amarnath, K., Bennett, D.I.G., Schneider, A.R., Fleming, G.R., 2016. Multiscale model of light harvesting by photosystem II in plants. Proc. Natl. Acad. Sci. U. S. A. 113, 1156–61. https://doi.org/10.1073/pnas.1524999113

Atkins, P.W., Friedman, R.S., 2011. Molecualr Quantum Mechanics, FIfth. ed. Oxford University Press, New York.

Avenson, T.J., Ahn, T.K., Niyogi, K.K., Ballottari, M., Bassi, R., Fleming, G.R., 2009. Lutein can act as a switchable charge transfer quencher in the CP26 light-harvesting complex. J. Biol. Chem. 284, 2830–5. https://doi.org/10.1074/jbc.M807192200

Avenson, T.J., Ahn, T.K., Zigmantas, D., Niyogi, K.K., Li, Z., Ballottari, M., Bassi, R., Fleming, G.R., 2008. Zeaxanthin radical cation formation in minor light-harvesting complexes of higher plant antenna. J. Biol. Chem. 283, 3550–8. https://doi.org/10.1074/jbc.M705645200

Bennett, D.I.G., Amarnath, K., Fleming, G.R., 2013. A Structure-Based Model of Energy Transfer Reveals the Principles of Light Harvesting in Photosystem II Supercomplexes. J. Am. Chem. Soc. 135, 9164–9173. https://doi.org/10.1021/ja403685a

Bennett, D.I.G., Fleming, G.R., Amarnath, K., 2017. Feedback de-excitation adjusts the excitation diffusion length to regulate photosynthetic light harvesting, ArXiv e-prints.

Bernhardt, K., Trissl, H.-W., 1999. Theories for kinetics and yields of fluorescence and photochemistry: how, if at all, can different models of antenna organization be distinguished experimentally? Biochim. Biophys. Acta 1409, 125–142. https://doi.org/10.1016/S0005-2728(98)00149-2

Bittner, T., Irrgang, K.-D., Renger, G., Wasielewski, M.R., 1994. Ultrafast Excitation Energy Transfer and Exciton-Exciton Annihilation Processes in Isolated Light Harvesting Complexes of Photosystem II (LHC II) from Spinach. J. Phys. Chem. 98, 11821–11826. https://doi.org/10.1021/j100097a004

Bittner, T., Wiederrecht, G.P., Irrgang, K.-D., Renger, G., Wasielewski, M.R., 1995. Femtosecond transient absorption spectroscopy on the light-harvesting Chl a/b protein complex of Photosystem II at room temperature and 12 K. Chem. Phys. 194, 311–322. https://doi.org/10.1016/0301-0104(95)00045-P

Blankenship, R.E., 2014. Molecular mechanisms of photosynthesis, 2nd ed. Wiley Blackwell, Oxford.

Bode, S., Quentmeier, C.C., Liao, P.-N., Hafi, N., Barros, T., Wilk, L., Bittner, F., Walla, P.J., 2009. On the regulation of photosynthesis by excitonic interactions between carotenoids

and chlorophylls. Proc. Natl. Acad. Sci. U. S. A. 106, 12311–6. https://doi.org/10.1073/pnas.0903536106

Brixner, T., Stenger, J., Vaswani, H.M., Cho, M., Blankenship, R.E., Fleming, G.R., 2005. Two-dimensional spectroscopy of electronic couplings in photosynthesis. Nature 434, 625–628. https://doi.org/10.1038/nature03429

Calhoun, T.R., Ginsberg, N.S., Schlau-Cohen, G.S., Cheng, Y.-C., Ballottari, M., Bassi, R., Fleming, G.R., 2009. Quantum Coherence Enabled Determination of the Energy Landscape in Light-Harvesting Complex II. J. Phys. Chem. B 113, 16291–16295. https://doi.org/10.1021/jp908300c

Cheng, Y.-C., Fleming, G.R., 2009. Dynamics of Light Harvesting in Photosynthesis. Annu. Rev. Phys. Chem. 60, 241–262. https://doi.org/10.1146/annurev.physchem.040808.090259

Cho, M., Vaswani, H.M., Brixner, T., Stenger, J., Fleming, G.R., 2005. Exciton Analysis in 2D Electronic Spectroscopy. J. Phys. Chem. B 109, 10542–10556. https://doi.org/10.1021/JP050788D

Connelly, J.P., Müller, M.G., Hucke, M., Gatzen, G., Mullineaux, C.W., Ruban, A. V., Horton, P., Holzwarth, A.R., 1997. Ultrafast Spectroscopy of Trimeric Light-Harvesting Complex II from Higher Plants. J. Phys. Chem. B 101, 1902–1909. https://doi.org/10.1021/JP9619651

Daskalakis, V., Papadatos, S., 2017. The Photosystem II Subunit S under Stress. Biophys. J. 113, 2364–2372. https://doi.org/10.1016/j.bpj.2017.09.034

Demmig-Adams, B., Adams III, W.W., 1992. Photoprotection and other responses of plants to high light stress. Annu. Rev. Plant Physiol. Plant Micorbial Biol. 43, 599–626. https://doi.org/10.1146/annurev.pp.43.060192.003123

Demmig-Adams, B., Cohu, C.M., Muller, O., Adams, W.W., 2012. Modulation of photosynthetic energy conversion efficiency in nature: from seconds to seasons. Photosynth. Res. 113, 75–88. https://doi.org/10.1007/s11120-012-9761-6

Demmig-Adams, B., Cohu, C.M., Stewart, J.J., Adams III, W.W., 2014. Non-Photochemical Quenching and Energy Dissipation in Plants, Algae and Cyanobacteria, Photosynthesis and Respiration. Springer Netherlands. https://doi.org/10.1007/978-94-017-9032-1

Den Hollander, W.T.F., Bakker, J.G.C., Van Grondelle, R., 1983. Trapping, loss and annihilation of excitations in a photosynthetic system. I. Theoretical aspects. Biochim. Biophys. Acta - Bioenerg. 725, 492–507. https://doi.org/10.1016/0005-2728(83)90190-1

Dreuw, A., Fleming, G.R., Head-Gordon, M., 2005. Role of electron-transfer quenching of chlorophyll fluorescence by carotenoids in non-photochemical quenching of green plants. Biochem. Soc. Trans. 33, 858–862. https://doi.org/10.1042/BST0330858

Dreuw, A., Fleming, G.R., Head-Gordon, M., 2003a. Charge-Transfer State as a Possible Signature of a Zeaxanthin−Chlorophyll Dimer in the Non-photochemical Quenching Process in Green Plants. J. Phys. Chem. B 107, 6500–6503. https://doi.org/10.1021/JP034562R

Dreuw, A., Fleming, G.R., Head-Gordon, M., 2003b. Chlorophyll fluorescence quenching by xanthophylls. Phys. Chem. Chem. Phys. 5, 3247. https://doi.org/10.1039/b304944b

Duffy, C.D.P., Chmeliov, J., Macernis, M., Sulskus, J., Valkunas, L., Ruban, A. V., 2013. Modeling of Fluorescence Quenching by Lutein in the Plant Light-Harvesting Complex LHCII. J. Phys. Chem. B 117, 10974–10986. https://doi.org/10.1021/jp3110997

Duffy, C.D.P., Ruban, A. V, 2015. Dissipative pathways in the photosystem-II antenna in plants. J. Photochem. Photobiol. B Biol. 152, 215–226. https://doi.org/10.1016/j.jphotobiol.2015.09.011

Eads, D.D., Castner, E.W., Alberte, R.S., Mets, L., Fleming, G.R., 1989. Direct observation of energy transfer in a photosynthetic membrane: chlorophyll b to chlorophyll a transfer in LHC. J. Phys. Chem. 93, 8271–8275. https://doi.org/10.1021/j100363a001

Fassioli, F., Dinshaw, R., Arpin, P.C., Scholes, G.D., 2014. Photosynthetic light harvesting: excitons and coherence. J. R. Soc. Interface 11, 20130901. https://doi.org/10.1098/rsif.2013.0901

Fenna, R.E., Matthews, B.W., 1975. Chlorophyll arrangement in a bacteriochlorophyll protein from Chlorobium limicola. Nature 258, 573–577. https://doi.org/10.1038/258573a0

Foresman, J.B., Head-Gordon, M., Pople, J.A., Frisch, M.J., 1992. Toward a systematic molecular orbital theory for excited states. J. Phys. Chem. 96, 135–149. https://doi.org/10.1021/j100180a030

Förster, T., 1948. Zwischenmolekulare Energiewanderung und Fluoreszenz. Ann. Phys. 437, 55–75. https://doi.org/10.1002/andp.19484370105

Frank, H.A., Bautista, J.A., Josue, J.S., Young, A.J., 2000. Mechanism of nonphotochemical quenching in green plants: Energies of the lowest excited singlet states of violaxanthin and zeaxanthin. Biochemistry 39, 2831–2837. https://doi.org/10.1021/bi9924664

Frank, H.A., Chynwat, V., Desamero, R.Z.B., Farhoosh, R., Erickson, J., Bautista, J., 1997. On the photophysics and photochemical properties of carotenoids and their role as light-harvesting pigments in photosynthesis. Pure Appl. Chem. 69, 2117–2124. https://doi.org/10.1351/pac199769102117

Frank, H.A., Cogdell, R.J., 1996. Carotenoids in Photosynthesis. Photochem. Photobiol. 63, 257–264. https://doi.org/10.1111/j.1751-1097.1996.tb03022.x

Gradinaru, C.C., Ozdemir, S., Gülen, D., van Stokkum, I.H., van Grondelle, R., van Amerongen, H., 1998. The flow of excitation energy in LHCII monomers: implications for the structural model of the major plant antenna. Biophys. J. 75, 3064–77. https://doi.org/10.1016/S0006-3495(98)77747-1

Gülen, D., van Grondelle, R., van Amerongen, H., 1997. Structural Information on the Light-Harvesting Complex II of Green Plants That Can Be Deciphered from Polarized Absorption Characteristics. J. Phys. Chem. B 101, 7256–7261. https://doi.org/10.1021/JP963364F

Hager, A., Holocher, K., 1994. Localization of the xanthophyll-cycle enzyme violaxanthin de-epoxidase within the thylakoid lumen and abolition of its mobility by a (light-dependent) pH decrease. Planta 192, 581–589. https://doi.org/10.1007/BF00203597

Hirata, S., Head-Gordon, M., 1999. Time-dependent density functional theory within the Tamm–Dancoff approximation. Chem. Phys. Lett. 314, 291–299. https://doi.org/10.1016/S0009-2614(99)01149-5

Holleboom, C.-P., Walla, P.J., 2014. The back and forth of energy transfer between carotenoids and chlorophylls and its role in the regulation of light harvesting. Photosynth. Res. 119, 215–221. https://doi.org/10.1007/s11120-013-9815-4

Holt, N.E., Zigmantas, D., Valkunas, L., Li, X.-P., Niyogi, K.K., Fleming, G.R., 2005. Carotenoid cation formation and the regulation of photosynthetic light harvesting. Science 307, 433–6. https://doi.org/10.1126/science.1105833

Horton, P., Ruban, A.V., Rees, D., Pascal, A.A., Noctor, G., Young, A.J., 1991. Control of the light-harvesting function of chloroplast membranes by aggregation of the LHCII chlorophyll–protein complex. FEBS Lett. 292, 1–4. https://doi.org/10.1016/0014-5793(91)80819-O

Horton, P., Ruban, A. V., Young, A.J., 1999. Regulation of the Structure and Function of the Light Harvesting Complexes of Photosystem II by the Xanthophyll Cycle, in: The Photochemistry of Carotenoids. Kluwer Academic Publishers, Dordrecht, pp. 271–291. https://doi.org/10.1007/0-306-48209-6_15

Horton, P., Ruban, A. V, Walters, R.G., 1996. Regulation of light harvesting in green plants. Annu. Rev. Plant Physiol. Plant Mol. Biol 47, 655–84. https://doi.org/10.1146/annurev.arplant.47.1.655

Hu, X., Ritz, T., Damjanovic, A., Autenrieth, F., Schulten, K., 2002. Photosynthetic apparatus of purple bacteria. Q. Rev. Biophys. 35, 1–62. https://doi.org/10.1017/S0033583501003754

Ilioaia, C., Johnson, M.P., Horton, P., Ruban, A. V, 2008. Induction of efficient energy dissipation in the isolated light-harvesting complex of Photosystem II in the absence of protein aggregation. J. Biol. Chem. 283, 29505–12. https://doi.org/10.1074/jbc.M802438200

İşeri, E.İ., Gülen, D., 2001. Chlorophyll transition dipole moment orientations and pathways for flow of excitation energy among the chlorophylls of the major plant antenna, LHCII. Eur. Biophys. J. 30, 344–353. https://doi.org/10.1007/s002490100151

Ishizaki, A., Fleming, G.R., 2009a. On the adequacy of the Redfield equation and related approaches to the study of quantum dynamics in electronic energy transfer. J. Chem. Phys. 130, 234110. https://doi.org/10.1063/1.3155214

Ishizaki, A., Fleming, G.R., 2009b. Unified treatment of quantum coherent and incoherent hopping dynamics in electronic energy transfer: Reduced hierarchy equation approach. J. Chem. Phys. 130. https://doi.org/10.1063/1.3155372

Ishizaki, A., Fleming, G.R., 2009c. Theoretical examination of quantum coherence in a photosynthetic system at physiological temperature. Proc. Natl. Acad. Sci. U. S. A. 106, 17255–60. https://doi.org/10.1073/pnas.0908989106

Jahns, P., Holzwarth, A.R., 2012. The role of the xanthophyll cycle and of lutein in photoprotection of photosystem II. Biochim. Biophys. Acta 1817, 182–193. https://doi.org/10.1016/J.BBABIO.2011.04.012

Jahns, P., Latowski, D., Strzalka, K., 2009. Mechanism and regulation of the violaxanthin cycle: The role of antenna proteins and membrane lipids. Biochim. Biophys. Acta 1787, 3–14. https://doi.org/10.1016/J.BBABIO.2008.09.013

Jang, S., Jung, Y., Silbey, R.J., 2002. Nonequilibrium generalization of Förster–Dexter theory for excitation energy transfer. Chem. Phys. 275, 319–332. https://doi.org/10.1016/S0301-0104(01)00538-9

Jang, S., Newton, M.D., Silbey, R.J., 2004. Multichromophoric Förster Resonance Energy Transfer. Phys. Rev. Lett. 92, 218301. https://doi.org/10.1103/PhysRevLett.92.218301

Kalituho, L., Beran, K.C., Jahns, P., 2007. The transiently generated nonphotochemical quenching of excitation energy in Arabidopsis leaves is modulated by zeaxanthin. Plant Physiol. 143, 1861–70. https://doi.org/10.1104/pp.106.095562

Kanazawa, A., Kramer, D.M., 2002. In vivo modulation of nonphotochemical exciton quenching (NPQ) by regulation of the chloroplast ATP synthase. Proc. Natl. Acad. Sci. 99, 12789–12794. https://doi.org/10.1073/pnas.182427499

Kleima, F.J., Gradinaru, C.C., Florentine Calkoen, Ivo H. M. van Stokkum, Rienk van Grondelle, A., Amerongen, H. van, 1997. Energy Transfer in LHCII Monomers at 77K Studied by Sub-Picosecond Transient Absorption Spectroscopy. Biochemistry 36, 15262–15268. https://doi.org/10.1021/BI9716480

Kondo, T., Chen, W.J., Schlau-Cohen, G.S., 2017a. Single-Molecule Fluorescence Spectroscopy of Photosynthetic Systems. Chem. Rev. 117, 860–898. https://doi.org/10.1021/acs.chemrev.6b00195

Kondo, T., Pinnola, A., Chen, W.J., Dall'Osto, L., Bassi, R., Schlau-Cohen, G.S., 2017b. Single-molecule spectroscopy of LHCSR1 protein dynamics identifies two distinct states responsible for multi-timescale photosynthetic photoprotection. Nat. Chem. 9, 772–778. https://doi.org/10.1038/nchem.2818

Krause, G.H., Weis, E., 1991. Chlorophyll Fluorescence and Photosynthesis: The Basics. Annu. Rev. Plant Physiol. Plant Mol. Biol. 42, 313–349. https://doi.org/10.1146/annurev.pp.42.060191.001525

Kreisbeck, C., Aspuru-Guzik, A., 2016. Efficiency of energy funneling in the photosystem II supercomplex of higher plants. Chem. Sci. 7, 4174. https://doi.org/10.1039/c5sc04296h

Krishnan, M., Moolenaar, G.F., Gupta, K.B.S.S., Goosen, N., Pandit, A., 2017. Large-scale in vitro production, refolding and dimerization of PsbS in different microenvironments. Sci. Rep. 7, 15200. https://doi.org/10.1038/s41598-017-15068-3

Kromdijk, J., Głowacka, K., Leonelli, L., Gabilly, S.T., Iwai, M., Niyogi, K.K., Long, S.P., 2016. Improving photosynthesis and crop productivity by accelerating recovery from photoprotection. Science 354, 857–861. https://doi.org/10.1126/science.aai8878

Krüger, T.P.J., Ilioaia, C., Johnson, M.P., Ruban, A. V, Papagiannakis, E., Horton, P., van Grondelle, R., 2012. Controlled disorder in plant light-harvesting complex II explains its photoprotective role. Biophys. J. 102, 2669–76. https://doi.org/10.1016/j.bpj.2012.04.044

Kühlbrandt, W., 1988. Structure of light-harvesting chlorophyll a b protein complex from plant photosynthetic membranes at 7Å resolution in projection. J. Mol. Biol. 202, 849–864. https://doi.org/10.1016/0022-2836(88)90563-3

Kühlbrandt, W., Wang, D.N., 1991. Three-dimensional structure of plant light-harvesting complex determined by electron crystallography. Nature 350, 130–134. https://doi.org/10.1038/350130a0

Kühlbrandt, W., Wang, D.N., Fujiyoshi, Y., 1994. Atomic model of plant light-harvesting complex by electron crystallography. Nature 367, 614–621. https://doi.org/10.1038/367614a0

Külheim, C., Agren, J., Jansson, S., 2002. Rapid regulation of light harvesting and plant fitness in the field. Science 297, 91–93. https://doi.org/10.1126/science.1072359

Kwa, S.L.S., van Amerongen, H., Lin, S., Dekker, J.P., van Grondelle, R., Struve, W.S., 1992. Ultrafast energy transfer in LHC-II trimers from the Chl a b light-harvesting antenna of Photosystem II. Biochim. Biophys. Acta 1102, 202–212. https://doi.org/10.1016/0005-2728(92)90101-7

Laisk, A., Nedbal, L., Govindjee, 2009. Photosynthesis in silico, Advances in Photosynthesis and Respiration. Springer Netherlands, Dordrecht. https://doi.org/10.1007/978-1-4020-9237-4

Lavorel, J., Joliot, P., 1972. A connected model of the photosynthetic unit. Biophys. J. 12, 815–831. https://doi.org/10.1016/S0006-3495(72)86125-3

Leuenberger, M., Morris, J.M., Chan, A.M., Leonelli, L., Niyogi, K.K., Fleming, G.R., 2017. Dissecting and modeling zeaxanthin- and lutein-dependent nonphotochemical quenching in Arabidopsis thaliana. Proc. Natl. Acad. Sci. U. S. A. 114, E7009–E7017. https://doi.org/10.1073/pnas.1704502114

Lewis, N.H.C., Gruenke, N.L., Oliver, T.A.A., Ballottari, M., Bassi, R., Fleming, G.R., 2016. Observation of Electronic Excitation Transfer Through Light Harvesting Complex II Using Two-Dimensional Electronic–Vibrational Spectroscopy. J. Phys. Chem. Lett. 7, 4197–4206. https://doi.org/10.1021/acs.jpclett.6b02280

Li, X.-P., Björkman, O., Shih, C., Grossman, A.R., Rosenquist, M., Jansson, S., Niyogi, K.K., 2000. A pigment-binding protein essential for regulation of photosynthetic light harvesting. Nature 403, 391–395. https://doi.org/10.1038/35000131

Li, X.-P., Gilmore, A.M., Caffarri, S., Bassi, R., Golan, T., Kramer, D., Niyogi, K.K., 2004. Regulation of photosynthetic light harvesting involves intrathylakoid lumen pH sensing by the PsbS protein. J. Biol. Chem. 279, 22866–74. https://doi.org/10.1074/jbc.M402461200

Li, X., Parrish, R.M., Liu, F., Kokkila Schumacher, S.I.L., Martínez, T.J., 2017. An Ab Initio Exciton Model Including Charge-Transfer Excited States. J. Chem. Theory Comput. 13, 3493–3504. https://doi.org/10.1021/acs.jctc.7b00171

Li, Z., Ahn, T.K., Avenson, T.J., Ballottari, M., Cruz, J.A., Kramer, D.M., Bassi, R., Fleming, G.R., Keasling, J.D., Niyogi, K.K., 2009. Lutein Accumulation in the Absence of Zeaxanthin Restores Nonphotochemical Quenching in the Arabidopsis thaliana npq1 Mutant. Plant Cell 21, 1798–812. https://doi.org/10.1105/tpc.109.066571

Liguori, N., Novoderezhkin, V., Roy, L.M., van Grondelle, R., Croce, R., 2016. Excitation dynamics and structural implication of the stress-related complex LHCSR3 from the green alga Chlamydomonas reinhardtii. Biochim. Biophys. Acta 1857, 1514–1523. https://doi.org/10.1016/J.BBABIO.2016.04.285

Liguori, N., Roy, L.M., Opacic, M., Durand, G., Croce, R., 2013. Regulation of Light Harvesting in the Green Alga Chlamydomonas reinhardtii : The C-Terminus of LHCSR Is the Knob of a Dimmer Switch. J. Am. Chem. Soc. 135, 18339–18342. https://doi.org/10.1021/ja4107463

Liu, Z., Yan, H., Wang, K., Kuang, T., Zhang, J., Gui, L., An, X., Chang, W., 2004. Crystal structure of spinach major light-harvesting complex at 2.72 Å resolution. Nature 428, 287–292. https://doi.org/10.1038/nature02373

Lokstein, H., Tian, L., Polle, J.E.W., DellaPenna, D., 2002. Xanthophyll biosynthetic mutants of Arabidopsis thaliana: altered nonphotochemical quenching of chlorophyll fluorescence is

due to changes in Photosystem II antenna size and stability. Biochim. Biophys. Acta 1553, 309–319. https://doi.org/10.1016/S0005-2728(02)00184-6

Macernis, M., Sulskus, J., Duffy, C.D.P., Ruban, A. V., Valkunas, L., 2012. Electronic Spectra of Structurally Deformed Lutein. J. Phys. Chem. A 116, 9843–9853. https://doi.org/10.1021/jp304363q

Miloslavina, Y., Wehner, A., Lambrev, P.H., Wientjes, E., Reus, M., Garab, G., Croce, R., Holzwarth, A.R., 2008. Far-red fluorescence: A direct spectroscopic marker for LHCII oligomer formation in non-photochemical quenching. FEBS Lett. 582, 3625–3631. https://doi.org/10.1016/j.febslet.2008.09.044

Mirkovic, T., Ostroumov, E.E., Anna, J.M., van Grondelle, R., Govindjee, Scholes, G.D., 2017. Light Absorption and Energy Transfer in the Antenna Complexes of Photosynthetic Organisms. Chem. Rev. 117, 249–293. https://doi.org/10.1021/acs.chemrev.6b00002

Müh, F., Madjet, M.E.-A., Renger, T., 2012. Structure-based simulation of linear optical spectra of the CP43 core antenna of photosystem II. Photosynth. Res. 111, 87–101. https://doi.org/10.1007/s11120-011-9675-8

Müh, F., Madjet, M.E.-A., Renger, T., 2010. Structure-Based Identification of Energy Sinks in Plant Light-Harvesting Complex II. J. Phys. Chem. B 114, 13517–13535. https://doi.org/10.1021/jp106323e

Müh, F., Renger, T., 2012. Refined structure-based simulation of plant light-harvesting complex II: Linear optical spectra of trimers and aggregates. Biochim. Biophys. Acta - Bioenerg. 1817, 1446–1460. https://doi.org/10.1016/J.BBABIO.2012.02.016

Mukamel, S., 1995. Principles of Nonlinear Optical Spectroscopy. Oxford University Press, New York.

Müller, M.G., Lambrev, P., Reus, M., Wientjes, E., Croce, R., Holzwarth, A.R., 2010. Singlet Energy Dissipation in the Photosystem II Light-Harvesting Complex Does Not Involve Energy Transfer to Carotenoids. ChemPhysChem 11, 1289–1296. https://doi.org/10.1002/cphc.200900852

Nilkens, M., Kress, E., Lambrev, P., Miloslavina, Y., Müller, M., Holzwarth, A.R., Jahns, P., 2010. Identification of a slowly inducible zeaxanthin-dependent component of non-photochemical quenching of chlorophyll fluorescence generated under steady-state conditions in Arabidopsis. Biochim. Biophys. Acta 1797, 466–475. https://doi.org/10.1016/J.BBABIO.2010.01.001

Niyogi, K.K., 1999. Photoprotection Revisited: Genetic and Molecular Approaches. Annu. Rev. Plant Physiol. Plant Mol. Biol. 50, 333–359. https://doi.org/10.1146/annurev.arplant.50.1.333

Niyogi, K.K., Björkman, O., Grossman, A.R., 1997. The roles of specific xanthophylls in photoprotection. Proc. Natl. Acad. Sci. 94. https://doi.org/10.1073/pnas.94.25.14162

Novoderezhkin, V.I., Marin, A., van Grondelle, R., 2011a. Intra- and inter-monomeric transfers in the light harvesting LHCII complex: the Redfield–Förster picture. Phys. Chem. Chem. Phys. 13, 17093. https://doi.org/10.1039/c1cp21079c

Novoderezhkin, V.I., Palacios, M.A., van Amerongen, H., van Grondelle, R., 2004. Energy-Transfer Dynamics in the LHCII Complex of Higher Plants: Modified Redfield Approach†. J. Phys. Chem. B 108, 10363–10375. https://doi.org/10.1021/JP0496001

Novoderezhkin, V.I., Palacios, M.A., Van Amerongen, H., Van Grondelle, R., 2005. Excitation Dynamics in the LHCII Complex of Higher Plants: Modeling Based on the 2.72 Å Crystal Structure. J. Phys. Chem. B 109, 10493–10504. https://doi.org/10.1021/jp044082f

Novoderezhkin, V.I., Romero, E., Dekker, J.P., van Grondelle, R., 2011b. Multiple Charge-Separation Pathways in Photosystem II: Modeling of Transient Absorption Kinetics. ChemPhysChem 12, 681–688. https://doi.org/10.1002/cphc.201000830

Novoderezhkin, V.I., Salverda, J.M., van Amerongen, H., van Grondelle, R., 2003. Exciton Modeling of Energy-Transfer Dynamics in the LHCII Complex of Higher Plants: A Redfield Theory Approach. J. Phys. Chem. B 107, 1893–1912. https://doi.org/10.1021/JP027003D

Paillotin, G., Swenberg, C.E., Breton, J., 1979. Analysis of picosecond laser-induced fluorescence phenomena in photosynthetic membranes using a master equation approach. Biophys. J. 25, 513–533. https://doi.org/10.1016/S0006-3495(79)85320-5

Pan, X., Li, M., Wan, T., Wang, L., Jia, C., Hou, Z., Zhao, X., Zhang, J., Chang, W., 2011. Structural insights into energy regulation of light-harvesting complex CP29 from spinach. Nat. Struct. Mol. Biol. 18, 309–315. https://doi.org/10.1038/nsmb.2008

Pascal, A.A., Liu, Z., Broess, K., van Oort, B., van Amerongen, H., Wang, C., Horton, P., Robert, B., Chang, W., Ruban, A., 2005. Molecular basis of photoprotection and control of photosynthetic light-harvesting. Nature 436, 134–137. https://doi.org/10.1038/nature03795

Peers, G., Truong, T.B., Ostendorf, E., Busch, A., Elrad, D., Grossman, A.R., Hippler, M., Niyogi, K.K., 2009. An ancient light-harvesting protein is critical for the regulation of algal photosynthesis. Nature 462, 518–521. https://doi.org/10.1038/nature08587

Pogson, B.J., Niyogi, K.K., Björkman, O., DellaPenna, D., 1998. Altered xanthophyll compositions adversely affect chlorophyll accumulation and nonphotochemical quenching in Arabidopsis mutants. Proc. Natl. Acad. Sci. U. S. A. 95, 13324–9. https://doi.org/10.1073/PNAS.95.22.13324

Polívka, T., Herek, J.L., Zigmantas, D., Åkerlund, H.-E., Sundstrom, V., 1999. Direct observation of the (forbidden) S1 state in carotenoids. Proc. Natl. Acad. Sci. 96, 4914–4917. https://doi.org/10.1073/pnas.96.9.4914

Polívka, T., Zigmantas, D., Sundström, V., Formaggio, E., Cinque, G., Bassi, R., 2002. Carotenoid S1 state in a recombinant light-harvesting complex of photosystem II. Biochemistry 41, 439–450. https://doi.org/10.1021/bi011589x

Raszewski, G., Diner, B.A., Schlodder, E., Renger, T., 2008. Spectroscopic properties of reaction center pigments in photosystem II core complexes: revision of the multimer model. Biophys. J. 95, 105–19. https://doi.org/10.1529/biophysj.107.123935

Raszewski, G., Renger, T., 2008. Light Harvesting in Photosystem II Core Complexes Is Limited by the Transfer to the Trap: Can the Core Complex Turn into a Photoprotective Mode? J. Am. Chem. Soc. 130, 4431–4446. https://doi.org/10.1021/ja7099826

Raszewski, G., Saenger, W., Renger, T., 2005. Theory of Optical Spectra of Photosystem II Reaction Centers: Location of the Triplet State and the Identity of the Primary Electron Donor. Biophys. J. 88, 986–998. https://doi.org/10.1529/biophysj.104.050294

Redfield, G., 1957. On the Theory of Relaxation Processes. IBM J. Res. Dev. 1, 19. https://doi.org/10.1147/rd.11.0019

Remelli, R., Varotto, C., Sandonà, D., Croce, R., Bassi, R., 1999. Chlorophyll binding to monomeric light-harvesting complex. A mutation analysis of chromophore-binding residues. J. Biol. Chem. 274, 33510–21. https://doi.org/10.1074/JBC.274.47.33510

Renger, T., Madjet, M.E., Knorr, A., Müh, F., 2011. How the molecular structure determines the flow of excitation energy in plant light-harvesting complex II. J. Plant Physiol. 168, 1497–1509. https://doi.org/10.1016/J.JPLPH.2011.01.004

Renger, T., May, V., Kühn, O., 2001. Ultrafast excitation energy transfer dynamics in photosynthetic pigment–protein complexes. Phys. Rep. 343, 137–254. https://doi.org/10.1016/S0370-1573(00)00078-8

Robinson, G.W., 1967. Excitation Transfer and Trapping in Photosynthesis, in: Brookhaven Symposia in Biology Number 19: Energy Conversion by the Photosynthetic Apparatus, Report of Symposium Held at Upton, June 6-9, 1966. Upton, NY (United States). https://doi.org/10.2172/4444017

Roden, J.J.J., Bennett, D.I.G., Birgitta Whaley, K., 2016. Long-range energy transport in photosystem II. J. Chem. Phys. J. Chem. Phys. J. Chem. Phys. J. Chem. Phys. 144, 245101–174106. https://doi.org/10.1063/1.4932307

Rogl, H., Kühlbrandt, W., 1999. Mutant Trimers of Light-Harvesting Complex II Exhibit Altered Pigment Content and Spectroscopic Features. Biochemistry 38, 16214–16222. https://doi.org/10.1021/BI990739P

Ruban, A. V., Berera, R., Ilioaia, C., van Stokkum, I.H.M., Kennis, J.T.M., Pascal, A.A., van Amerongen, H., Robert, B., Horton, P., van Grondelle, R., 2007. Identification of a mechanism of photoprotective energy dissipation in higher plants. Nature 450, 575–578. https://doi.org/10.1038/nature06262

Ruban, A. V., Johnson, M.P., 2010. Xanthophylls as modulators of membrane protein function. Arch. Biochem. Biophys. 504, 78–85. https://doi.org/10.1016/j.abb.2010.06.034

Ruban, A. V., Johnson, M.P., Duffy, C.D.P., 2012. The photoprotective molecular switch in the photosystem II antenna. Biochim. Biophys. Acta 1817, 167–181. https://doi.org/10.1016/J.BBABIO.2011.04.007

Ruban, A. V, 2016. Nonphotochemical Chlorophyll Fluorescence Quenching: Mechanism and Effectiveness in Protecting Plants from Photodamage. Plant Physiol. 170, 1903–16. https://doi.org/10.1104/pp.15.01935

Runge, E., Gross, E.K.U., 1984. Density-Functional Theory for Time-Dependent Systems. Phys. Rev. Lett. 52, 997–1000. https://doi.org/10.1103/PhysRevLett.52.997

Salverda, J.M., Vengris, M., Krueger, B.P., Scholes, G.D., Czarnoleski, A.R., Novoderezhkin, V., van Amerongen, H., van Grondelle, R., 2003. Energy transfer in light-harvesting complexes LHCII and CP29 of spinach studied with three pulse echo peak shift and transient grating. Biophys. J. 84, 450–65. https://doi.org/10.1016/S0006-3495(03)74865-6

Schlau-Cohen, G.S., Calhoun, T.R., Ginsberg, N.S., Read, E.L., Ballottari, M., Bassi, R., van Grondelle, R., Fleming, G.R., 2009. Pathways of Energy Flow in LHCII from Two-Dimensional Electronic Spectroscopy. J. Phys. Chem. B 113, 15352–15363. https://doi.org/10.1021/jp9066586

Schlau-Cohen, G.S., Yang, H.-Y., Krüger, T.P.J., Xu, P., Gwizdala, M., van Grondelle, R., Croce, R., Moerner, W.E., 2015. Single-Molecule Identification of Quenched and Unquenched States of LHCII. J. Phys. Chem. Lett. 6, 860–867. https://doi.org/10.1021/acs.jpclett.5b00034

Schneider, A.R., Geissler, P.L., 2013a. Coexistence of fluid and crystalline phases of proteins in photosynthetic membranes. Biophys. J. 105, 1161–70. https://doi.org/10.1016/j.bpj.2013.06.052

Schneider, A.R., Geissler, P.L., 2013b. Coarse-grained computer simulation of dynamics in thylakoid membranes: methods and opportunities. Front. Plant Sci. 4, 555. https://doi.org/10.3389/fpls.2013.00555

Scholes, G.D., Jordanides, X.J., Fleming, G.R., 2001. Adapting the Förster Theory of Energy Transfer for Modeling Dynamics in Aggregated Molecular Assemblies. https://doi.org/10.1021/JP003571M

Scholes, G.D., Rumbles, G., 2006. Excitons in nanoscale systems. Nat. Mater. 5, 683–696. https://doi.org/10.1038/nmat1710

Schulten, K., Ohmine, I., Karplus, M., 1976. Correlation effects in the spectra of polyenes. J. Chem. Phys. 64, 4422–4441. https://doi.org/10.1063/1.432121

Standfuss, J., Terwisscha van Scheltinga, A.C., Lamborghini, M., Kühlbrandt, W., 2005. Mechanisms of photoprotection and nonphotochemical quenching in pea light-harvesting complex at 2.5 A resolution. EMBO J. 24, 919–28. https://doi.org/10.1038/sj.emboj.7600585

Starcke, J.H., Wormit, M., Schirmer, J., Dreuw, A., 2006. How much double excitation character do the lowest excited states of linear polyenes have? Chem. Phys. 329, 39–49. https://doi.org/10.1016/J.CHEMPHYS.2006.07.020

Strümpfer, J., Schulten, K., 2012. Open Quantum Dynamics Calculations with the Hierarchy Equations of Motion on Parallel Computers. J. Chem. Theory Comput. 8, 2808–2816. https://doi.org/10.1021/ct3003833

Sumi, H., 1999. Theory on Rates of Excitation-Energy Transfer between Molecular Aggregates through Distributed Transition Dipoles with Application to the Antenna System in Bacterial Photosynthesis. J. Phys. Chem B 103, 252–260. https://doi.org/10.1021/JP983477U

Sylak-Glassman, E.J., Malnoë, A., De Re, E., Brooks, M.D., Fischer, A.L., Niyogi, K.K., Fleming, G.R., 2014. Distinct roles of the photosystem II protein PsbS and zeaxanthin in the regulation of light harvesting in plants revealed by fluorescence lifetime snapshots. Proc. Natl. Acad. Sci. U. S. A. 111, 17498–503. https://doi.org/10.1073/pnas.1418317111

Sylak-Glassman, E.J., Zaks, J., Amarnath, K., Leuenberger, M., Fleming, G.R., 2016. Characterizing non-photochemical quenching in leaves through fluorescence lifetime snapshots. Photosynth. Res. 127, 69–76. https://doi.org/10.1007/s11120-015-0104-2

Takizawa, K., Cruz, J.A., Kanazawa, A., Kramer, D.M., 2007. The thylakoid proton motive force in vivo. Quantitative, non-invasive probes, energetics, and regulatory consequences of light-induced pmf. Biochim. Biophys. Acta 1767, 1233–1244. https://doi.org/10.1016/J.BBABIO.2007.07.006

Terazono, Y., Kodis, G., Bhushan, K., Zaks, J., Madden, C., Moore, A.L., Moore, T.A., Fleming, G.R., Gust, D., 2011. Mimicking the Role of the Antenna in Photosynthetic Photoprotection. J. Am. Chem. Soc. 133, 2916–2922. https://doi.org/10.1021/ja107753f

Trinkunas, G., Connelly, J.P., Müller, M.G., Valkunas, L., Holzwarth, A.R., 1997. Model for the Excitation Dynamics in the Light-Harvesting Complex II from Higher Plants. J. Phys. Chem B 101. https://doi.org/10.1021/JP963968J

Tutkus, M., Chmeliov, J., Rutkauskas, D., Ruban, A. V., Valkunas, L., 2017. Influence of the Carotenoid Composition on the Conformational Dynamics of Photosynthetic Light-Harvesting Complexes. J. Phys. Chem. Lett. 8, 5898–5906. https://doi.org/10.1021/acs.jpclett.7b02634

van Amerongen, H., Valkunas, L., van Grondelle, R., 2000. Photosynthetic Excitons. World Scientific Publishing Co. Pte. Ltd., Singapore.

van Kooten, O., Snel, J.F.H., 1990. The use of chlorophyll fluorescence nomenclature in plant stress physiology. Photosynth. Res. 25, 147–150. https://doi.org/10.1007/BF00033156

van Oort, B., Roy, L.M., Xu, P., Lu, Y., Karcher, D., Bock, R., Croce, R., 2018. Revisiting the Role of Xanthophylls in Nonphotochemical Quenching. J. Phys. Chem. Lett. 9, 346–352. https://doi.org/10.1021/acs.jpclett.7b03049

van Stokkum, I.H.M., Larsen, D.S., van Grondelle, R., 2004. Global and target analysis of time-resolved spectra. Biochim. Biophys. Acta 1657, 82–104. https://doi.org/10.1016/J.BBABIO.2004.04.011

Visser, H.M., Kleima, F.J., van Stokkum, I.H.M., van Grondelle, R., van Amerongen, H., 1996. Probing the many energy-transfer processes in the photosynthetic light-harvesting complex II at 77 K using energy-selective sub-picosecond transient absorption spectroscopy. Chem. Phys. 210, 297–312. https://doi.org/10.1016/0301-0104(96)00092-4

Vulto, S.I.E., Baat, M.A. de, Louwe, R.J.W., Permentier, H.P., Neef, T., Miller, M., Amerongen, H. van, Aartsma, T.J., 1998. Exciton Simulations of Optical Spectra of the FMO Complex from the Green Sulfur Bacterium Chlorobium tepidum at 6 K. https://doi.org/10.1021/JP982095L

Walla, P.J., Linden, P.A., Ohta, K., Fleming, G.R., 2001. Excited-State Kinetics of the Carotenoid S1 State in LHC II and Two-Photon Excitation Spectra of Lutein and β-Carotene in Solution: Efficient Car S1→Chl Electronic Energy Transfer via Hot S1 States? J. Phys. Chem. A 106, 1909–1916. https://doi.org/10.1021/JP011495X

Wilk, L., Grunwald, M., Liao, P.-N., Walla, P.J., Kühlbrandt, W., 2013. Direct interaction of the major light-harvesting complex II and PsbS in nonphotochemical quenching. Proc. Natl. Acad. Sci. U. S. A. 110, 5452–6. https://doi.org/10.1073/pnas.1205561110

Wilkins, D.M., Dattani, N.S., 2015. Why Quantum Coherence Is Not Important in the Fenna–Matthews–Olsen Complex. J. Chem. Theory Comput. 11, 3411–3419. https://doi.org/10.1021/ct501066k

Wraight, C.A., Crofts, A.R., 1970. Energy-Dependent Quenching of Chlorophyll a Fluorescence in Isolated Chloroplasts. Eur. J. Biochem. 17, 319–327. https://doi.org/10.1111/j.1432-1033.1970.tb01169.x

Yang, C., Kosemund Kirstin, Cornet, C., Paulsen, H., 1999. Exchange of Pigment-Binding Amino Acids in Light-Harvesting Chlorophyll a/b Protein. Biochemistry 38, 16205–16213. https://doi.org/10.1021/BI990738X

Yang, M., Fleming, G.R., 2002. Influence of phonons on exciton transfer dynamics: comparison of the Redfield, Förster, and modified Redfield equations. Chem. Phys. 275, 355–372. https://doi.org/10.1016/S0301-0104(01)00540-7

Zaks, J., Amarnath, K., Kramer, D.M., Niyogi, K.K., Fleming, G.R., 2012. A kinetic model of rapidly reversible nonphotochemical quenching. Proc. Natl. Acad. Sci. U. S. A. 109, 15757–62. https://doi.org/10.1073/pnas.1211017109

Zhang, W.M., Meier, T., Chernyak, V., Mukamel, S., 1998. Exciton-migration and three-pulse femtosecond optical spectroscopies of photosynthetic antenna complexes. J. Chem. Phys. 108, 7763. https://doi.org/10.1063/1.476212

Zhu, X.-G., Ort, D.R., Whitmarsh, J., Long, S.P., 2004. The slow reversibility of photosystem II thermal energy dissipation on transfer from high to low light may cause large losses in carbon gain by crop canopies: a theoretical analysis. J. Exp. Bot. 55, 1167–1175. https://doi.org/10.1093/jxb/erh141

Chapter 2: Dissecting and modeling zeaxanthin- and lutein-dependent non-photochemical quenching in *Arabidopsis thaliana*

This chapter reproduces an article entitled "Dissecting and modeling zeaxanthin- and lutein-dependent non-photochemical quenching in Arabidopsis thaliana, by M. Leuenberger, J. M. Morris, A. M. Chan, L. Leonelli, K. K. Niyogi, and G. R. Fleming, appearing in *Proc. Natl. Acad. Sci. U S A*. 114(33):E7009-E7017 (2017). M. Leuenberger and J. M. Morris contributed equally to this work.

As described in Chapter 1, zeaxanthin plays an important role in quenching. It is proposed to play both a direct role as a site for dissipation (through either an energy transfer quenching process or a charge transfer and recombination quenching process) and having impact on the regulatory dynamics, where it has been identified to play a role in both q_E and q_Z. Zeaxanthin accumulates over the course of high light exposure due to the VAZ cycle, where violaxanthin is de-epoxidated twice into antheraxanthin and zeaxanthin. In contrast, in *Arabidopsis*, lutein is not regulated by a chemical cycle and has also been proposed to play a direct role as a site of energy dissipation.

However, in *Nannochlroropsis oceanica*, lutein is regulated in a lutein-lutein epoxide (LxL) cycle due the presence of a zeaxanthin epoxidase enzyme that functions on lutein. In order to attempt to distinguish the regulatory effects of quenching intrinsic to each xanthophyll, as opposed to the accumulation of the xanthophyll, a set of mutants including a line with a transgenic insert of the zeaxanthin epoxidase from *Nanno*, resulting in a LxL cycle in *Arabidopsis* were investigated.

Because zeaxanthin, once accumulated, takes much longer to return to violaxanthin, the zeaxanthin will remain after a short period of dark exposure subsequent to the traditional initial high light exposure period. In a second high light exposure period, the induction of quenching that is intrinsic to the presence of zeaxanthin can be observed in a manner distinct from the induction of quenching in the initial high light exposure period, where the zeaxanthin or must accumulate. Comparing the results of measurements on *Arabidopsis* that naturally contains a VAZ cycle with the transgenic line that replaces the VAZ cycle with an LxL cycle verifies that a difference observed between the first and second high light exposure period is due to the accumulation in the first period.

Upon analysis, a change was observed between the two periods: when the zeaxanthin or lutein needed to accumulate in the initial period, the observed timescale of induction of quenching was slower, indicating that regulatory dynamics in the first period depended on both the intrinsic regulation of zeaxanthin or lutein dependent mechanisms and the accumulation of the zeaxanthin or lutein. In addition, a mathematical model was constructed to model the regulatory dynamics. The model was able to reproduce both the change between the first and second period reproduce wild type quenching from mutant lines that isolated contributions from lutein dependent quenching and zeaxanthin quenching, providing insight into the relative contributions of two different mechanisms of quenching.

Abstract

Photosynthetic organisms employ various photoprotective mechanisms to dissipate excess photoexcitation as heat in a process called non-photochemical quenching (NPQ). Regulation of NPQ allows for a rapid response to changes in light intensity and in vascular plants is primarily triggered by a pH gradient across the thylakoid membrane (ΔpH). The response is mediated by the PsbS protein and various xanthophylls. Time correlated single photon counting (TCSPC) measurements were performed on Arabidopsis thaliana to quantify the dependence of the response of NPQ to changes in light intensity on the presence and accumulation of zeaxanthin and lutein. Measurements were performed on wild type and mutant plants deficient in one or both of the xanthophylls, as well as a transgenic line that accumulates lutein via an engineered lutein epoxide cycle. Changes in the response of NPQ to light acclimation in wild type and mutant plants were observed between two successive light acclimation cycles, suggesting that the character of the rapid and reversible response of NPQ in fully dark-acclimated plants is substantially different than in conditions plants are likely to experience due to changes in light intensity during daylight. Mathematical models of the response of zeaxanthin- and lutein-dependent reversible NPQ were constructed that accurately describe the observed differences between the light acclimation periods. Finally, the wild-type response of NPQ was reconstructed from isolated components present in mutant plants with a single common scaling factor, which enabled deconvolution of the relative contributions of zeaxanthin- and lutein-dependent NPQ.

Significance Statement

The balance between light harvesting and photoprotection is a critical component of photosynthetic efficiency, and this balance must be maintained in response to fluctuating light conditions. Two xanthophylls play key roles in the vascular plant response to changes in light intensity: zeaxanthin and lutein. Fluorescence decay studies of *Arabidopsis thaliana* mutants enabling the isolation of individual contributions of zeaxanthin and lutein to the response and a kinetic model of quenching make it possible to model the mutant data and predict the combined influence of zeaxanthin and lutein on non-photochemical quenching in wild type *A. thaliana* with the use of a single scaling factor. The model informs efforts to improve the response of plants to fluctuating light in natural environments and to increase crop yields.

Introduction

Photosynthesis begins with solar driven electron transfer in reaction centers [1], but often the energy available from sunlight outpaces the capacity for productive photochemistry in photosynthetic organisms. This can cause serious damage to the proteins that make up the photosynthetic apparatus. The fluctuations in light intensity experienced by higher plants necessitate both the rapid induction of photoprotective processes in response to high light conditions to prevent photodamage, as well as subsequent relaxation of quenching, to ensure optimal photosynthetic activity upon return to low light conditions [2, 3]. Although both of the photosynthetic reaction center complexes of higher plants, photosystem I (PSI) and photosystem II (PSII), experience photodamage and have photoprotective mechanisms, they are spectroscopically distinct primarily due to the shallow nature of the PSII reaction center trap and the reversibility of primary charge separation in the PSII reaction center (P680+) relative to PSI. These features lead to longer lived excitation in the PSII reaction center and therefore a higher probability of damage when reaction centers are closed. Moreover, the shallow trap and reversibility of charge transfer in PSII reaction centers contribute to variability in fluorescence from PSII which allows for the study of NPQ via fluorescence yield and lifetime measurements [4]. The fluorescence from PSI is far less variable at room temperature.

Here we discuss photoprotective mechanisms of PSII as observed via fluorescence lifetime measurements. The suite of photoprotective mechanisms that protect PSII collectively result in, and are referred to as, non-photochemical quenching (NPQ): the reduction in chlorophyll *a* fluorescence yield due to the dissipation of excess excitation by mechanisms other than photochemistry [5, 6, 7]. Although NPQ's various mechanisms allow for rapid response to excess light conditions, the overall response is slow to recover, leading to a period of potentially suboptimal photosynthetic efficiency [8]. Understanding the multiple processes underlying NPQ could inform engineering of photoprotective systems to increase crop yields [3] or systems to protect bio-inspired energy devices [9].

NPQ is a broad term encompassing several constituent components historically categorized by rate of induction and relaxation. For the quenching response of photosystem II (PSII) in vascular plants, the components are often separated into qE, the rapidly reversible, energy-dependent quenching component, and qI, the slowly reversible component associated with PSII photoinhibition [10, 11]. Although important in many photosynthetic systems, qT, a component of NPQ associated with excitation balance between PSI and PSII by altering the relative antenna size, does not contribute significantly in vascular plants exposed to high light [5]. The historic decoupling of rapidly reversible mechanisms from slower ones may not be as feasible as previously understood: subsequent work has indicated the complicated nature of qI [12, 13, 14, 15,16] and the roles of zeaxanthin in qE [17, 18, 19, 20, 21, 22] and another NPQ component termed qZ [23], making the distinction less clear and, at times, arbitrary [24].

As of yet, there is little consensus surrounding the molecular mechanisms underlying the quenching pathways intrinsic to NPQ in PSII. However, several important players impacting the regulation of PSII photoprotection are widely agreed upon. qE in higher plants is triggered by a high pH gradient, ΔpH, formed across the thylakoid membrane as charge separation due to productive photochemistry outpaces the activity of ATP synthase and other downstream processes

[25]. PsbS, which contains exposed protonatable residues, has been shown to be a sensor of ΔpH [26], and is necessary for qE in vivo [27]. Finally, upon the formation of ΔpH, violaxanthin de-epoxidase (VDE) is activated, converting violaxanthin to antheraxanthin and zeaxanthin [28] in the VAZ cycle. Some evidence suggests that zeaxanthin plays a direct role in quenching [19, 20], while other evidence suggests that zeaxanthin simply regulates lutein-dependent quenching allosterically [29, 30]. So far, the direct roles of zeaxanthin and lutein in NPQ, either as participants in the molecular mechanism of quenching or in the molecular regulation of quenching, remain unclear.

While the accumulation of zeaxanthin from violaxanthin under high light conditions is ubiquitous among higher plants and has been studied extensively, an analogous cycle reflecting the accumulation of lutein from lutein epoxide (the LxL cycle), found in about 60% of plant species studied thus far, has recently become of interest [31, 32, 33, 34]. Because this LxL cycle regulates lutein levels in response to light intensity changes in a similar way to the regulation of zeaxanthin in the VAZ cycle, the LxL cycle is of interest to help determine the impact of different xanthophyll cycles on the activation and recovery of NPQ in PSII. Recently, transgenic lines of *Arabidopsis thaliana* modified to express zeaxanthin epoxidase from the alga *Nannochloropsis oceanica* have been produced [35], allowing the study of the isolated LxL cycle in a well-characterized model system. In this paper, we present spectroscopic studies of these lines and other xanthophyll mutants, and we examine the contribution of zeaxanthin- and lutein-dependent activation of NPQ in PSII to the full wild-type response.

Results and Discussion

In order to distinguish lutein-dependent quenching from zeaxanthin-dependent quenching, chlorophyll fluorescence lifetime snapshot measurements of whole leaves of *A. thaliana* sensitive to changes in chlorophyll a fluorescence in PSII were collected via time correlated single photon counting (TCSPC). The genetic lines studied include wild type (*wt*; Col-0 ecotype), the *szl1* mutant that lacks VAZ cycle xanthophylls and accumulates high levels of lutein [36], the double mutant *szl1npq1* that is also defective in VDE activity [36], the lutein-deficient mutant *lut2* [37], the novel lutein epoxide cycle transgenic mutant *szl1+NoZEP1* [35], and lastly the transgenic mutant *szl1npq1+NoZEP1*, which constitutively accumulates lutein epoxide and lacks zeaxanthin and therefore cannot induce any rapidly reversible qE [35]. A table of the mutants studied and their properties is supplied in Table S1.

After 30 min of initial dark acclimation, TCSPC snapshots were collected during two periods of high light each followed by a period of dark relaxation. The first cycle consisted of 20 min of high light, which is long enough to achieve quasi-steady-state quenching lifetimes, followed by 10 min of darkness, chosen to be long enough to allow a return to steady-state unquenched lifetimes but short enough to maintain high levels of de-epoxidized xanthophylls in plants with appropriate epoxidase and de-epoxidase enzymatic cycles. The second cycle, which immediately followed the first, consisted of 7 min of high light, followed by 3 min of darkness, and served to demonstrate the response of the fluorescence lifetimes when the de-epoxidized carotenoids are present at the onset of the induction of rapidly reversible qE. Additionally, the pigments present in leaf samples exposed to the same light cycles were quantified via high-performance liquid chromatography (HPLC). Fig. S1 summarizes these data.

Representative fluorescence decays measured via TCSPC in the quenched and relaxed states of *wt* leaves are provided in Fig. 1. For the two decays shown, the dark-acclimated or relaxed average lifetime was 1.42 ns and the quenched average lifetime obtained after 270 s of 745 µmol photons m^{-2} s^{-1} actinic light acclimation was 0.52 ns. The average lifetimes were obtained from an amplitude-weighted average of the fit of data to two lifetime components. The decision to fit the data to two lifetime components was made upon analysis of a singular value decomposition of the data set (Fig. S2) that resulted in two singular vectors containing structure and remaining singular vectors displaying noise. This indicates that fitting more than two components does not extract additional meaningful information, reflecting the tradeoff between limited data collection time of snapshot measurements and the dynamic range of the fluorescence decay curves.
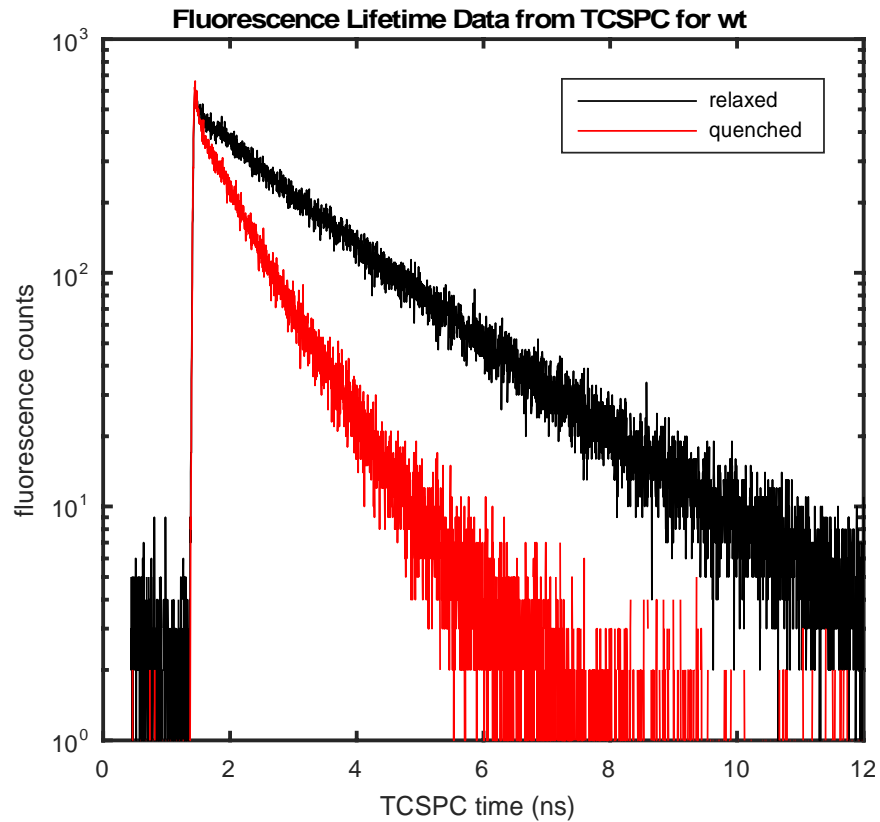
Figure 1. Representative fluorescence lifetime decays for dark-acclimated (relaxed) and light-acclimated (quenched) wild type *A. thaliana* leaves. The average lifetime obtained for the sample shown was 1.42 ns for the relaxed state and 0.52 ns for the quenched state after 270 s of exposure to 745 µmol photons m^{-2} s^{-1} actinic light.

Fluorescence decays were collected from 20 samples per mutant over the course of the light acclimation scheme and fitted to determine the amplitude-weighted average lifetimes. The

traces of average lifetimes for the different mutants over the course of acclimation are shown in Fig. 2. Mutants containing only a constant high level of lutein (*szl1* and *szl1npq1*, Fig. 2c and 2f) display a rapid overshoot and relaxation to the steady-state quenching level in response to both light acclimation periods. Mutants containing a xanthophyll cycle (*lut2*, which accumulates zeaxanthin via the VAZ cycle, and *szl1+NoZEP1*, which accumulates lutein via the LxL cycle, Fig. 2b and 2e) do not display this overshoot in the first light acclimation period. The *szl1npq1+NoZEP1* strain (Fig. 2d) containing neither xanthophyll cycle, does not show any reversible quenching. *wt* plants (Fig. 2a) acclimate faster than *lut2* mutants containing only the VAZ cycle but do not show the initial overshoot of *szl1*.

Observed Average Lifetimes in whole leaves of *A. thaliana*
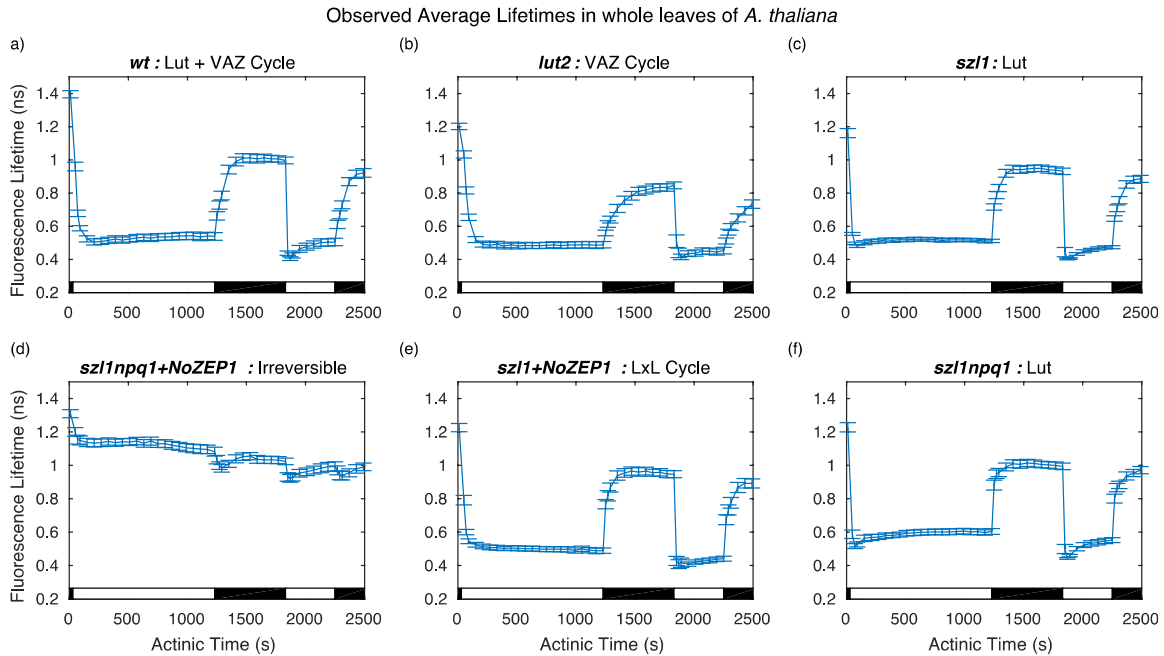
Figure 2. Average fluorescence lifetime traces over a two-cycle light acclimation scheme, shown by the light and dark bars superimposed on the bottom of each plot for the six *A. thaliana* strains. Error bars denote SD for n = 20. a) *wt* contains lutein and a VAZ cycle to form zeaxanthin in high light conditions. b) *lut2* lacks lutein and has an active VAZ cycle. c) *szl1* lacks zeaxanthin due to a partially blocked ß-carotene biosynthesis pathway and contains more lutein than *wt*. d) The *szl1npq1+NoZEP1* strain does not have either xanthophyll cycle. e) *szl1+NoZEP1* lacks zeaxanthin and contains a non-native zeaxanthin epoxidase that functions on lutein, converting lutein to lutein epoxide that can be converted back to lutein by native VDE in high light. f) *szl1npq1* contains lutein but lacks zeaxanthin due to blocking of the ß-carotene biosynthesis pathway and inhibition of VDE.

Modeling

In order to model the quenching processes observed in the data, a quenching parameter Q, is calculated from the normalized average lifetimes, τ, allowing for direct comparison of the quenching behavior between different plant lines. The amplitude-weighted average lifetimes are proportional to fluorescence yield, ϕ, which is given by the ratio of the rate of fluorescence to the sum of the rates of all relaxation processes, including fluorescence, quenching, and other processes such as energy transfer and intersystem crossing. The expression relating the average lifetimes to the quenching parameter is given in Eqn. 1. The rates used for the various processes were obtained from Zaks et al. [38].

$$\tau \propto \phi = \frac{k_{fluo}}{k_{fluo} + k_{other} + k_{quenching}Q} \quad (1)$$

The parameter Q is a dimensionless modifier of the effective quenching rate, and is a function of activated PsbS, lutein, zeaxanthin, and other variables. The product of $k_{quenching}$ and Q produces an effective rate of quenching that results in the observed lifetimes. Although previous work has attributed Q to a fraction of activated quenching sites [38], this type of analysis is also valid for more complicated underlying mechanistic details of energy dissipation, such as the alterations to the rate of quenching at an individual site, the density of quenching sites, or multiple types of quenching sites. For simplicity, a single constant rate of quenching at each site, $k_{quenching}$ is assumed, and Q can be considered an effective fraction within these caveats. The particular choice of the value of $k_{quenching}$ does not severely impact the observed behavior of the quenching dynamics, but linearly scales the numerical values of Q obtained from the average lifetime, and the numerical values of parameters that describe the dynamical behavior. Q is similar to the usual NPQ parameter [1] calculated from, for example, PAM fluorescence traces, but is scaled to reflect estimates of the physical processes involved and emphasizes the competition in the experiment between quenching and fluorescence or productive photochemical pathways.

Because the denominator of Eqn. 1 is the sum of rates of various processes, using the parameter Q allows for the direct addition and subtraction of various quenching processes within and across mutant strains. In this work, Q is partitioned into a reversible component and an irreversible component based on the observed behavior, per Eqn. 2.

$$Q = Q_{rev} + Q_{irr} \quad (2)$$

The *szl1npq1+NoZEP1* strain contains no lutein or zeaxanthin and displays nearly monotonically increasing quenching over the course of the experiment. The Q values calculated from *szl1npq1+NoZEP1* lifetimes via Eqn. 1 are identified solely as irreversible quenching, Q_{irr}. These values can be subtracted from the values of Q calculated from other strains to isolate the values of reversible quenching, Q_{rev}.

Reversible quenching was modeled using differential equations describing a pair of two-state systems. The systems individually represent lutein- and zeaxanthin-dependent quenching and each system contains "active" and "inactive" quenching states. The solution to the differential equation for the active quenching states, Q^{active}, gives predicted values of Q_{rev} due to either lutein

39

or zeaxanthin for comparison to experimental results. The differential equations are simple kinetic rate equations with activation rates given by functions of the variables ΔpH across the membrane, concentration of activated PsbS, and the concentration of the appropriate xanthophyll(s).

The dynamics of ΔpH and the activation of PsbS and VDE in response to ΔpH were obtained from the model described by Zaks et al. [38]. Their work concluded that the temporal behavior of ΔpH across the thylakoid membrane was insensitive to the detailed parameters of the model of quenching. Therefore, ΔpH is a function solely of time for a given light acclimation scheme and does not depend on the differential equations. Qualitatively, ΔpH has a fast initial rise on the timescale of seconds upon exposure to high light, which then peaks and decays to a steady state level on the timescale of a few minutes. Upon initiation of dark relaxation, ΔpH decays from the high light steady state level to a dark-adapted steady state level on the timescale of seconds. The plot of ΔpH in terms of the $[H^+]$ concentration gradient and normalized activity of PsbS and VDE is shown in Fig. S3.

The kinetics of the xanthophyll cycles depend on the activation of VDE by ΔpH; concentrations of the xanthophylls were obtained by fitting a first-order kinetic model with ΔpH-dependent rates of de-epoxidation described by Zaks et al. [38] for each relevant mutant to HPLC data in order to interpolate between measurements. A plot of the *wt* xanthophyll cycle showing the fractional concentrations of each pigment normalized to the total concentration of the three pigments available for interconversion is shown in Fig. 3. Similar fits were performed for the *szl1+NoZEP1* strain, containing the LxL cycle, showing the expected conversion from lutein epoxide to lutein in response to high light conditions, and the *lut2* mutant, containing the same VAZ cycle as *wt* (Figs. S4, S5).
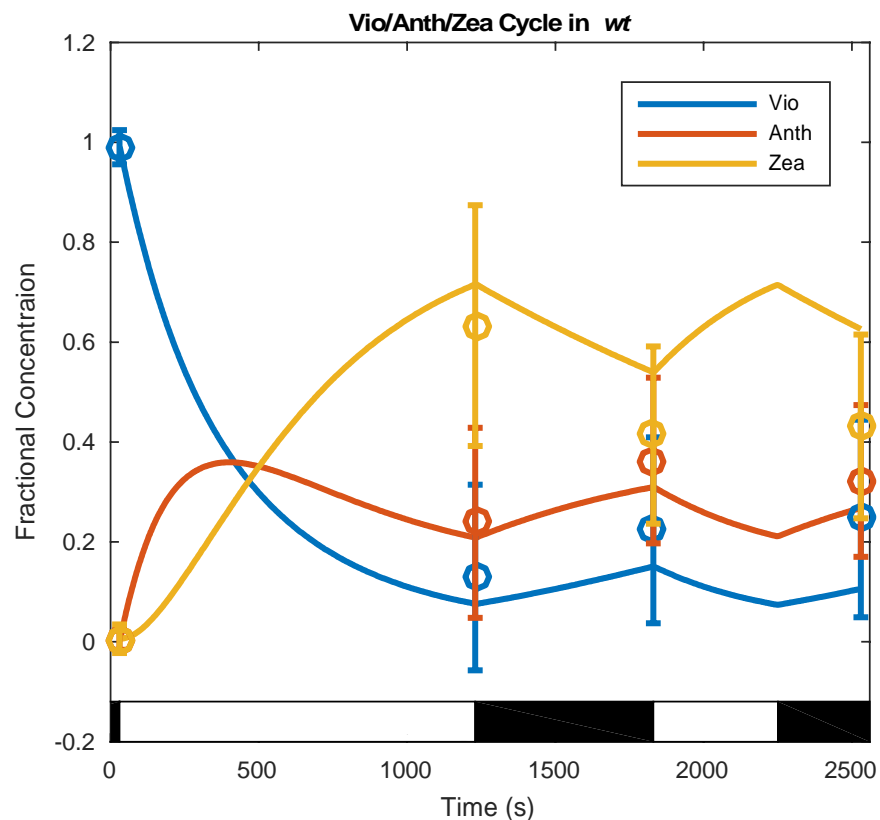
Figure 3. Dynamics of the *wt* xanthophyll cycle in response to the light acclimation scheme shown in the light and dark bars superimposed on the plot fit to HPLC data are shown here. The data are represented by a fit of the fractional concentration of the available pool of violaxanthin, antheraxanthin, and zeaxanthin to the available pool of xanthophylls determined from analysis of HPLC measurements (see Methods section of the text) at four time points (open circles with error bars denoting SD for n=8) using a first-order kinetic model with a pH gradient dependent rate of de-epoxidation (solid lines).

The pool of violaxanthin available for de-epoxidation was quantified using Monte Carlo methods to determine the minimum quantity of violaxanthin present using bootstrap resampling of the HPLC data. This technique, described in detail in the methods section, indicated that approximately 60% of the measured violaxanthin was unavailable for de-epoxidation on the timescales of light acclimation in the experiment, in good agreement with previous work [39]. The same technique was used to remove background antheraxanthin and zeaxanthin present in the dark-acclimated state. The fractional concentration was calculated as the fraction of each individual xanthophyll over the sum of the available pool of xanthophylls.

Lutein-Dependent Quenching

The constant value of lutein in the mutant *szl1*, which contains no zeaxanthin, is the simplest system to model. The constant-lutein-dependent reversible quenching model is:

$$\frac{d}{dt}Q_{[\text{Lut}]}^{active} = k_{Q_{[\text{Lut}]}}^{activation}(t)Q_{[\text{Lut}]}^{inactive} - k_{Q_{[Lut]}}^{recovery}Q_{[\text{Lut}]}^{active} \quad (3)$$

$$\frac{d}{dt}Q_{[\text{Lut}]}^{inactive} = -k_{Q_{[\text{Lut}]}}^{activation}(t)Q_{[Lut]}^{inactive} + k_{Q_{[Lut]}}^{recovery}Q_{[\text{Lut}]}^{active} \quad (4)$$

The time-dependence of $k_{Q_{[\text{Lut}]}}^{activation}$ is due to the time-dependence of the activated fraction of PsbS, [PsbS*], which in turn depends on the ΔpH. The time-dependent activation constant is defined in the form of a Hill equation,

$$k_{Q_{[\text{Lut}]}}^{activation}(t) \equiv \frac{[\text{PsbS}^*]^n}{K_{\text{PsbS}^*} + [\text{PsbS}^*]^n} \kappa_{Q_{[\text{Lut}]}}^{activation} \quad (5)$$

The constants K_{PsbS^*} and n, respectively, describe an equilibrium point and interaction coefficient of quenching sites activated by PsbS. Together with $\kappa_{Q_{[\text{Lut}]}}^{activation}$, a scaling constant, these constants, which determine the activation, $k_{Q_{[\text{Lut}]}}^{activation}$, and recovery, $k_{Q_{[\text{Lut}]}}^{recovery}$, rates of the quenching were obtained by fitting solutions of $Q_{[Lut]}^{active}$ in Eqn. 3 to values of Q_{rev} calculated from *szl1* lifetime values via Eqn. 1 and 2. A plot of the resulting model, comparing the fit values of $Q_{[Lut]}^{active}$ to the values of Q_{rev} calculated from *szl1* lifetime values and the predicted lifetimes for *szl1*, is shown in Fig. 4.
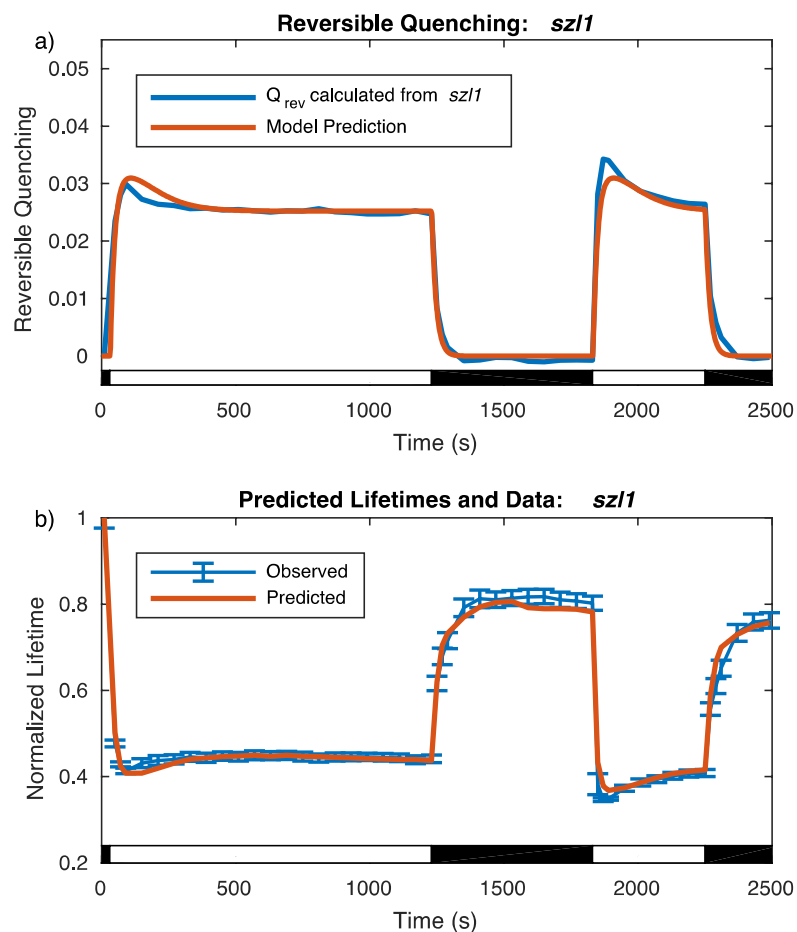
Figure 4. Comparison of model to reversible quenching calculated from *szl1* lifetime data via Eqns. 1 and 2 and predicted lifetime to data for *szl1*. a) The modeled reversible lutein-dependent quenching (red line) compared to the reversible quenching values calculated from *szl1* lifetime data after background subtraction of the irreversible quenching present in *szl1npq1+NoZEP1* (blue line). b) Normalized fluorescence lifetimes predicted by the model upon reconstruction of fluorescence yield from the model for lutein-dependent reversible quenching in *szl1* and the irreversible quenching extracted from *szl1npq1+NoZEP1* (red line) compared to data (blue line; data points with error bars denoting SD for n=20).

The two plots, of Q_{rev} and the lifetime values, are essentially reciprocals as a consequence of Eqns. 1 and 2. What appears as a slight dip in the lifetime at early acclimation times is reflected in a larger apparent spike, or overshoot of the steady state, in the value of the Q_{rev}. The model is able to describe the initial overshoot of quenching in response to high light, the steady state level during light exposure, and the recovery in dark. Small discrepancies remain between the light-acclimation periods, with the initial overshoot overestimated in the first period and underestimated in the second period. Upon recovering the predicted lifetimes from the model for *szl1* and the irreversible quenching from *szl1npq1+NoZEP1*, it is apparent that these discrepancies are commensurate in scale with the uncertainty in the data. In this simple system, reversible quenching, $Q_{rev,}$ appears to track directly with the previously predicted ΔpH.

Next, we modeled the *szl1+NoZEP1* strain, which contains the LxL cycle, adding a further complication to account for in our model. In the LxL cycle lutein epoxide is de-epoxidated to lutein in response to the formation of ΔpH. Therefore, in addition to the activation of quenching in response to high light, lutein accumulates. This was verified by HPLC and fit to a first-order kinetic model as discussed above and shown in Fig. S3. To account for the impact of the accumulation of lutein on the quenching behavior, the activation rate in the previous model of *szl1* quenching was modified to contain the product of two responses: one to the activated PsbS as shown previously, and a second response to the concentration of lutein, also in the form of a Hill equation. The time-dependent activation rate is redefined as

$$k_{Q_{[Lut]}}^{activation}(t) \equiv \frac{[\text{PsbS}^*]^n}{K_{\text{PsbS}^*} + [\text{PsbS}^*]^n} \frac{[\text{Lut}]^m}{K_{[\text{Lut}]} + [\text{Lut}]^m} \kappa_{Q_{[Lut]}}^{activation} \quad (6)$$

which incorporates an additional $K_{[\text{Lut}]}$, an equilibrium value, and *m*, an interaction coefficient, in the Hill type response to lutein. A comparison of predicted lifetimes associated with best fit solutions of $Q_{[Lut]}^{active}$ to values of Q_{rev}, calculated from *szl1+NoZEP1* lifetime data using Eqns. 1 and 2, is shown in Fig. 5a.

The model captures much of the behavior of the lutein-dependent quenching in *szl1+NoZEP1*: a smooth transition from the dark acclimated lifetime to a steady state quenched lifetime in the first acclimation period, followed by a sharp spike in the second acclimation period. Due to the additional complicating factor of the accumulation of lutein, the direct correspondence between ΔpH and Q_{rev} seen in *szl1* mutants is obscured. The initial accumulation of lutein suppresses the overshoot that is seen in the second acclimation period, when lutein is present at the outset due to the slower rate of re-epoxidation.
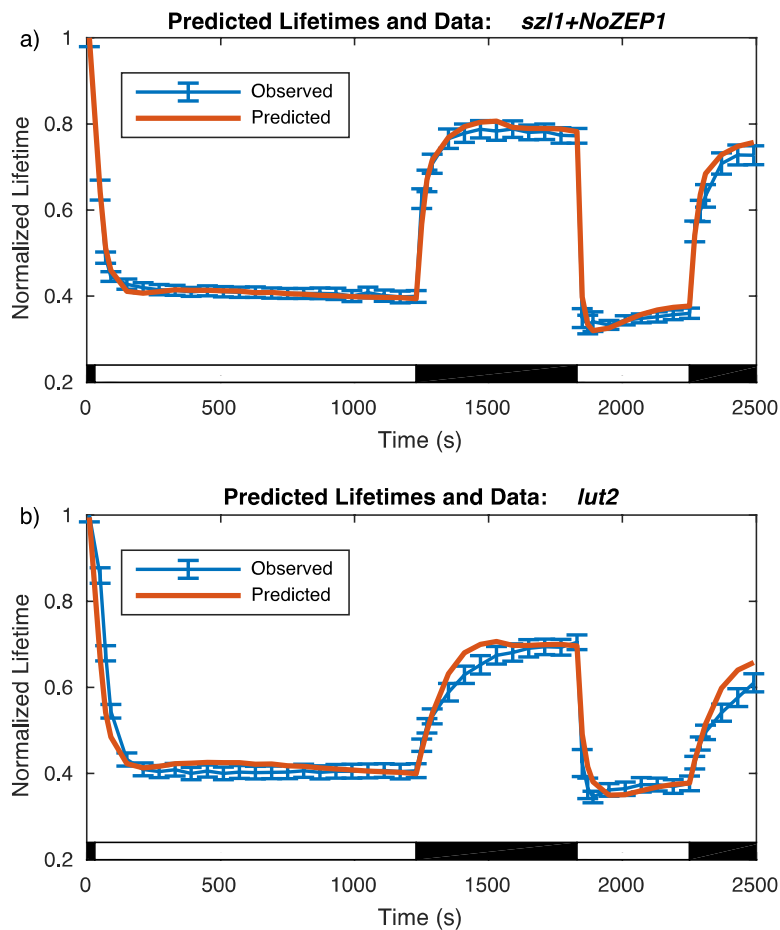
Figure 5. Comparison of predicted to observed lifetimes for *szl1+NoZEP1* and *lut2*. a) Normalized fluorescence lifetimes predicted by the model of reversible quenching for the LxL cycle mutant *szl1+NoZEP1* and irreversible quenching from *szl1npq1+NoZEP1* (red line) compared to *szl1+NoZEP1* lifetime data (blue line; with data points with error bars denoting SD for n=20). b) Normalized fluorescence lifetimes predicted by the model of reversible quenching for the lutein-less VAZ cycle mutant *lut2* and irreversible quenching from *szl1npq1+NoZEP1* (red line) compared to *lut2* lifetime data (blue line; with data points with error bars denoting SD for n=20).

Zeaxanthin-Dependent Quenching

The lifetime data show similar characteristics for the LxL cycle strain *szl1+NoZEP1* (Fig. 5a) and the lutein-less mutant *lut2* (Fig. 5b), which only contains the native *A. thaliana* VAZ cycle, suggesting that a similar model can be used to describe zeaxanthin dependent quenching. The same two-state system, with analogous terms containing an activation rate formed from the product of response to activated PsbS and the xanthophyll, and a constant recovery rate was used, but with

zeaxanthin substituted for lutein. This is sufficient to account for the zeaxanthin- and ΔpH-dependent portion of the quenching response (usually thought of as a portion of qE).

However, upon close examination, there is a discrepancy between the reversible quenching behavior of the LxL cycle *szl1+NoZEP1* mutant and the VAZ cycle *lut2* mutant seen in the recovery displayed in the dark. While the reversible quenching of the LxL cycle *szl1+NoZEP1* strain recovers fully upon dark relaxation, the reversible quenching of the VAZ cycle *lut2* mutant does not fully recover upon dark relaxation due to the contribution of zeaxanthin-dependent, but non-ΔpH-dependent quenching (qZ [23]). In order to account for this difference, an additional term is required in the model differential equations. The additional term is independent of $Q_{[Zea]}^{active}$ and linearly dependent on the concentration of zeaxanthin. It carries the opposite sign as the recovery term, and shifts the steady-state recovery level when zeaxanthin is present. Although the non-ΔpH-dependent quenching operates on a time scale slower than the ΔpH-dependent quenching, it is still included in the values of Q_{rev} determined from the partitioning scheme. The model system therefore is given by

$$\frac{d}{dt}Q_{[Zea]}^{active} = k_{Q_{[Zea]}}^{activation}(t)Q_{[Zea]}^{inactive} - k_{Q_{[Zea]}}^{recovery}Q_{[Zea]}^{active} + k_{qZ}[Zea] \quad (7)$$

$$\frac{d}{dt}Q_{[Zea]}^{inactive} = -k_{Q_{[Zea]}}^{activation}(t)Q_{[Zea]}^{inactive} + k_{Q_{[Zea]}}^{recovery}Q_{[Zea]}^{active} - k_{qZ}[Zea] \quad (8)$$

$$k_{Q_{[Zea]}}^{activation}(t) \equiv \frac{[PsbS^*]^n}{K_{PsbS^*} + [PsbS^*]^n}\frac{[Zea]^m}{K_{[Zea]} + [Zea]^m}\kappa_{Q_{[Zea]}}^{activation}(9)$$

where the first two terms, including $k_{Q_{[Zea]}}^{activation}(t)$, are analogous to the model for the LxL cycle *szl1+NoZEP1* strain and the final term accounts for the zeaxanthin dependent, non-ΔpH-dependent quenching behavior unique to zeaxanthin. The predicted lifetimes associated with fit of values of $Q_{[Zea]}^{active}$ to values of Q_{rev} calculated from *lut2* lifetime values by the same method as previously described, are shown in Fig. 5b. The fit values again capture the differences between the first and second light acclimation periods, this time due to the accumulation of zeaxanthin but analogous to the accumulation of lutein. The additional term unique to this model also captures the shift in the recovery level due to the zeaxanthin-dependent, non-ΔpH-dependent qZ behavior.

Constructing *wt* Quenching from Components

The zeaxanthin and lutein dependent quenching in the mutants containing just one of the two xanthophylls allows for a comparison of the ability to quench on a per lutein or zeaxanthin basis. Quantities of lutein and zeaxanthin determined from HPLC were normalized to the quantity of chlorophyll *a*, and in turn, the quasi-steady-state values of quenching associated with lutein and zeaxanthin were compared upon normalizing by the quantity of lutein and zeaxanthin present at quasi-steady state. The quasi-steady-state quenching values for the lutein-dependent quenching in *szl1*, normalized to the quantity of lutein, were approximately ten times lower than the quasi-steady-state values of zeaxanthin-dependent quenching in *lut2*, normalized to the quantity of zeaxanthin. This indicates that, on average, each zeaxanthin molecule contributes ten times more to the overall quenching than each lutein molecule. The difference could either be due to a

difference in actual rate of quenching, or a difference in the fraction of time in which each molecule is in a quenching state when activated, resulting in a reduced density of quenching sites not accounted for by the concentrations. However, this analysis relies on homogeneous contributions and does not account for potentially non-uniform contributions of the lutein and zeaxanthin molecules – e.g. if only a specific and unique fraction of the lutein molecules present contribute to quenching dynamics, the analysis fails.

One way to test whether the models developed for *szl1* and *lut2* have captured the essence of the quenching process involving these two xanthophylls is to use these models to predict the *wt* response. To do this, the zeaxanthin-dependent reversible quenching calculated from *lut2* lifetime measurements using Eqns. 1 and 2, denoted Q_{rev}^{lut2}, and the lutein-dependent reversible quenching calculated from *szl1* lifetime measurements, again using Eqns. 1 and 2, denoted Q_{rev}^{szl1}, were each weighted by the ratio of the average concentrations of the relevant carotenoids present in *wt* relative to the mutant overexpression levels and added to obtain a predicted *wt* quenching value containing the behavior of both lutein- and zeaxanthin-dependent quenching. This value was multiplied by a single common scaling factor, α, to fit the value of Q_{rev} calculated using Eqns. 1 and 2 from *wt* lifetime measurements, denoted Q_{rev}^{wt}. The expression for the predicted *wt* reversible quenching is

$$Q_{rev}^{wt} = \alpha \left(\frac{< [\text{Lut}] >_{wt}}{< [\text{Lut}] >_{szl1}} Q_{rev}^{szl1} + \frac{< [\text{Zea}] >_{wt}}{< [\text{Zea}] >_{lut2}} Q_{rev}^{lut2} \right) (10)$$

The lutein and zeaxanthin ratios in Eqn. 10 were determined from the HPLC data to be 0.67 and 0.24, respectively. The scaling factor, α, was fitted to 1.37.

Plots of the reconstructed *wt* quenching parameter, Q_{rev}^{wt}, are compared to values calculated from *wt* lifetime data via Eqns. 1 and 2 in Fig. 6a; the *wt* lifetimes predicted from the reconstruction are compared to the measured *wt* lifetime data in Fig. 6b. The reversible quenching values, Q_{rev}^{szl1} and Q_{rev}^{lut2}, calculated from lifetime data from *lut2* and *szl1,* are plotted, after scaling by the ratio of the concentrations and α, together with their sum, the predicted reversible quenching for *wt*, Q_{rev}^{wt}. The predicted value of the reversible quenching for *wt* from the components agrees well with the value calculated directly from the *wt* lifetime data. The lifetimes resulting from these values in Fig. 6b show the variation from the observed *wt* lifetime data is on the order of the uncertainty of the measurement.
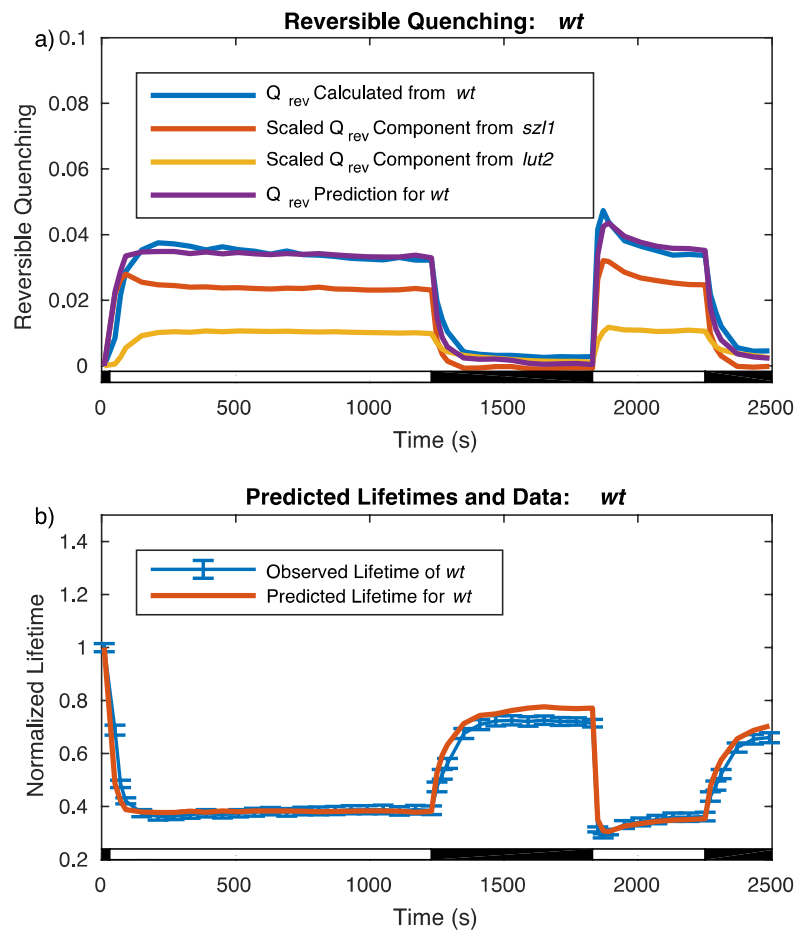
Figure 6. Comparison of *wt* reversible quenching calculated from lifetime data via Eqns. 1 and 2 to predicted values calculated from *szl1* and *lut2* mutant lifetime data via Eqn. 10 and corresponding lifetimes. a) Reversible quenching calculated via Eqns. 1 and 2 from *wt* lifetime data (blue) agrees well with the predicted reversible quenching (purple) obtained from *szl1* (red) and *lut2* (yellow) contributions via Eqn. 10 (see text). b) The *wt* lifetimes (red) predicted from the *wt* reversible quenching obtained via Eqn. 10 and irreversible quenching from *szl1npq1+NoZEP1* is within the error of the observed lifetimes of *wt* (blue, including error bars indicating SD for n = 20.)

The success of our approach in reproducing both the steady state quenching and the quantitative value of the overshoot in the second light acclimation period with only a single common scaling factor has several implications. First, the finding supports the previous analysis of the relative average contributions to quenching of each xanthophyll. Linear scaling by the xanthophyll concentrations reproduces the observed *wt* quenching across a range of quenching values. This suggests that for the range of concentrations found in the mutants studied, the contributions of each molecule in the xanthophyll pool is indeed homogenous. Microscopically,

48

this corresponds to a regime where the activation of quenching sites is limited by the availability of the xanthophylls, and not a regime limited by binding sites capable of quenching. In the alternative regime, the ratio of participating sites to concentration of the xanthophylls would not scale linearly across the range of observed quenching values. Instead, the quenching would scale linearly with the available binding sites. At yet higher concentrations of xanthophylls, e.g. in mutants that more strongly over-express the xanthophylls, these regimes may no longer hold true.

Secondly, despite correctly predicting the ratio between the steady state and overshoot quenching upon scaling the contributions by the average concentrations of the xanthophylls, the additional common scaling factor, α, is still required to quantitatively predict the observed *wt* quenching values. There are several possible explanations for the scaling factor. For example, the presence of both xanthophylls may increase the density of quenching sites for a given concentration of each xanthophyll due to more efficient binding of the correct xanthophyll in certain sites. Furthermore, there is evidence that substitution at lutein or zeaxanthin sites occurs in mutants lacking the preferred xanthophyll [36]. Upon substitution, changes in quenching rate due to the substitute xanthophyll could result in reduced quenching for a given density of quenchers in mutants lacking the correct xanthophyll. Finally, in sites where zeaxanthin and lutein are in close proximity to both one another and a chlorophyll, the combined presence may work to cooperatively increase the quenching rate beyond the rates of quenching possible in the presence of either xanthophyll individually [29, 30]. However, because both lutein- and zeaxanthin-dependent quenching are able to operate independently, it seems that zeaxanthin is unlikely to function solely as an allosteric regulator. Reasonable physical models [40] could help evaluate the extent that various possibilities could explain the behavior observed for *wt* quenching. Determining the density of quenching sites required to predict the lutein- and zeaxanthin-dependent quenching and comparing to *wt* would indicate which, if any, of these effects is consistent with the observed behavior, but it may be difficult to decouple the product of quenching rate and quenching site density thus requiring additional constraints to separate these quantities.

Conclusion

There are multiple mechanisms that contribute to NPQ in *wt* plants. We have demonstrated the use of NPQ data from various mutants to isolate specific contributions from lutein and zeaxanthin and use these to reconstruct the response of the *wt*, that results from several (two or more) different contributions. The success of the approach of Kromdijk et al. in increasing plant productivity by changing expression levels of VDE, zeaxanthin epoxidase, and PsbS [3] indicates that optimizing the rates of violaxanthin to zeaxanthin and lutein epoxide to lutein interconversion along with the concentration of PsbS is a viable route to increased photosynthetic yield. The kinetic model developed here will enable optimal values of concentrations and yields to be explored and tested in real field trials to determine if the 15% increase described in *Nicotiana* (tobacco) [3] can be further improved upon. From the perspective of refining the model, the distinct differences observed between the two light-acclimation periods suggest that varying frequency periodic illumination periods could enable the separation of the multiple quenching processes that occur on different timescales, but, for example, all depend on the presence of zeaxanthin.

Materials and Methods

<u>Plant Material and Growth Conditions</u>

A. thaliana wild-type plants (Col-0) and mutant plants *lut2*, *szl1*, *szl1npq1*, *szl1+NoZEP1*, and *szl1npq1+NoZEP1* were germinated on plates, transplanted to pots and grown in growth chambers under 110 μmol photons m^{-2} s^{-1} on a 10-hour day, 14-hour night schedule at 23°C. A table of the mutant descriptions is shown in Table S1. The LxL cycle strains [35] were screened for homozygosity on plates containing Basta. The NPQ phenotype of these mutants, which contain zeaxanthin epoxidase from *Nannochloropsis oceanica* [41], was confirmed using an IMAGING-PAM M-series (Heinz Walz) instrument to monitor NPQ capacity. Lastly, HPLC data confirmed the presence of lutein epoxide, which is conclusive evidence of the functionality of the non-native NoZEP1 in *A. thaliana* plants. All plants were between 6 and 9 weeks of age at the time of experiments and all measurements were completed before the stage of bolting as described previously [42].

<u>TCPSC Measurements</u>

Each sample set was comprised of 20 whole leaves from each respective genotype. Before TCSPC snapshot experiments, plants were dark-acclimated for 30 min to ensure that the relevant xanthophylls in plants containing xanthophyll cycles were in their inactive, epoxidized state at the start of the experiment. All plants lines except for *lut2* were exposed to 745 μmol photons m^{-2} s^{-1} during high light periods. *Lut2* plants were subjected to 620 μmol photons m^{-2} s^{-1} during periods of high light to achieve similar quenched average lifetimes as *szl1+NoZEP1* exposed to 745 μmol photons m^{-2} s^{-1} high light periods to facilitate comparison of the shape of the two decay curves at intensities where the average lifetimes of the two mutants are the same. The decay curves of lut2 and szl1+NoZEP1 were very similar, as were the fitted parameters, limiting the extraction of any mechanistic implications. However, the change from 745 μmol photons m^{-2} s^{-1} to 620 μmol photons m^{-2} s^{-1} should not significantly impact the analysis reported in this work. In contrast to PAM traces, data from TCPSC measurements are relatively insensitive to changes in high light intensity, as time resolving the fluorescence eliminates sensitivity to non-quenching processes including chloroplast avoidance [42]. The remaining differences that could have implications for the reconstruction of *wt* from components were subsequently accounted for by normalization of the average lifetimes and by the resulting zeaxanthin concentration in *lut2* compared to *wt*. Plants were kept under 100 μmol photons m^{-2} s^{-1} of light when not being dark-acclimated and no plant was dark-acclimated more than once during any 1.5-hour period.

After initial dark acclimation, TCSPC snapshots were collected during two cycles of high light followed by dark relaxation. The first cycle consisted of 20 min of high light, followed by 10 min of darkness. The second cycle, immediately following the first cycle, consisted of 7 min of high light, followed by 3 min of darkness. Leaves were removed from dark-acclimated plants immediately prior to TCSPC experiments and placed in a home-built holder that allows the leaf surface to be mostly exposed to air to avoid overheating and drying during the experiment, and

has a small well to hold water for the petiole to take up during the experiment as described previously [42].

The TCSPC setup was similar to the one described in Sylak-Glassman et al. [42] and in Amarnath et al. [43]. A 532 nm Coherent Verdi G10 diode laser pumped an ultrafast Ti:Sapph Coherent Mira 900f oscillator with the birefringence adjusted such that the center wavelength was 840 nm with a FWHM of approximately 9 nm. The 840 nm output pulses from the Mira were then frequency doubled to 420 nm using a beta barium borate (BBO) crystal in order to excite the soret band of chlorophyll a (Chla). Before the sample area, the beam was split by a beam splitter so that a small portion was sent to a sync photodiode and acted as a reference pulse for the TCSPC measurements, while the remainder was sent to the sample area where it was incident on the leaf. Data were acquired using a Becker & Hickl SPC-850 data acquisition card in conjunction with the appropriate Becker & Hickl software and the sequence of shutter operations executed using LabView. The portion of the beam that reached the sample was incident on the leaf at a 70° angle to the adaxial side of the leaf. The average power of the laser at the sample was 1.75 mW, corresponding to about 1800 µmol photons $m^{-2} s^{-1}$ of light, which is enough to reach saturation of closed reaction centers [44], with a pulse energy of 19.8 pJ. A monochromator (HORIBA Jobin-Yvon; H-20) set to transmit 684±8 nm was placed before the MCP PMT detector (Hamamatsu R3809U MCP-PMT) in order to selectively observe fluorescence from the Q_y band of Chla molecules in PSII. The actinic light source was a Leica KL1500 LCD with dual gooseneck fiber optic cables to allow for acclimation of two samples to the same light conditions simultaneously.

The detector was cooled to -30°C and the gain was set to 94% (controlled by Becker & Hickl software), yielding an instrument response function with a FWHM of 36-38 ps. Each fluorescence lifetime snapshot consisted of a one second period of laser exposure and data collection. The lifetime data was partitioned into five 0.2-s steps. During subsequent analysis, the step with the longest average lifetime, which corresponds to the step with the highest fluorescence yield in a PAM trace, was retained as the measurement with the reaction centers closed, similar to [42].

Data Analysis

In order to avoid the need for additional, physically meaningless lifetime components each curve was fitted individually to a biexponential function using non-linear least squares analysis rather than aligning the curves according to their maxima and summing them to average the data before fitting. This method also allowed for the step with the reaction center closed to be chosen before any averaging was done ensuring that the reaction centers were closed in each leaf for each snapshot rather than just on average. Standard deviations on each fit parameter were calculated from the Jacobian and a reduced χ^2 value was calculated for each fit in order to confirm goodness of fit. Residuals of several curves from each dataset were examined as an additional check on goodness of fit. Furthermore, singular value decomposition revealed only two components, validating the use of a bi- exponential function to fit the data (Fig. S2).

Once each curve was fitted to a bi-exponential decay function, the amplitude weighted average lifetime associated with each decay was calculated and the uncertainty associated with it

determined from the standard deviation of the fit parameters. Next, the step with the longest lifetime was chosen as the step with the reaction centers closed to saturation. At this point, the rest of the data were discarded and only the data collected when the reaction centers were identified as closed to saturation were further analyzed. The fits for each snapshot were used to calculate uncertainty-weighted averages of each of the components across 20 leaf samples. Due to normal variability in fluorescence yield from different leaves it was necessary to normalize the amplitudes associated with the decay times to sum to one in order to make them comparable across all samples. The average amplitude weighted lifetime across 20 samples was calculated for each snapshot from the uncertainty weighted averages of the fit parameters and the uncertainties on the parameters were then used to calculate the uncertainty on the average amplitude weighted lifetime for each decay. Each decay time, amplitude and average amplitude weighted lifetime for each snapshot/decay was then bootstrapped by examining the variation across resampling of the data from the 20 samples collected for each snapshot during TCSPC. Since the amplitudes were normalized to sum to one, their uncertainties cannot be decoupled. The uncertainty on the amplitude of the shorter decay time was calculated first, and the uncertainty on the amplitude of the larger decay time was then back calculated. The standard deviations were obtained by calculating a 68% confidence interval from the resampled dataset generated during bootstrapping. These confidence intervals were used to generate error bars on the traces of amplitude weighted average lifetimes during TCSPC measurements.

Monte Carlo Methods to Determine Available Xanthophyll Pools.

In order to estimate the fraction of the detected xanthophylls available to undergo de-epoxidation, Monte Carlo methods were employed to determine a constant background pool. Many samples of time series for each xanthophyll were generated from a normal distribution using the mean and standard deviation observed from the measurements at each point in the light acclimation scheme. The minimum value of the concentration of each xanthophyll across a sample time series was selected as the value of background xanthophyll in the time series. For, e.g., violaxanthin, the minimum within a single time series usually occurred following twenty minutes of light acclimation. The mean minimum values were subsequently determined and identified as the portion of the measured xanthophyll concentrations that did not contribute to the kinetic behavior of de-epoxidation and re-epoxidation observed.

Model Estimation.

Models of the kinetic behavior of the carotenoids and of quenching were fit to HPLC data points and values of reversible quenching described previously. The nonlinear greybox estimation tools provided in MATLAB were used to determine best fit values of the parameters, by evaluating the normalized mean square error, expressed as a percentage. Sets of parameters were initialized on a grid in order to determine global best fits for each model. Because the algorithm requires equally spaced time points, when a missing time point was required as in the case for the carotenoid kinetic modeling, a dummy point was inserted and allowed to vary by resetting to the predicted value of the fit and repeating until the results converged. The normalized mean square error values, expressed as percentages, were greater than 80% for each mutant model fit; and 68% for the fit of the *wt* model to data. Values for the carotenoid fit were all greater than 60% for the active xanthophyll, but due to the small number of time series data points, the fits to HPLC data are only

valuable as estimates. 0% corresponds to a straight line at the mean value of the data; 100% is a perfect fit.

Acknowledgements

References

[1]   R. E. Blankenship. Molecular Mechanisms of Photosynthesis, Second Edition. Wiley-Blackwell, 2014.

[2]   C. Külheim, J. Agren, and S. Jansson. Rapid regulation of light harvesting and plant fitness in the field. *Science*, 297(5578):91, 2002.

[3]   J. Kromdijk, K. Głowacka, L. Leonelli, S. T. Gabilly, M. Iwai, K. K. Niyogi, and S. P. Long. Improving photosynthesis and crop productivity by accelerating recovery from photoprotection. *Science*, 354(6314):857-861, 2016

[4]   Schatz GH, Brock H, Holzwarth AR. Kinetic and energetic model for the primary processes of photosystem II. *Biophys. J.* 54:397-405, 1988

[5]   K. K. Niyogi. Photoprotection revisited: genetic and molecular approaches. *Annual Review of Plant Physiology and Plant Molecular Biology*, 50(1):333–359, Jun 1999.

[6]   B. Demmig-Adams and W. W. Adams III. Photoprotection and other responses of plants to high light stress. *Annual Review of Plant Physiology and Plant Molecular Biology*, 43:599–626, 1992.

[7]   Ruban, A. V. Nonphotochemical Chlorophyll Fluorescence Quenching: Mechanism and Effectiveness in Protecting Plants from Photodamage. *Plant Physiology*, *170*(4), 1903–16, 2016

[8]   X.-G. Zhu, D. R. Ort, J. Whitmarsh, and S. P. Long. The slow reversibility of photosystem II thermal energy dissipation on transfer from high to low light may cause large losses in carbon gain by crop canopies: a theoretical analysis. *Journal of Experimental Botany*, 55(400):1167–1175, 2004.

[9]   Y. Tarazona, G. Kodis, K. Bhushan, J. Zaks, C. Madden, A.L. Moore, T. A. Moore, G.R. Fleming, and D. Gust. Mimicking the Role of the Antenna in Photosynthetic Photoprotection. *Journal of the American Chemical Society*, 133(9):2916-2922, 2011.

[10]   C. A. Wraight and A. R. Crofts. Energy-Dependent Quenching of Chlorophyll a Fluorescence in Isolated Chloroplasts. *European Journal of Biochemistry*, 17(2):319–327, Dec 1970.

[11]   G. H. Krause and E. Weis. Chlorophyll Fluorescence and Photosynthesis: The Basics. *Annual Review of Plant Physiology and Plant Molecular Biology*, 42(1):313–349, Jun 1991.

[12]   Verhoeven. Sustained energy dissipation in winter evergreens. *New Phytologist*, 201: 57–65, 2014.

[13] V. Ruban, A. J. Young, and P. Horton. Induction of NonphotochemicaI Energy Dissipation and Absorbance Changes in Leaves. Plant physiology, 102:741–750, 1993.

[14] V. Ruban and P. Horton. An investigation of the sustained component of non-photochemical quenching of chlorophyll fluorescence in isolated chloroplasts and leaves of spinach. *Plant Physiology*, 108(2):721–726, 1995.

[15] M. A. Ware, V. Giovagnetti, E. Belgio, and A. V. Ruban. PsbS protein modulates non-photochemical chlorophyll fluorescence quenching in membranes depleted of photosystems. *Journal of Photochemistry and Photobiology B*: Biology, 152:301–307, 2015.

[16] Brooks, M. D., Sylak-Glassman, E. J., Fleming, G. R., & Niyogi, K. K. A thioredoxin-like/β-propeller protein maintains the efficiency of light harvesting in Arabidopsis. *Proceedings of the National Academy of Sciences of the United States of America*, *110*(29), E2733-40, 2013

[17] P. Xu, L. Tian, M. Kloz, and R. Croce. Molecular insights into zeaxanthin-dependent quenching in higher plants. *Scientific Reports*, 5:13679, Sep 2015.

[18] P. Horton, A.V. Ruban, and M. Wentworth. Allosteric regulation of the light-harvesting system of photosystem II. *Philosophical Transactions of the Royal Society of London B*: *Biological Sciences*, 355:1361–1370, 2000.

[19] N. E. Holt, D. Zigmantas, L. Valkunas, X. Li, K. K. Niyogi, and G. R. Fleming. Carotenoid cation formation and the regulation of photosynthetic light harvesting. *Science,* 307(5708):433–436, 2005.

[20] T. J. Avenson, T. K. Ahn, D. Zigmantas, K. K. Niyogi, Z. Li, M. Ballottari, R. Bassi, and G. R. Fleming. Zeaxanthin radical cation formation in minor light-harvesting complexes of higher plant antenna. *The Journal of Biological Chemistry*, 283(6):3550–8, Feb 2008.

[21] T. K. Ahn, T. J. Avenson, M. Ballottari, Y. Cheng, K. K. Niyogi, R. Bassi, and G. R. Fleming. Architecture of a charge-transfer state regulating light harvesting in a plant antenna protein. *Science*, 320(5877):794, 2008.

[22] S. Bode, C. C. Quentmeier, P. Liao, N. Hafi, T. Barros, L. Wilk, F. Bittner, and P. J. Walla. On the regulation of photosynthesis by excitonic interactions between carotenoids and chlorophylls. *Proceedings of the National Academy of Sciences of the United States of America*, 106(30):12311–6, Jul 2009.

[23] M. Nilkens, E. Kress, P. Lambrev, Y. Miloslavina, M. Müller, A. R. Holzwarth, and P. Jahns. Identification of a slowly inducible zeaxanthin- dependent component of non-photochemical quenching of chlorophyll fluorescence generated under steady-state conditions in Arabidopsis. *Biochimica et Biophysica Acta (BBA) - Bioenergetics*, 1797(4):466–475, 2010.

[24] V. Ruban. Nonphotochemical chlorophyll fluorescence quenching: mechanism and effectiveness in protecting plants from photodamage. *Plant Physiology*, 170(4):1903–16, 2016.

[25] Demmig-Adams, C. M. Cohu, J. J. Stewart, and W. W. Adams III. *Non-photochemical Quenching and Energy Dissipation in Plants, Algae and Cyanobacteria*, Volume 40. Springer Netherlands, 2014.

[26] X.-P. Li, A. M. Gilmore, S. Caffarri, R. Bassi, T. Golan, D. Kramer, and K. K. Niyogi. Regulation of photosynthetic light harvesting involves intrathylakoid lumen pH sensing by the PsbS protein. *The Journal of Biological Chemistry*, 279(22):22866–74, May 2004.

[27] X.-P. Li, O. Björkman, C. Shih, A. R. Grossman, M. Rosenquist, S. Jansson, and K. K. Niyogi. A pigment-binding protein essential for regulation of photosynthetic light harvesting. *Nature*, 403(6768):391–395, Jan 2000.

[28] P. Jahns, D. Latowski, and K. Strzalka. Mechanism and regulation of the violaxanthin cycle: The role of antenna proteins and membrane lipids. *Biochimica et Biophysica Acta (BBA) – Bioenergetics*, 1787(1):3-14, Jan 2009.

[29] P. Horton, M. Wentworth, and A.V. Ruban. Control of the light harvesting function of chloroplast membranes: the LHCII aggregation model for non-photochemical quenching. *Federation of European Biochemical Societies Letters*, 579:4201–4206, 2005.

[30] M. P. Johnson, M. L. Pérez-Bueno, A. Zia, P. Horton, and A. V. Ruban. The zeaxanthin-independent and zeaxanthin-dependent qE components of nonphotochemical quenching involve common conformational changes within the photosystem II antenna in Arabidopsis. *Plant Physiology*, 149(2):1061–1075, 2009.

[31] H. D. Rabinowitch, P. Budowski, and N. Kedar. Carotenoids and epoxide cycles in mature-green tomatoes. *Planta*, 122(1):91–97, 1975.

[32] R. A. Bungard, A. V. Ruban, J. M. Hibberd, M. C. Press, P. Horton, and J. D. Scholes. Unusual carotenoid composition and a new type of xanthophyll cycle in plants. *Proceedings of the National Academy of Sciences of the United States of America*, 96(3):1135–9, Feb 1999.

[33] J. I. García-Plazaola, S. Matsubara, and C. B. Osmond. The lutein epoxide cycle in higher plants: its relationships to other xanthophyll cycles and possible functions. *Functional Plant Biology*, 34(9):759, 2007.

[34] J. I. García-Plazaola, K. Hormaetxe, A. Hernández, J. M. Olano, and J. M. Becerril. The lutein epoxide cycle in vegetative buds of woody plants. *Functional Plant Biology*, 31(8):815, 2004.

[35] L. Leonelli, M.D. Brooks, and K.K. Niyogi. Engineering the lutein epoxide cycle into Arabidopsis thaliana. *Proceedings of the National Academy of Sciences of the United States of America*, submitted 2017.

[36] Z. Li, T. K. Ahn, T. J. Avenson, M. Ballottari, J. A. Cruz, D. M. Kramer, R. Bassi, G. R. Fleming, J. D. Keasling, and K. K. Niyogi. Lutein accumulation in the absence of zeaxanthin restores nonphotochemical quenching in the Arabidopsis thaliana npq1 mutant. *The Plant Cell*, 21(6):1798–812, Jun 2009.

[37] Pogson, K. A. McDonald, M. Truong, G. Britton, and D. DellaPenna. Arabidopsis carotenoid mutants demonstrate that lutein is not essential for photosynthesis in higher plants. *The Plant Cell*, 8(9):1627–39, Sep 1996.

[38] J. Zaks, K. Amarnath, D. M. Kramer, K. K. Niyogi, and G. R. Fleming. A kinetic model of rapidly reversible nonphotochemical quenching. *Proceedings of the National Academy of Sciences of the United States of America*, 109(39):15757–62, Sep 2012.

[39] Wehner, T. Grasses, and P. Jahns. De-epoxidation of violaxanthin in the minor antenna proteins of photosystem II, LHCB4, LHCB5, and LHCB6. *The Journal of Biological Chemistry*, 281(31):21924–33, Aug 2006.

[40] K. Amarnath, D. I. G. Bennett, A. R. Schneider, and G. R. Fleming. Multiscale modeling of light harvesting by photosystem II in plants. *Proceedings of the National Academy of Sciences of the United States of America*, 113(5):1156–1161, Dec 2015.

[41] Leonelli, L., Erickson, E., Lyska, D., & Niyogi, K. K. Transient expression in *Nicotiana benthamiana* for rapid functional analysis of genes involved in non-photochemical quenching and carotenoid biosynthesis. *The Plant Journal*, 1–12, 2016

[42] E. J. Sylak-Glassman, J. Zaks, K. Amarnath, M. Leuenberger, and G. R. Fleming. Characterizing non-photochemical quenching in leaves through fluorescence lifetime snapshots. *Photosynthesis Research*, 127(1):69–76, Jan 2016.

[43] K. Amarnath, J. Zaks, S. D. Park, K. K. Niyogi, and G. R. Fleming. Fluorescence lifetime snapshots reveal two rapidly reversible mechanisms of photoprotection in live cells of *Chlamydomonas reinhardtii*. *Proceedings of the National Academy of Sciences of the United States of America*, 109(22):8405–10, May 2012.

[44] G. Schansker, S. Z. Toth, and R. J. Strasser. Dark recovery of the Chl a fluorescence transient (OJIP) after light adaptation: The qT-component of non- photochemical quenching is related to an activated photosystem I acceptor side. *Biochimica et Biophysica Acta (BBA) - Bioenergetics*, 1757(7):787–797, 2006.

Supporting Information
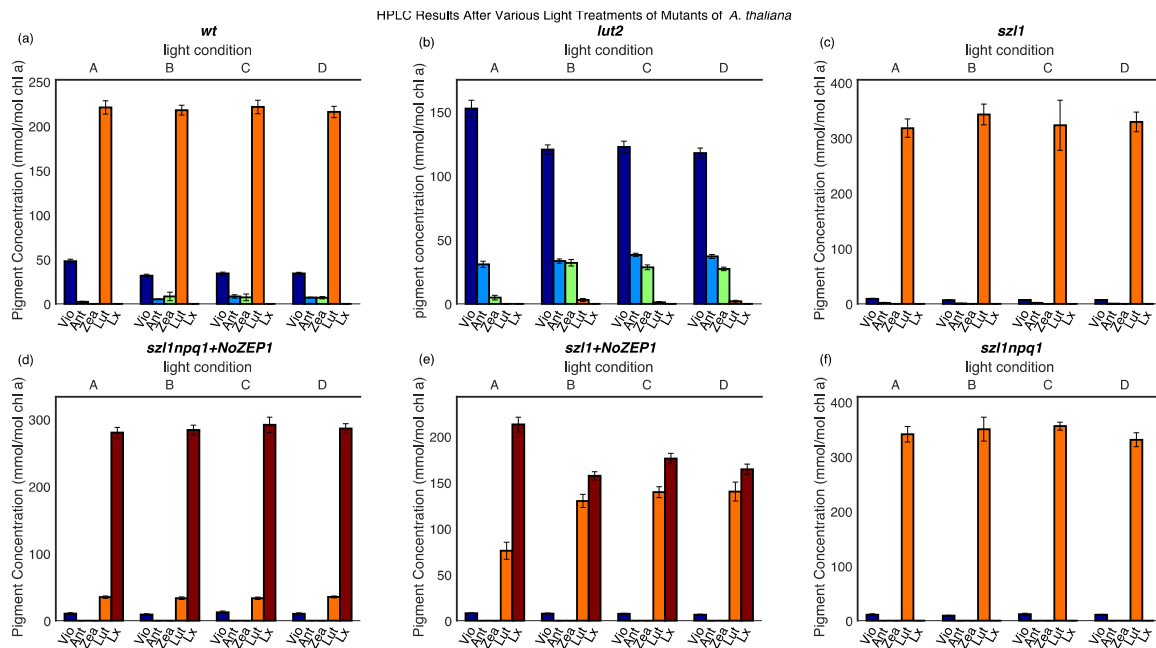
Figure S1. HPLC Results for mutants of *A. thaliana* after light treatment corresponding to TCSPC snapshot measurements.   (a)-(f) Light conditions for each set A-D consist of initial dark acclimation (Set A) followed by a scheme corresponding to the light acclimation scheme used for TCPSC measurement. (See text.) Set B corresponds to samples after the first twenty minutes of light acclimation of the scheme. Set C corresponds to samples after the next ten minutes of dark acclimation. Set D corresponds to samples acclimated to the subsequent light-dark cycle of seven minutes of high light followed by five minutes of dark.
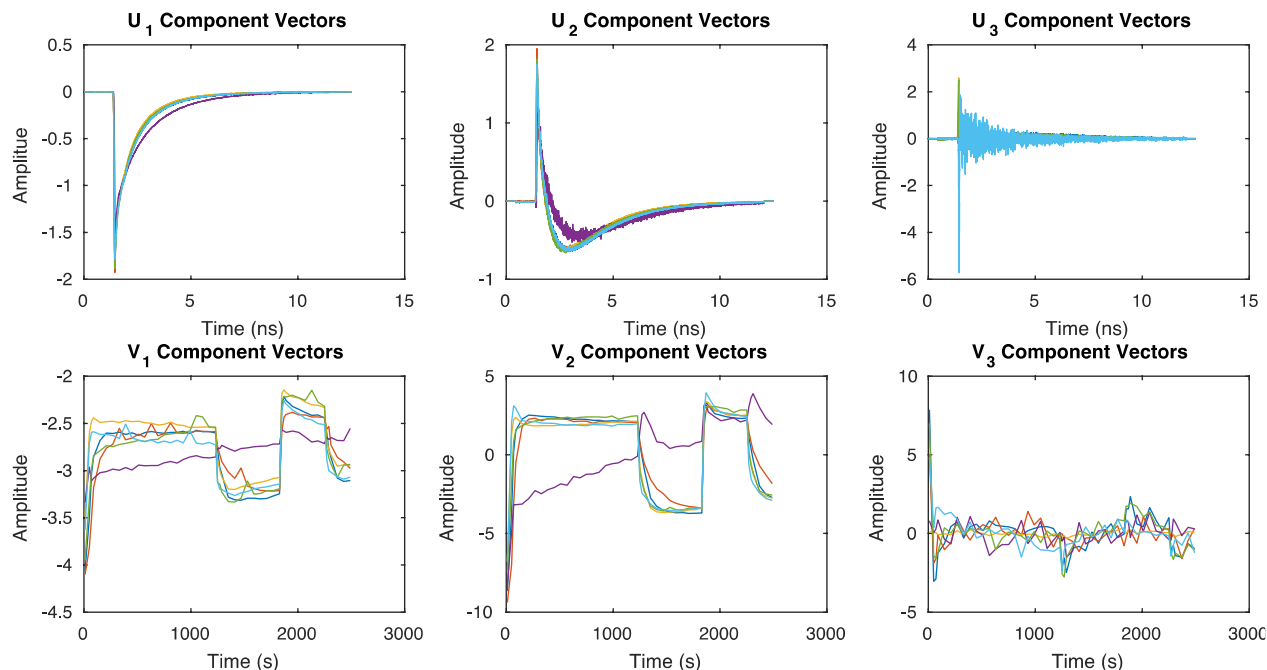
Figure S2. Singular Value Decomposition (SVD) results for the whole data set. The average U and V vectors corresponding to the largest three singular values are shown for *wt* (blue), *lut2* (red), *szl1* (yellow), *szl1npq1+NoZEP1* (purple), *szl1+NoZEP1* (green), and *szl1npq1* (cyan). Using the standard definition of the SVD, X = USV*, the decompositions were performed on matrices, X, composed of the vectors of raw fluorescence lifetime data corresponding to the actinic time points observed for a sample. The resulting decompositions were averaged over the 20 samples for each line. In this construction, U is composed of the actinic light acclimation time basis vectors, V is composed of the ultrafast dynamics basis vectors, and S holds the singular values. The first two basis vectors of the ultrafast dynamics basis set clearly exhibit structure; the third exhibits far less structure. The actinic light acclimation basis set vectors exhibit two components with structure; the third exhibits noise. The singular values corresponding to the sets {U_1, V_1}, {U_2, V_2}, and {U_3, V_3} drop by an order of magnitude between each set. This indicates that fitting more than two components does not extract additional meaningful information, reflecting the tradeoff between limited data collection time of snapshot measurements and the dynamic range of the fluorescence decay curves.
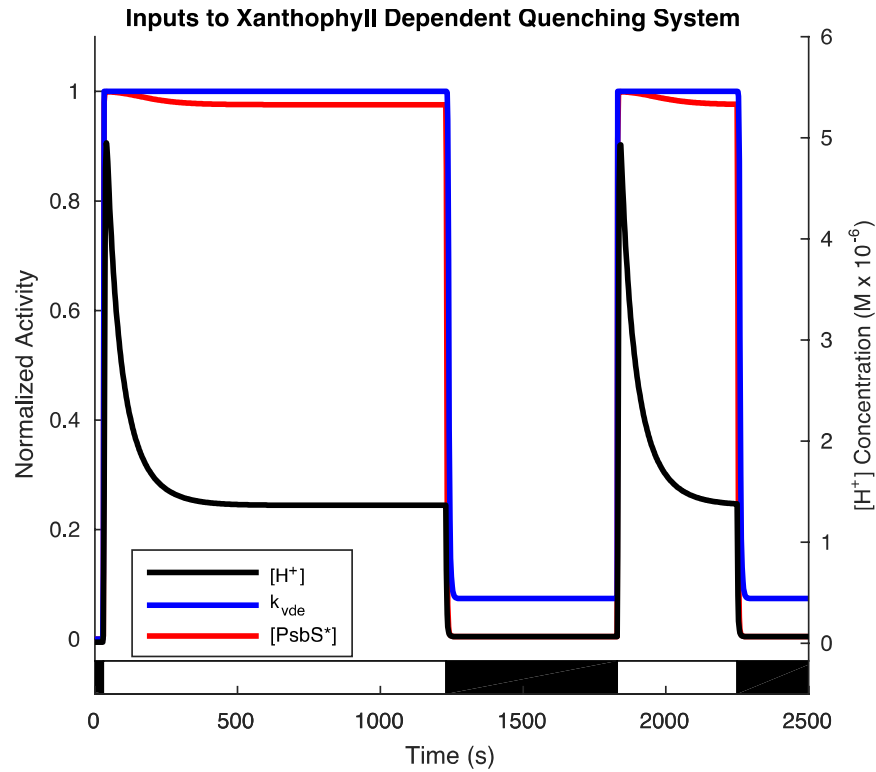
Figure S3. Dynamics of thylakoid membrane ΔpH in terms of [H$^+$] concentration gradient and activation of PsbS and VDE. The black line shows the [H$^+$] concentration for the light acclimation scheme shown in the light and dark bars superimposed on the plot. It displays a rapid spike upon high light exposure followed by a decay to a steady state value; upon dark acclimation, [H$^+$] concentration rapidly recovers to a dark adapted quasi-steady-state value. The blue line shows the normalized activity of VDE, which is activated upon the formation of the pH gradient. The red line shows the normalized activation of PsbS upon the formation of the pH gradient. All values were obtained from the model provided in Zaks et al. [38].
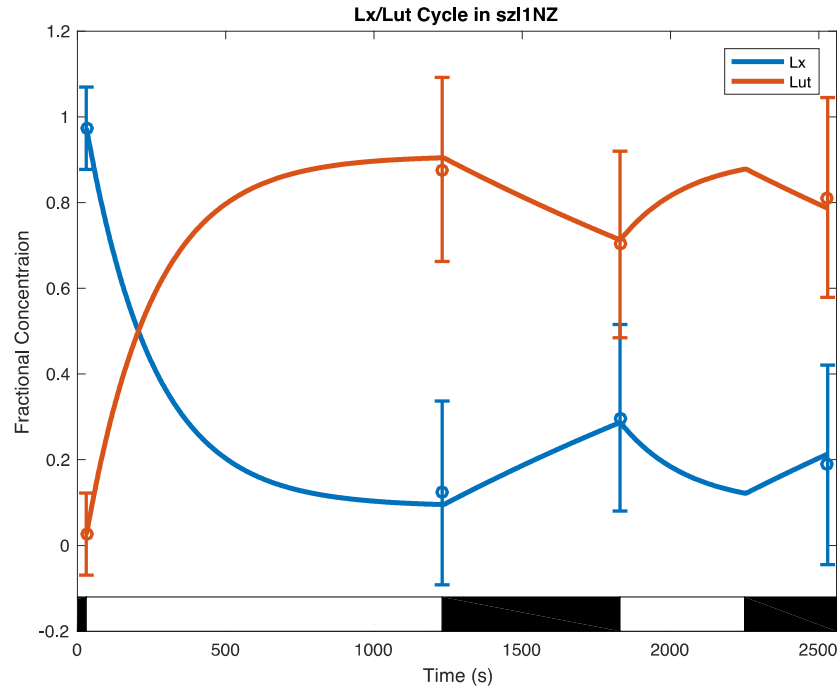
Figure S4. Dynamics of the *szl1+NoZEP1* LxL cycle in response to the light acclimation scheme shown in the light and dark bars superimposed on the plot fit to HPLC data are shown here. The data are represented by a fit of the fractional concentration of the available pool of lutein and lutein epoxide to the available pool of xanthophylls determined from analysis of HPLC measurements (see Methods section of the text) at four time points (open circles with error bars denoting SD for n=8) using a first-order kinetic model with a pH gradient dependent rate of de-epoxidation (solid lines).
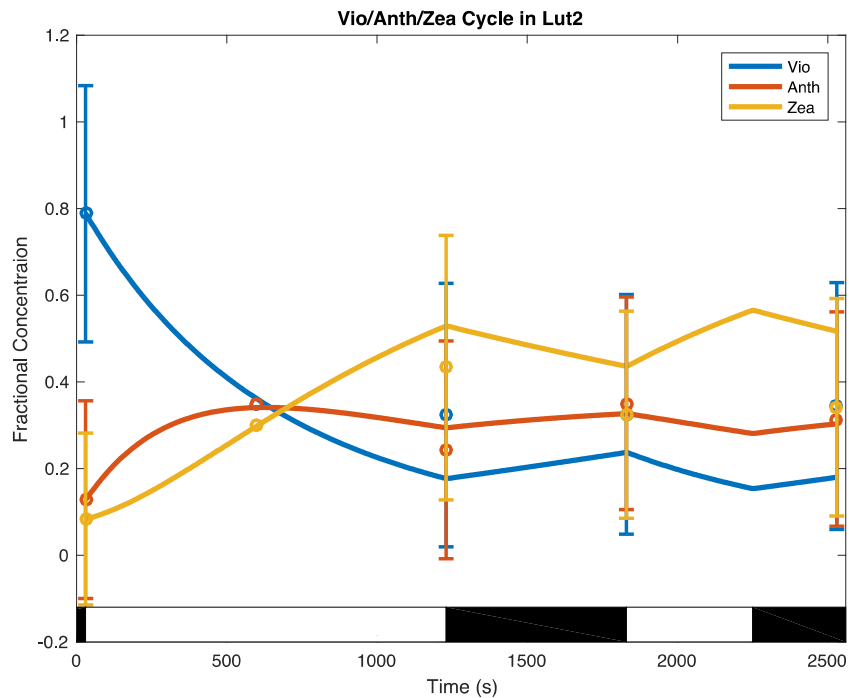
Figure S5. Dynamics of the *lut2* VAZ cycle in response to the light acclimation scheme shown in the light and dark bars superimposed on the plot fit to HPLC data are shown here. The data are represented by a fit of the fractional concentration of the available pool of violaxanthin, antheraxanthin, and zeaxanthin to the available pool of xanthophylls determined from analysis of HPLC measurements (see Methods section of the text) at four time points (open circles with error bars denoting SD for n=8) using a first-order kinetic model with a pH gradient dependent rate of de-epoxidation (solid lines).

Name	Mutation	Effect
Col-0 (*wt*)	N/A	N/A
lut2	Mutated lycopene ε-cyclase (LCYE)	Mutated LCYE inhibits formation of α-carotene and lutein.
szl1	Mutated lycopene β-cyclase (LCYB)	Mutated LCYB partially inhibits β-carotene formation and severely restricts accumulation of zeaxanthin, antheraxanthin, and violaxanthin.
szl1npq1	Mutated lycopene β-cyclase (LCYB) and mutated violaxanthin de-epoxidase (VDE)	Mutated LCYB partially inhibits β-carotene formation and severely restricts accumulation of zeaxanthin, antheraxanthin, and violaxanthin. Mutated VDE inhibits formation of zeaxanthin from antheraxanthin and violaxanthin.
szl1+NoZEP1	Mutated lycopene β-cyclase (LCYB), addition of zeaxanthin epoxidase from *Nannochloropsis oceanica* (NoZEP1)	Mutated LCYB partially inhibits β-carotene formation and severely restricts accumulation of zeaxanthin, antheraxanthin, and violaxanthin. Lutein is converted to lutein epoxide in dark conditions by NoZEP1, and lutein epoxide is converted to lutein in high light conditions by VDE, forming the LxL cycle.
szl1npq1+NoZEP1	Mutated lycopene β-cyclase (LCYB) and mutated violaxanthin de-epoxidase (VDE), addition of zeaxanthin epoxidase from *Nannochloropsis oceanica* (NoZEP1)	Mutated LCYB partially inhibits β-carotene formation and severely restricts accumulation of zeaxanthin, antheraxanthin, and violaxanthin. Mutated VDE inhibits formation of zeaxanthin from antheraxanthin and violaxanthin and lutein from lutein epoxide in high light conditions. Lutein is converted to lutein epoxide in dark conditions by NoZEP1.

Table S1: Lines of *A. thaliana* studied with explanation of mutations and effect on xanthophyll content and dynamics.

Chapter 3: Periodic actinic light exposure reveals complex roles of PsbS and zeaxanthin in the regulation of nonphotochemical quenching in *Arabidopsis thaliana*

This chapter reproduces an manuscript entitled "Periodic actinic light exposure reveals complex roles of PsbS and zeaxanthin in the regulation of nonphotochemical quenching in Arabidopsis thaliana," by J. M. Morris, K. K. Niyogi, and G. R. Fleming, prepared for submission to *J. Chem. Phys. B.*

The analysis and modeling performed in the work described in Chapter 2 indicated that the observed timescales of the induction of quenching upon initial exposure to high light after full dark acclimation included both the effect of an intrinsic regulation of zeaxanthin dependent quenching and the regulatory effect of the accumulation of zeaxanthin in Arabidopsis. However, the effects of longer term quenching processes may also prevent the observed timescale in the second period from representing a regulatory rate intrinsic to the activation of a zeaxanthin dependent quenching mechanism: longer term quenching mechanisms were accounted for by comparison to a mutant line deficient in zeaxanthin and lutein.

In addition, although the mathematical model was able to reproduce the combined effects of zeaxanthin- and lutein-dependent quenching in wild type from the mutant lines with isolated contributions of zeaxanthin and lutein, the process of fitting the differential equation based model using greybox estimation techniques has little predictive power for changes in regulatory protein concentrations. Such predictive power is necessary to develop models suitable for the optimization of protein expression levels of various regulatory proteins to increase crop yields.

A natural refinement of the two light exposure period measurement is in turn a multiple light exposure period measurement, able to isolate regulatory timescales of multiple processes within a single mutant line. This is particularly useful to investigate separate regulatory processes that may depend on common biochemical regulators, such as zeaxanthin that appears to influence the regulation of quenching on multiple timescales that cannot easily be isolated via genetic manipulation.

This chapter describes measurements that were performed on a series of mutants including the wild type, *szl1* that lacks zeaxanthin, and *L17* and *npq4* that overexpress another important regulatory protein, PsbS, respectively over a series of periodic actinic light exposure. Over successive periods, the quenching induction and recovery within a period oscillated in response to high and dark light inside an envelope of the maximum quenching and recovery over successive periods. After several periods, the envelopes equilibrated, allowing the intrinsic rapid regulatory induction and relaxation timescales of each line to be determined without relying on isolating the contributions of components from multiple mutant lines. The measurements revealed important roles of zeaxanthin and PsbS that are suggested to depend on protein conformational changes and membrane reorganization.

Abstract

Photosynthetic organisms employ various photoprotective mechanisms to dissipate excess photoexcitation as heat in a process called non-photochemical quenching (NPQ). Regulation of NPQ in response to varying light intensity operates on multiple timescales, but often the regulation at different timescales depends on shared biochemical regulatory components, such as the accumulation of the carotenoid zeaxanthin or the presence of the pH-sensitive PsbS protein. This makes distinguishing contributions of different regulatory responses to the overall response by comparing the initial step response of various mutant lines difficult. In order to simultaneously resolve timescales of regulatory processes operating on different timescales, but with shared biochemical regulators, time correlated single photon counting (TCSPC) measurements were performed on several Arabidopsis thaliana mutants during periodic actinic light exposure. Over successive periods of actinic light, TCSPC measurements show distinct intra-period and inter-period dynamics and demonstrate complex roles of the biochemical regulators PsbS and zeaxanthin in both fast and slow timescale responses of NPQ. Comparison between mutant lines suggests evidence of a role of PsbS in the longer timescale quenching response not previously emphasized. Finally, a mathematical model was constructed demonstrating how short timescale, rapidly reversible quenching processes and longer timescale quenching processes combine to produce the overall quenching response.

Introduction

The initial step of photosynthesis requires absorption of light to drive charge separation via photochemistry [1]. However, fluctuating incident sunlight can transiently exceed the ability of photosynthetic organisms to use the absorbed energy for productive charge separation and can damage the photosynthetic apparatus. Photosynthetic organisms therefore regulate photoprotective processes in response to light conditions to ensure that excess absorbed light is dissipated safely across a range of light intensities [2]. Recent work has shown that increasing photosynthetic organisms' ability to rapidly match the level of photoprotection to the incident light can improve crop yields [3].

Of the two major photosystems and their photoprotective mechanisms, photosystem II (PSII) experiences longer lived excitation kinetics and is more susceptible to damage than photosystem I when incident light absorption outpaces charge separation [4]. The suite of photoprotective mechanisms that protect PSII have been the subject of intense study. The mechanisms result in a phenomenon called non-photochemical quenching (NPQ), the reduction in the observed chlorophyll a fluorescence due to the dissipation of excess excitation by mechanisms other than photochemistry [5, 6, 7]. NPQ processes allow for rapid induction of photoprotection in response to excess light, but slower timescale processes are also present that lead to a period of suboptimal photosynthetic efficiency [8] when transient high light intensities return to lower light intensities. Detailed understanding of the complex regulatory processes that constitute NPQ could allow for optimizing photoprotective systems to improve crop yields [3] or utilizing biomimetic protective schemes in bio-inspired energy devices [9].

In plants, "components" of NPQ have historically been separated by the timescales of the induction and relaxation of the phenomena. At the two extremes are qE, the rapidly reversible, energy-dependent quenching component, and qI, the slowly reversible component associated with PSII photoinhibition [10, 11]. The different induction and relaxation timescales used to classify components are fundamentally regulatory signatures, but the interpretation of these timescales usually also relies on an underlying assumption that each regulatory-based component is attributable to a distinct underlying photochemical mechanism – a specific physical process by which the excess excitation energy is dissipated. There is a key distinction between the regulatory processes and mechanisms: the regulatory processes are the means by which dissipative photochemical mechanisms (that operate on ultrafast timescales) are controlled as opposed to dissipative mechanisms themselves. Identifying molecular mechanisms of energy dissipation and relating these mechanisms the observed regulatory responses by monitoring unique signatures would help to resolve the nature of the various regulatory components, but as of yet, there is little consensus on the roles of specific molecular mechanisms in NPQ [12, 13].

Further complicating the difficulties in identifying molecular mechanisms associated with each NPQ component, there are a number of ambiguities in the temporal separation of these components [14]. Attempts to isolate the contributions of biochemical players have led to conflicting evidence about the regulatory functions and mechanisms involved. The literature suggests that qI depends on some combination of the presence of zeaxanthin [15, 16], membrane reorganization [17- 21], the protein PsbS (that also primarily influences qE) [18,19], and other proteins [22]. Zeaxanthin appears to also play a role in both qE, serving as a direct participant in

the molecular mechanism of quenching [23-27] or as an allosteric regulator [28], and another component "qZ" that depends on zeaxanthin but operates at timescales between qE and qI [29].

Despite difficulties in identifying specific molecular mechanisms of energy dissipation associated with each component of the quenching response, many important biochemical regulatory processes affecting rapidly reversible qE have been identified. qE is triggered by a pH gradient, ΔpH, formed across the thylakoid membrane when charge separation due to productive photochemistry outpaces the activity of ATP synthase and other downstream processes [30]. PsbS, which contains exposed protonatable residues, has been shown to be a sensor of ΔpH [31], and is necessary for the rapid regulation characteristic of qE [32] that occur via interactions with other pigment protein complexes [33]. In parallel, upon the formation of ΔpH, violaxanthin de-epoxidase (VDE) is activated, converting violaxanthin to antheraxanthin and zeaxanthin in the VAZ cycle. The VAZ cycle is necessary for the complete induction of qE [34] and influences the rapid regulatory effects of PsbS [35]. However, zeaxanthin is also linked to changes in slower timescale processes, including qI and qZ [15, 29]. Therefore, distinguishing the unique roles these shared biochemical regulators play in each component, in order to determine opportunities to optimize yields or design biomimetic devices, requires experimental methods that can distinguish between the regulatory components without relying on modifications of the biochemical regulatory system.

Fluorescence measurements are the most common experimental probe of quenching in intact photosynthetic systems. However, a quantitative interpretation of the meaning of fluorescence measurements used to observe NPQ requires an underlying physical understanding of the energy transfer and quenching processes incorporated into mathematical models. Traditionally, these models fell into either "lake" or "puddle" regimes [36], that describe opposing limits of the connectivity of energy transfer amongst pigment-protein complexes containing antenna, reaction centers, and quenching sites. Energy enters the system upon absorption by a chlorophyll, and can diffuse through the membrane much like ink dropped into water. In the limit of a highly connected energy transfer network, many reaction centers are accessible by excitations originating in an antenna, as if the reaction centers were spread out in a "lake" of antennae. In the opposing limit, only one reaction center is accessible to excitations originating in the antenna near that reaction center, as if the membrane could be pictured as a group of antenna "puddles" each with a reaction center.

Modern membrane-scale computational models of energy transfer and quenching [37, 38] suggest that the photosynthetic membrane operates somewhere between these two limits, and in the presence of quenching, can be pictured using a new "contracting lake" model. In the new "contracting lake" model, quenching serves to decrease the effective diffusion length of an exciton when quenching sites are active and function as traps, thereby decreasing the size of the "lake." The observed fluorescence lifetime in this picture is a function of the product of an intrinsic rate of quenching of a particular quenching site and the density of available quenching sites. The intrinsic rate of quenching includes contributions from both the rate of energy transfer to a state that can quench and the rate at which that state dissipates energy. In macroscopic fluorescence lifetime measurements, these two factors cannot be disentangled. This makes drawing conclusions about photochemical mechanisms of dissipation from fluorescence lifetime measurements difficult. However, the regulatory timescales of induction and relaxation of quenching apparent

in fluorescence lifetime measurements still provide insight into constraints that any proposed underlying photochemical mechanism or combination of mechanisms, regulated individually or together by various components, must be able to satisfy.

In accordance with the traditional view that each regulatory component of NPQ operates independently with distinct associated photochemical mechanisms, much of the literature measures the change in the quenching response during a single time period of high light exposure after a sample is fully dark acclimated, followed by a single time period of dark recovery, usually in a pulse amplitude modulated (PAM) fluorescence yield measurement [14, 16-18, 22, 23, 27-29, 31-33, 35]. Recent experiments with two consecutive light and dark periods have shown that the lifetime decays [39], the regulatory character, and the magnitude [40] of the initial induction of quenching upon exposure to high light are different in the subsequent re-exposure to high light. These experiments suggest deficiencies in the view that each component operates independently. At the very least, the regulation of different mechanisms must be coupled in some manner in order to achieve the different behaviors of the rapidly reversible quenching that depend on the state of other regulatory mechanisms. Although counter to the prevailing view, a simple proposed explanation is that the coupling occurs because different regulatory components affect shared dissipative photochemical mechanisms [41].

Amongst many proposed mechanisms of dissipation, two leading candidates include: 1) excitation energy transfer (EET) to a carotenoid like zeaxanthin or lutein, followed by non-radiative decay of energy and 2) the formation of a radical cation charge transfer (CT) complex between a carotenoid like zeaxanthin and a neighboring chlorophyll, followed by charge recombination to dissipate the energy [12,13]. Because the electronic states of the carotenoids are so close in energy, even small transient changes in the coupling of excited states of adjacent chlorophylls to the various excited states of the carotenoids could result in either mechanism of dissipation at the same quenching site [42-44], suggesting that the two mechanisms could easily co-occur in a macroscopic collection of sites. Both transient absorption studies that observe simultaneous signals of charge transfer quenching and excitation energy transfer quenching [45, 46, 47] and single-molecule fluorescence experiments showing that pigment-protein complexes rapidly transition between multiple states that all display quenching behavior [48,49] further support this view.

Within a "contracting lake" picture [38], excitations may visit multiple quenching sites before dissipation occurs. The probability that quenching occurs during any given visit to a particular quenching site depends on the intrinsic rate of quenching at that site. In either case, the rates of energy transfer to a carotenoid or formation of a charge transfer complex are potentially sensitive to small conformational changes of the pigment-protein complex. Larger changes in protein conformation may reduce the rate of energy transfer to a suitable quenching site so much that the quenching site is effectively inactive, changing the perceived density of quenching sites, further complicating attempts to distinguish experimentally between intrinsic quenching rate and density of quenching sites. Apart from conformational changes, chemical composition of the pigment-protein complex (e.g. the presence of violaxanthin vs. zeaxanthin) could also impact the nature of the quenching. This complexity suggests that attempts to assign distinct photochemical mechanisms (or, alternately, quenching sites) to traditional components of quenching may not be feasible or even representative of the underlying physical processes. A diagram depicting possible

regulatory mechanisms operating on shared photochemical mechanisms of dissipation, occurring at quenching sites, is shown in Figure 1.
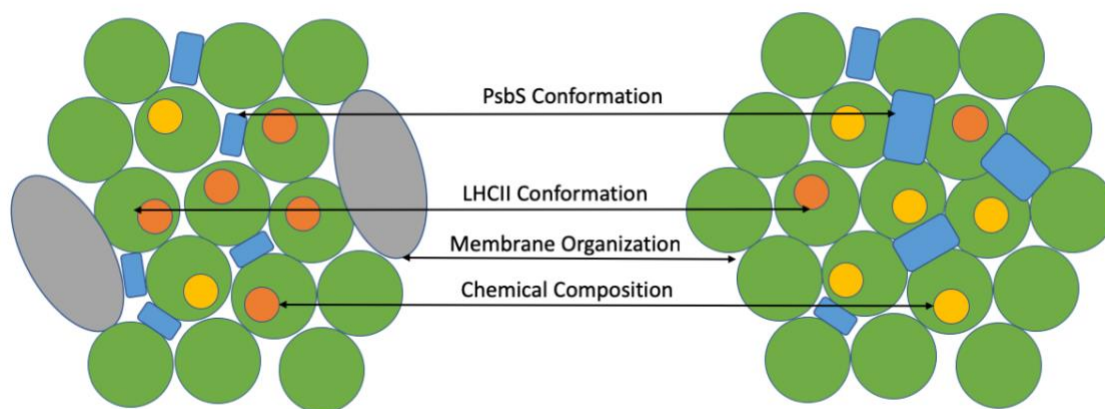
Figure 1. Diagrammatic representation of the photosynthetic membrane in two hypothetical states resulting in quenching via a carotenoid, with annotations indicating potential physical changes that can be described with a kinetic scheme for the regulation of macroscopic quenching behavior. Each change between the left and right states may impact the observed quenching by altering either the intrinsic quenching rate or the effective density of quenching sites, but with macroscopic measurements, only the product of these two factors determines the observed quenching. Green circles represent light harvesting complex II (LHCII). Orange and yellow circles within the LHCII represent various carotenoids that may be substituted or interconverted as part of the regulatory process, including e.g. zeaxanthin from violaxanthin via the VAZ cycle. Changes in the location of the carotenoid within the LHCII conceptually represent (potentially complex) changes in LHCII conformation. PsbS conformational changes in response to the formation of ΔpH are represented by the change in size of the blue rectangles. Membrane organization changes are represented by the presence or absence of core photosystem II complexes, shown in grey.

     The maximum observable quenching requires a combination of factors to occur simultaneously: the presence of PsbS inducing conformational changes in antenna proteins such as light-harvesting complex II (LHCII) in response to ΔpH [16, 30-33, 35] under optimal chemical composition of carotenoids in LHCII [16, 34, 35] and optimal membrane organization [18-21]. This is the case for either the traditional formulation or a formulation where regulatory components

operate on shared quenching sites. Upon initial exposure of a fully dark-acclimated sample to high light, each of the regulatory processes begins simultaneously to induce (turn on) quenching. However, each causes effects on different timescales. The initial response of the rapid induction of quenching that is observed experimentally when a fully dark-acclimated sample is exposed to high light is therefore due to the combination of effects and not solely the fastest timescale component. In general, this is valid (in the macroscopic kinetic sense) for either formulation.

Upon subsequent exposure to dark, the fastest timescale processes rapidly recover from (turn off) quenching, but slower timescale processes limit the ability of the sample to return to a fully unquenched state. After an incomplete recovery, when exposed again to high light, the faster regulatory processes are again induced, but because quenching has not fully recovered, the observed induction of quenching in subsequent periods will be different than the initial period. Again, this is valid (in the macroscopic kinetic sense) for either formulation.

The two cases differ in how the effects combine. In the case of independent mechanisms, without coupling, the combination of the regulatory timescales would simply add to result in the observed quenching, with the magnitude and timescale of rapid quenching unaffected by the states of slower quenching components. This is often implied in the determination of NPQ components from measurements of a single light exposure and relaxation period via subtraction [7]. However, in the case that the regulatory processes operate on shared dissipative mechanisms or quenching sites, the processes are inherently coupled and the magnitudes and intrinsic timescales of the rapidly reversible quenching may change in subsequent re-exposure to high light.

Fluorescence measurements under periodic actinic light exposure allow for the simultaneous observation of the fast and slow regulation of quenching, without relying on modification of the biochemical regulatory system. Isolating the response components by comparison across mutants requires the assumption that the biochemical regulatory process deficiencies that occur due to mutation (e.g. a violaxanthin de-epoxidase knockout that inhibits the ability of a plant to accumulate zeaxanthin) only influence a single response component, despite strong evidence to the contrary - specifically the dual role of zeaxanthin in "qE" and "qZ." [21-27]. Separating the regulatory response dynamics by timescale with periodic exposure instead allows the subsequent comparison between the mutant lines to directly address the effects of the presence or absence of the biochemical regulatory processes on individual components of the quenching responses, and the dependence of rapid regulation on slower regulatory processes. These considerations are necessary to develop a quantitative understanding of contributions of the various regulatory elements under realistic light exposure conditions.

Periodic light exposure patterns are also more representative of the light exposure patterns plants are subjected to in natural conditions [50]. Various A. thaliana mutants with modified NPQ phenotypes display different levels of fitness under growth conditions with fluctuating light than in steady-state growth light [51]. In addition, long term exposure to periodic photoinhibitory light during growth influences seed yields, but with similar photochemical yields of photosynthesis compared to growth under constant light [52]. Therefore, attempts to optimize the quenching response to light fluctuations [3, 8] must account for how changes to the various biochemical regulators influence more than a single response component and how the various response components, in turn, influence yields. Here, time correlated single photon counting (TCSPC)

measurements of the fluorescence lifetime are performed on whole leaves under exposure to periodic actinic light.

Methods

Chlorophyll fluorescence lifetime "snapshot measurements" of whole leaves of A. thaliana were collected via time correlated single photon counting (TCSPC) in order to measure changes in the fluorescence lifetimes (ps-ns) of chlorophyll a (Chla) of PSII in response to actinic light exposure (s-min). TCSPC measurements of fluorescence lifetime are less sensitive to changes in absorbance, due to e.g. chloroplast avoidance, than traditional yield measurements [53], allowing longer actinic light exposure patterns to be studied. The genetic lines studied included wild type (wt; Col-0 ecotype), szl1, a mutant that does not accumulate zeaxanthin, but instead maintains high levels of lutein [54], a PsbS-overexpressing transgenic line L17 [55], and the PsbS-deficient mutant npq4 [56]. Plants were germinated on MS plates, transplanted to pots and grown in growth chambers under 110 μmol photons m-2 s-1 on a 10-hour day, 14-hour night cycle at 23◦C. All plants were between 5 and 8 weeks of age at the time of experiments, and all measurements were completed as described previously [39, 40]. These mutant lines allow for a comparison of the effects of both PsbS and zeaxanthin in rapid and moderate-to-long timescale quenching dynamics usually classified as qE, qZ, or qI.

After an hour of initial dark acclimation, leaves were removed from the plant and placed in a sample holder. A 532 nm Coherent Verdi G10 diode laser pumped an ultrafast Ti:Sapph Coherent Mira 900f oscillator with center wavelength of 840 nm and FWHM of approximately 9 nm. The 840 nm output pulses from the Mira were then frequency doubled to 420 nm using a beta barium borate crystal in order to excite the Soret band of Chla. The beam was split, with a portion directed to a sync photodiode providing a reference for TCSPC measurements, while the remainder was directed to the sample. The portion of the beam that reached the sample was incident on the leaf at a 70◦ angle to the adaxial side of the leaf. The average power of the laser at the sample was 1.75 mW, corresponding to approximately 18,000 μmol photons m-2 s-1 of light, saturating reaction centers [57]. Fluorescence was collected through a monochromator (HORIBA Jobin-Yvon; H-20) set to transmit 680±8 nm placed before the MCP PMT detector (Hamamatsu R3809U MCP-PMT) in order to selectively observe fluorescence from the Qy band of Chla molecules in PSII. The detector was cooled to -30◦C and the gain was set to 94% yielding an instrument response function with a FWHM of 36-38 ps. Data were acquired using a Becker & Hickl SPC-850 data acquisition card using a sequence of trigger and shutter operations executed using LabView. The actinic light source was a Leica KL1500 LCD.

TCSPC snapshots were collected at 30 s intervals over ten four-minute full periods of high light (700 μmol photons m-2 s-1) and dark. The full light and dark period consisted of 2 min of high light and 2 min of dark. Five fluorescence decays were collected for each 0.2 s step each during a 1 s snapshot measurement and fit to biexponential functions using re-convolution fitting with the measured instrument response function. The amplitude weighted average lifetime for each decay was calculated, and the step with the longest lifetime was chosen as the step with the reaction centers closed to saturation as described in previous work [39, 40].

High snapshot time resolution is required to resolve the timescale of the rapid induction of quenching upon the transition from dark to high light. The measurements at 30 s snapshot resolution were collected at two "phase offsets" describing the initial timepoint: one starting at 0 s (resulting in measurements at 0 s, 30 s, 60 s, and so on) and another at 15 s (resulting in measurements at 15 s, 45 s, 75 s, and so on). In order to achieve a 15 s snapshot resolution from the 30 s resolution data at each phase offset, pairwise combinations of leaf samples were combined and a 1st order Butter filter with a critical frequency of 15 s was applied to remove high frequency oscillation due to leaf-to-leaf variability. The resulting filtered traces were averaged using a standard mean at each time point to obtain fluorescence lifetime traces. Error was estimated as the standard deviation of the filtered pairwise combinations using a bootstrapping process.

To measure quenching, NPQ_τ values were calculated from the mean snapshot lifetime traces, as previously described [39, 40], and analogously to the traditional NPQ parameter(s) [1]. Error was estimated via the standard deviation of a bootstrap sampling process for the four mutants exposed to each periodic pattern. In order to quantify inter-period behavior, upper and lower envelope traces were obtained by selecting the NPQ_τ values at the light to dark transition (maximum quenching) and dark to light transition (maximum recovery).

Results and Discussion

Figure 2 shows a scatter plot of representative snapshot lifetime values collected from separate wt leaves at 30 s resolution and at the two phase offsets, overlaid with the mean and uncertainty values obtained by combining the data from the two phases to achieve 15 s resolution. Although individual series of snapshots obtained from a single leaf are consistent from snapshot to snapshot, there is noticeable leaf-to-leaf variability that introduces high frequency measurement error when interleaving the two phases that is eliminated with a 1st order Butter filter.

The mean snapshot traces for each mutant show the response pattern to the repeated light and dark exposure. In the high light portions of the periods, the lifetime rapidly decreases due to quenching. In subsequent dark recovery portions of the period, the lifetime recovers. Between successive periods, both the maximum reduction in the lifetimes due to quenching within a period and the recovery of the lifetimes within a period display longer timescale dynamics. After a few periods, the minimum lifetimes due to maximum quenching during high light saturate, followed a few periods later by the saturation of the maximum recovery lifetimes during dark relaxation. By the end of the ten periods, dynamics reach a quasi-periodic steady state, with only small variations between periods. This type of oscillatory behavior is common in electronic circuits and in signal processing, where the smooth curves that describe time dependent extrema or amplitudes of an oscillatory signal are referred to as "envelopes."
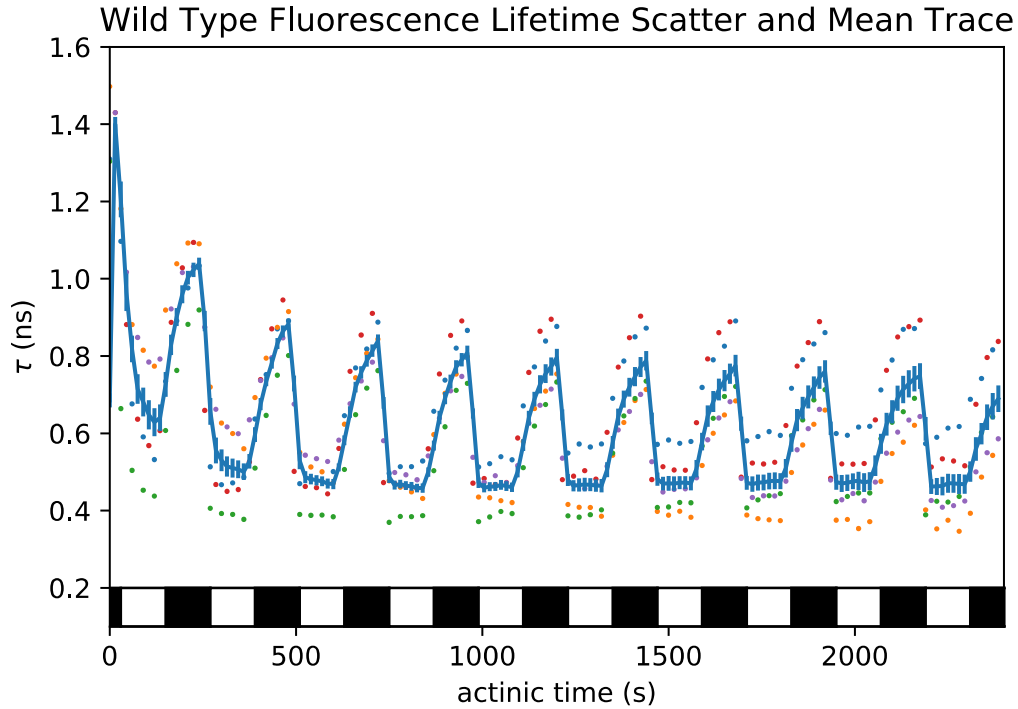
Figure 2. Scatter plot of scalar snapshot lifetime values collected from *wt* leaves (points, multiple colors corresponding to different leaf samples) at 30 s resolution at 0 s and 15 s phase offsets, overlaid with mean obtained from pairwise combination and application of a 1st order Butter filter (blue, error bars SD, n=9).

The intra- and inter-period dynamics separate the rapid and moderate-to-long timescale quenching dynamics that depend on common biochemical regulators. In later periods, the magnitude and timescales of rapidly reversible quenching (q_E) can be determined distinctly from magnitudes and timescales of moderate timescale dynamical components (q_Z or q_I) that appear in period-to-period comparison without requiring comparison between different mutant lines. In many experiments that only examine a single light period, the induction timescales of components can only truly be separated by comparing mutant lines deficient in one or more biochemical regulatory process(es). Experiments that separate magnitudes of components from within a single line rely on differences in relaxation timescales and are only able to separate the relative magnitudes of various components.

Inter-period Dynamics

Figure 3 shows traces of NPQ_τ values for wt, L17, *szl1*, and *npq4*. In order to quantify the inter-period behavior, both the upper and lower envelopes were fit to exponential decays. Although multiple regulatory processes occur at different timescales, such as the accumulation of zeaxanthin and long timescale structural reorganizations, only a single time constant was resolvable in the envelopes. Fit values are provided in Table 1.

In all periods, the *npq4* mutant deficient in PsbS displays very little rapidly reversible quenching, in agreement with previous observations [39]. However, it still shows a slow increase in NPQ_τ over successive periods, although the difference in the timescales between the maximum quenching in the light and the recovery levels in the dark is within a single standard deviation. Although *npq4* accumulates zeaxanthin, the difference in the timescale between de-epoxidation in high light and epoxidation in low light is greater than a factor of ten [58]. Zeaxanthin reaches near full accumulation in the first few periods, and does not significantly relax to antheraxanthin or violaxanthin in the short dark relaxation time, according to previous high-performance liquid chromatography measurements [40, 46]. Therefore, in later periods, the behavior of the inter-period dynamics should be attributable to slowly reversible or irreversible quenching processes occurring without changes due to zeaxanthin accumulation or the presence of PsbS.

A)
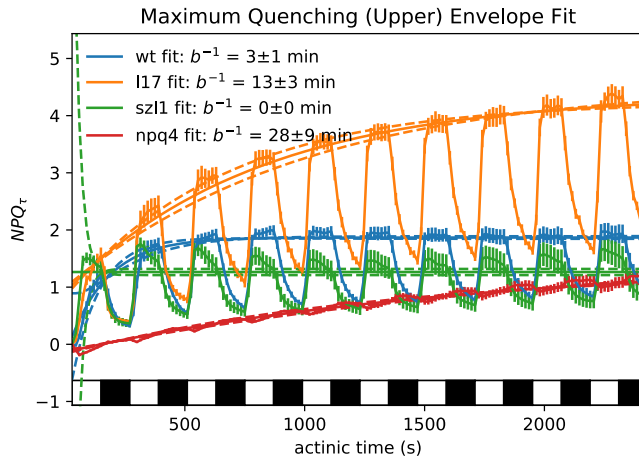
B)
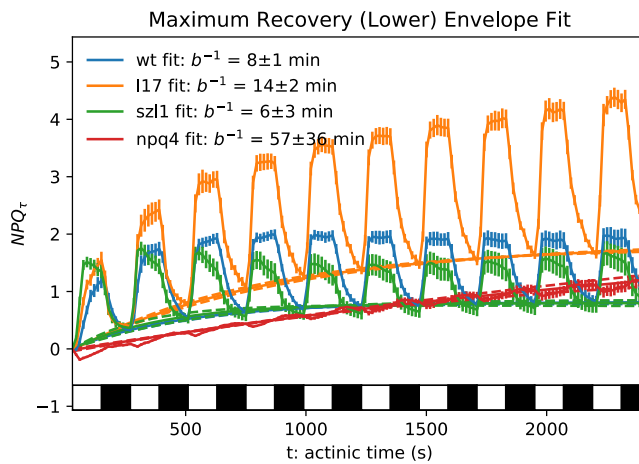
Figure 3. Comparison of NPQ_τ traces (error bars, SD via bootstrap resampling), envelope fit (solid line) and 1 σ fit confidence intervals (dashed lines) for each line: *wt* (blue), *L17* (orange), *szl1* (green) and *npq4* (red). The three PsbS-containing lines (*wt*, *L17*, and *szl1*) show rapid oscillatory quenching induction and relaxation within each period. The PsbS-deficient mutant *npq4* does not show the strong oscillatory behavior. A) Maximum quenching envelope obtained from the selection of trace values at the light to dark to dark transition and fit to a single exponential decay. B) Maximum recovery envelope obtained from selection of trace values at the dark to light transition and fit to a single exponential decay. Note that the similarities between the maximum recovery envelope of szl1 and WT in B make the fit plots difficult to distinguish visually, and due to the lack of strong oscillatory behavior in *npq4*, the envelope fit (dashed line) overlaps with the fluorescence lifetime trace (solid line) in A and B. Table 1 contains the fit values.

73

Table 1. Fit Values for Maximum Quenching and Recovery Envelopes

Maximum Quenching Fit Values: $NPQ_\tau^{\max}(t) = a\,e^{-bt} + c$

	a	$1/b$ (minutes)	c
wt	-2.09 ± 1.13	3 ± 1	1.86 ± 0.02
L17	-3.45 ± 0.08	13 ± 3	4.37 ± 0.16
szl1	-85 ± 126	0 ± 0	1.26 ± 0.01
npq4	-1.62 ± 0.25	29 ± 9	1.49 ± 0.28

Maximum Recovery Envelope Fit Values: $NPQ_\tau^{\min}(t) = a\,e^{-bt} + c$

	a	$1/b$ (minutes)	c
wt	-0.86 ± 0.02	8 ± 1	0.81 ± 0.04
L17	-1.91 ± 0.05	14 ± 2	1.82 ± 0.06
szl1	-0.86 ± 0.03	6 ± 3	0.79 ± 0.06
npq4	-2.42 ± 1.30	57 ± 36	2.38 ± 1.32

Table 1. Fit values reported for exponential fits of the moderate-to-long timescale envelope dynamics for A) maximum quenching (upper) envelope fit obtained from selection of trace values at the light to dark transition and B) the maximum recovery (lower) envelope fit obtained from selection of trace values at the dark to light transition. Fit values reported are the fit parameters obtained from the curves corresponding to the median values of the time constant, b, from fitting Monte Carlo bootstrap samples of NPQ_τ values. Errors reported are half the difference between parameters of curves corresponding to $+\sigma$ and $-\sigma$ percentile values of the time constant, b. Parameters a and c are unitless values of NPQ_τ, $1/b$ is reported in minutes.

In comparison, *szl1*, which does not detectibly accumulate zeaxanthin, shows both rapidly reversible quenching within individual periods and some combination of the moderate-to-long timescale reductions in fluorescence recovery. Focusing, momentarily, on the rapidly reversible dynamics not present in *npq4*, the lines that contain PsbS (*szl1*, *wt* and *L17*) all show the presence of significant intra-period responses, in agreement with previous conclusions about the role of PsbS in rapidly reversible quenching [12-14, 31-33, 35, 39, 55]. In the case of the moderate-to-long timescale dynamics, the envelopes of the maximum quenching and recovery of *szl1* show differing timescales outside of the uncertainty, suggesting the two envelopes are governed by different underlying regulatory dynamics. The difference between the maximum quenching and recovery envelopes is also resolvable in *wt*.

Turning to the fits in Figure 3A, the maximum induction timescale fit of zero for *szl1* suggests there are no maximum quenching dynamics present at this temporal resolution: the level is constant. In comparison, *wt* shows a timescale to achieve maximum quenching of 3 min. The difference between the *szl1* mutant and wt suggests that the maximum quenching envelope depends, in part, on zeaxanthin accumulation. This timescale is similar to the accumulation of zeaxanthin measured using high-performance liquid chromatography in various plant systems [40, 46]. There is no zeaxanthin accumulation in *szl1*, but *wt* accumulates zeaxanthin until steady state is reached within a few periods. This results in the appearance of a slower initial induction of the rapidly reversible component in *wt* compared to *szl1*, as is observed in single or few exposure measurements [40, 54]. Despite the conclusions of single period measurements, the difference is likely due to the accumulation of zeaxanthin and not a difference in the nature of the rapidly reversible quenching, as suggested by previous two-period measurements [40].

The recovery envelopes for *szl1* and *wt* (Figure 3B) are similar: differences are within the experimental uncertainty. Therefore, the recovery envelope does not appear to depend strongly on the accumulation of zeaxanthin. However, the similarities in the timescales between *szl1* and *wt*, that both contain PsbS, suggest a dependence on PsbS when the pair is compared to the much longer timescale of the recovery enevelope of *npq4* that lacks PsbS. This long timescale dependence on PsbS is not commonly identified in the literature, despite previous evidence of a role it may play in the magnitude of photo-inhibitory quenching [21, 55].

Both *szl1* and *wt* have a difference in the timescales their own maximum quenching and recovery envelopes. In order to achieve this result, the rapidly reversible quenching must change in magnitude over successive periods. Since *szl1* lacks zeaxanthin, the differences between the maximum quenching and maximum recovery within a single line cannot be attributed solely to a change in the chemical composition to regulate the rapidly reversible quenching magnitude. Therefore, the changes in magnitude over successive periods demonstrate that the rapidly reversible quenching is coupled to the slower regulatory processes. If rapidly reversible quenching utilized a distinct mechanism independent of the slower timescale processes, a constant magnitude of quenching between successive periods would be expected and result in common timescales and magnitudes of the maximum quenching and maximum recovery.

Finally, *L17*, which contains excess PsbS, displays higher values of maximum quenching. In addition, the recovery envelope displays higher values of quenching relative to other mutants. Although the dark recovery time period may not be long enough to completely relax the rapidly

reversible component, at least a portion of the excess quenching is likely due to excess long-timescale quenching as suggested by previous observations [21]. Finally, the net difference between the maximum quenching and the recovery is also larger than other mutants. This results in larger magnitudes of the rapidly reversible quenching, in agreement with single period measurements [55], field-scale experiments [3], and supports the view that the role of PsbS is to regulate rapidly reversible quenching.

However, unlike *szl1* and *wt*, the timescales of the maximum quenching and maximum recovery envelopes are similar for *L17* (Table 1). Within the uncertainty, both sets of timescales are longer than the corresponding sets of timescales in *szl1* and *wt*. In this case, the difference in magnitude alone indicates differences in the rapidly reversible quenching between successive periods. The differences again demonstrate coupling between the rapidly reversible quenching and the slower timescale components.

Although not as long as the timescale observed in *npq4*, the timescales of the envelope dynamics of *L17* appear to more closely match those of *npq4*, despite *L17* having excess PsbS and *npq4* lacking PsbS. The differences in NPQ_τ values between the PsbS-containing mutants and the *npq4* mutant deficient in PsbS highlight this behavior. Although the observed lifetime values cannot be directly subtracted, the unitless NPQ parameter, calculated traditionally by (Fm-Fm')/Fm' [1] under a Stern-Vollmer assumption, allows for a linear subtraction to investigate the differences between mutant traces. The analogous NPQ_τ values allow the same manipulation. Figure 4 shows the results of subtracting the *npq4* NPQ_τ values from the NPQ_τ values of the three PsbS-containing mutants for the recovery envelope.
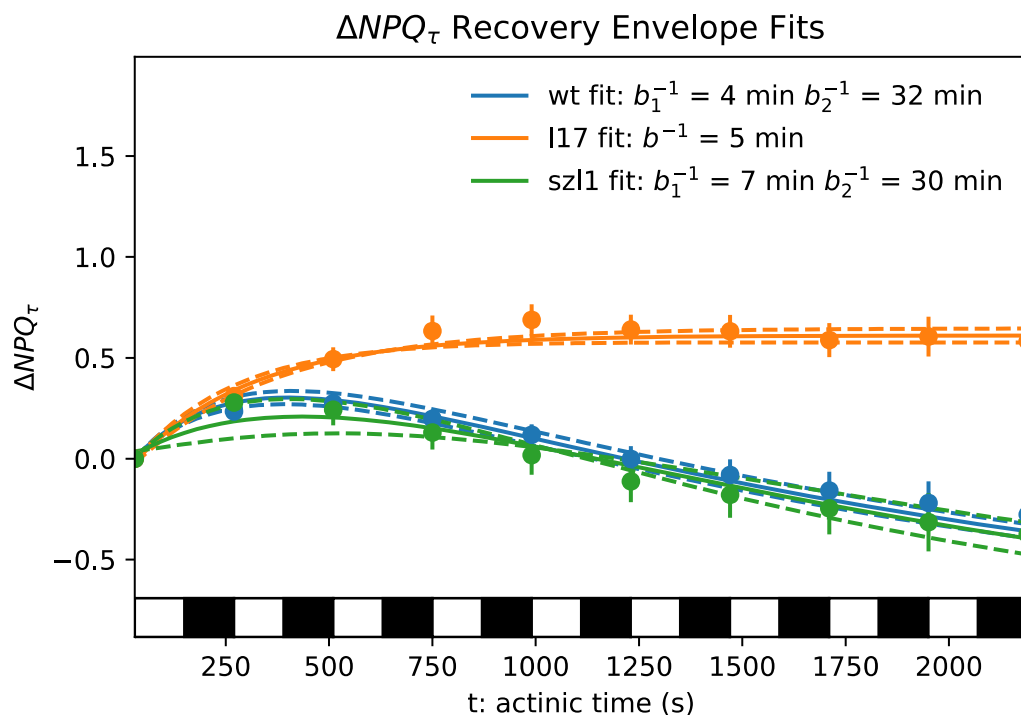
Figure 4. Results of performing subtraction of *npq4* NPQ_τ recovery values from the NPQ_τ values of the three PsbS containing mutants, *wt* (blue), *szl1* (green), and *L17* (orange), to obtain ΔNPQ_τ for the recovery envelopes. Fits to decays are overlaid (median, solid line; 1 σ confidence intervals, dashed line). *wt* and *szl1* are fit to biexponential decay with two time components, but *L17* fits to a single exponential decay with one timescale component. Fit values are provided in Table 2.

Table 2. ΔNPQ_τ Fit Values: $\Delta NPQ_\tau(t) = a_1\, e^{-b_1 t} + a_2 e^{-b_2 t} + c$

	a_1	$1/b_1$ (minutes)	a_2	$1/b_2$ (minutes)	c
wt	-0.9	4.4 ± 0.4	1.5	32 ± 3	-0.91
Ll17	-0.7	4.9 ± 0.2	N/A	N/A	-0.01 ± 0.04
szl1	-1	7.2 ± 2	1.78	29 ± 3	-0.71

Table 2. Fit values for ΔNPQ_τ traces obtained by subtracting the NPQ_τ values from *npq4* from the NPQ_τ values of the PsbS containing mutants. *wt* and *szl1* are fit to biexponentials with two time components. *L17* is fit to a single exponential. Fit values reported are the fit parameters obtained from the curves corresponding to the median values of the long time constant (b_2 for *wt* and *szl1*, b_1 for *L17*) from fitting Monte Carlo bootstrap samples of ΔNPQ_τ values. Initial parameters for the bi-exponential nonlinear fits were obtained by fitting a single exponential to later time points and subtracting the long component to fit a single exponential short time component. Errors reported are half the difference between parameters of curves corresponding to $+\sigma$ and $-\sigma$ percentile values of parameters. Errors for other parameters were at least an of magnitude smaller than the reported value. Parameters a_1, a_2, and c are unitless values of NPQ_τ; $1/b_1$ and $1/b_2$ are reported in minutes.

Upon performing the background subtraction of the *npq4* NPQ_τ values, each of the resulting ΔNPQ_τ traces were fit to decays with additional time components that were not reliably resolvable when comparing the overall envelopes. The *wt* and *szl1* traces were able to be fit to biexponential decays that show moderate timescale rises of about 4 and 7 min, followed by a long timescale decay of about half an hour. For the *L17* mutant that overexpresses PsbS, the trace was able to be fit only to a single exponential decay with a moderate timescale rise of 5 min. Attempts to resolve a long timescale component resulted in a value on the order of days, well beyond the timescale of the experiment. The moderate timescales are of similar timescales to the original envelopes, and difficult to draw conclusions from. Apart from the initial moderate timescale difference common to the three mutant lines, the lack of a long timescale component in *L17* relative to *npq4*, suggests the recovery envelope of *L17* decays at the same timescale as the *npq4* mutant, despite their totally different PsbS content. It is unlikely that this is attributable to a buildup of incomplete relaxation of a more rapidly reversible component, as upon induction, a quasi-equilibrium is reached within each period, indicating that decay occurs from similar maximum levels of the rapid quenching in spite of any incomplete relaxation in a previous period. In comparison, both *wt* and *szl1*, containing normal concentrations of PsbS, show an additional long timescale relative to *npq4*.

This suggests that the moderate-to-long timescale dynamics depend not just on the presence or absence of PsbS or a simple linear relationship to concentration, but rather a nonlinear dependence on PsbS concentration that initially rises to *wt* levels and then decreases at increased concentrations. PsbS concentration influences protein mobility and the ability of the thylakoid membrane to reorganize [18, 19, 20, 21], a mechanism suggested for multiple timescales of changes in quenching [18, 54, 55]. As PsbS does not bind pigments, it is thought that the role it plays as a sensor of ΔpH and actuator of quenching occurs through a conformation change of PsbS that results in interactions with pigment containing proteins that trigger associated conformational changes in the pigment protein complexes to induce quenching [33, 35].

These two processes likely operate on different timescales: conformational changes within individual pigment protein complexes can occur rapidly compared to reorganization of the protein itself within the membrane. As the most rapid influence of PsbS occurs within a period, the inter-period dynamics are likely associated with the longer timescale processes of membrane reorganization. A possible explanation for the nonlinear dependence of the 20-30 min timescale is that it is the result of interactions between two competing processes influencing the membrane organization that both influence the common quenching observable. Although chlorophyll-containing protein mobility is linearly associated with PsbS concentration between *npq4*, *wt*, and *L17* in confocal FRAP measurements, the sign of the linear trend changes from positive to negative after exposure to high light [21], suggesting competition between two processes influencing protein mobility. At the *wt* concentrations of PsbS, a competitive interaction between the light-dependent and the PsbS processes could result in the second timescale observed in *wt* and *szl1* relative to *npq4*. At excess concentrations of PsbS in *L17*, the interaction between the light-dependent and PsbS-dependent process could be overpowered, resulting in the loss of the second timescale relative to *npq4*.

Intra-period Dynamics

Figure 5 shows the typical dynamics of NPQ_τ within the periods for the PsbS-containing mutants, upon reaching a quasi-periodic steady state. The dynamics are referred to as quasi-periodic steady state because they are very nearly periodic: the same between successive periods of light and dark, due to the decay timescales of slower timescale dynamics. Within period traces were obtained by selecting the penultimate period and were verified against the proceeding periods to validate that periodic steady state had been reached. Although more complicated dynamics likely come into play when considering the mechanism of the rapidly reversible quenching, involving response to ΔpH [40, 59], induction and relaxation timescales were fit to simple exponential decays in order to describe characteristic timescales.

The intra-period traces allow for a comparison of the relative effects of the high light induced steady state concentration of zeaxanthin and PsbS on the rapidly reversible dynamics while the effects of the longer period dynamics that co-occur in initial periods are minimized. Within the physical picture described above, these dynamics reflect the influence of only the fastest regulatory components on the conformational preferences of individual pigment protein complexes – slower processes, such as the changes in the chemical composition via the *VAZ* cycle and membrane organization, have come to a quasi-periodic steady state near their equilibria that have much less impact on the dynamics than during initial periods. Traces of the *npq4* mutant are omitted, as PsbS is required for the presence of the rapidly reversible quenching observed within a single period.

After reaching quasi-steady state, the induction timescale for the *wt* and *szl1* mutants are the same, despite the presence or absence of zeaxanthin. This indicates that observations of induction timescales based solely on single period measurements are complicated by the simultaneous observation of a common rapidly reversible quenching process and slower regulatory control factors like the accumulation of zeaxanthin [54]. For the induction, the *L17* timescale is longer than *wt*, despite greater overall quenching. This indicates that the ability of PsbS to rapidly induce quenching and recovery begins to saturate at high concentrations, despite increased overall quenching. This could be a result of a saturation of the protein-protein interactions thought to be required for PsbS to actuate rapidly reversible quenching, or that the excess PsbS sufficiently influences membrane organization [18-20] to inhibit the rapidly reversible regulation (q_E).

A)
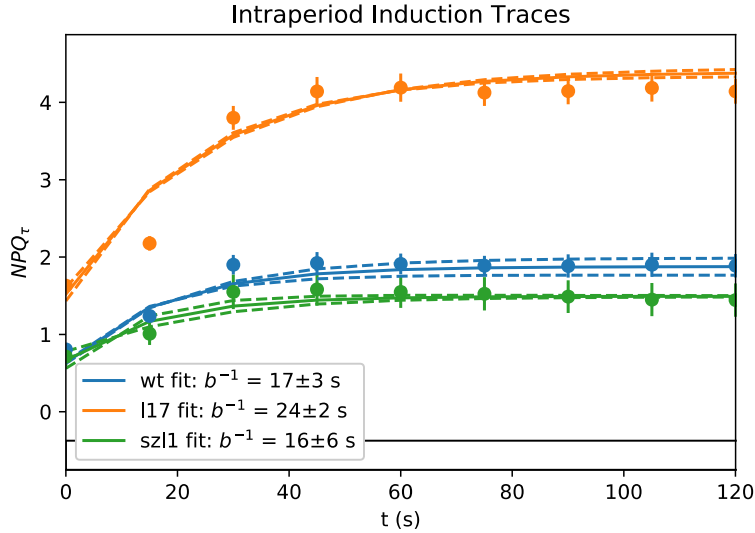
B)
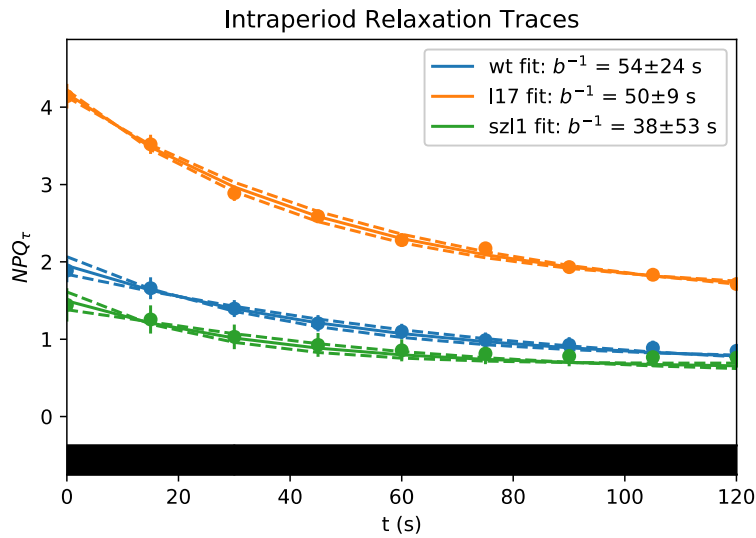
Figure 5. Quasi- periodic steady state dynamics of NPQ_τ within a single period for the PsbS containing mutants, *wt* (blue), *L17* (orange), and *szl1* (green). NPQ_τ values (points) with error bars derived from bootstrap sampling overlaid an exponential fit curve (solid line) and $1\ \sigma$ confidence intervals (dashed line) selected from fit curves corresponding to the median and $1\ \sigma$ confidence intervals for values of the decay constant. Inverse time constants in seconds, along with error estimates, are reported in the legend for convenience. Errors in the legend are estimated as average difference between the median and $1\ \sigma$ values of the time constant; error on *szl1* is asymmetric resulting in reported error value larger than median value. Full fit values and confidence intervals are provided in Table 3. A) High light quenching induction dynamics. B) Dark recovery dynamics.

Table 3. Rapidly Reversible Quenching Fit Values

Induction Fit Values: $NPQ_\tau(t) = a\,e^{-bt} + c$

	a	$1/b$ (s)	c
wt	-1.24 ± 0.13	17 ± 3	1.87 ± 0.11
L17	-2.87 ± 0.03	24 ± 2	4.39 ± 0.06
szl1	-0.82 ± 0.12	16 ± 6	1.49 ± 0.01

Relaxation Fit Values: $NPQ_\tau(t) = a\,e^{-bt} + c$

	a	$1/b$ (s)	c
wt	1.30 ± 0.02	54 ± 24	0.64 ± 0.13
L17	2.69 ± 0.08	50 ± 9	1.48 ± 0.12
szl1	0.87 ± 0.02	38 ± 53	0.62 ± 0.13

Table 3. Fit values for quasi- periodic steady state rapidly reversible NPQ_τ. Fit values reported are the fit parameters obtained from the curves corresponding to the median values of the time constant, b, from fitting Monte Carlo bootstrap samples of NPQ_τ values. Errors reported are half the difference between parameters of curves corresponding to +1 σ and -1 σ percentile values of the time constant, b. Error is asymmetric, resulting in large reported uncertainty on the time constant for *szl1* Parameters a and c are unitless values of NPQ_τ, $1/b$ is reported in seconds. A) High light induction decay fit values; B) dark recovery decay fit values.

Mathematical Model of Coupled Regulatory Processes

It is difficult to make conclusions about underlying photochemical mechanisms resulting in quenching based solely on macroscopic fluorescence lifetime measurements. However, kinetic regulatory models of quenching [40, 59], when combined with estimates of fluorescence lifetimes generated by various dissipation mechanisms [37], knowledge of the chemical composition of the biochemical regulatory state (e.g. the *VAZ* cycle [34, 40, 58, 59]), and the organization of the membrane [18-21], allow for important conclusions to be drawn about the nature of how any underlying mechanism must be regulated. Using an underlying physical picture such as the scheme shown in Figure 1, a model was constructed to demonstrate how rapidly reversible regulation of quenching occurs simultaneously to and alongside slower timescale regulatory processes.

This model treats slower regulatory processes (such as the accumulation of zeaxanthin or membrane reorganization) as constraints on the result of the rapidly reversible regulation of quenching (via e.g. conformational changes within individual pigment protein complexes) to achieve coupling between multiple timescales. Allowing coupling between the regulatory components is a key difference from a model where components (e.g. qE, qZ, and qI) arise from separate photochemical mechanisms and independent regulatory schemes. The regulatory model is agnostic of the underlying photochemical mechanisms of quenching due to the unsettled evidence regarding specific dissipative mechanisms associated with each regulatory component, and instead models an overall homogeneous value of quenching, similar to previous models [40, 59, 60] that combine overall quenching into a single modeled state.

A diagram of the regulatory model is shown in Figure 6. The observed quenching is modeled as a conservative two-state system representing the homogeneous quenching of the system using "quenching on" and "quenching off" states. Time-dependent rate values describe the rate of transitions from one state to the other (Figure 6A). The regulatory behavior at multiple timescales via physical processes (and, depending on particular choices of definitions, analogous to components of quenching e.g. qE, qZ, and qI) is contained within these time-dependent rate values. The time-dependent rate values, $k_1(t)$ and $k_2(t)$, are determined using (unitless) values of the maximum quenching and maximum recovery $q_{max}(t)$ and $q_{recovery}(t)$ and intrinsic, constant, rates of rapid response occurring in the light, $k_{induction}$, and the dark, k_{relax} (Figure 6B). $q_{max}(t)$ and $q_{recovery}(t)$ are modeled using a set of auxiliary differential equations. In the light, the rate values of the rapidly reversible quenching must be proportional to the time-dependent value of the maximum quenching, $q_{max}(t)$, capturing the behavior that quenching is driven to a steady state within each repeated light period. Upon a transition to dark, the rate values of the rapidly reversible quenching then switch to be proportional to the time-dependent maximum recovery values, $q_{recovery}(t)$, and recovery is driven to a separate steady state within each repeated dark period.

Despite the similarity in modeling a single quenching variable, the chosen model of the rapidly reversible regulation of quenching differs from previous models [40, 59, 60] that relate predicted states of biochemical regulatory cycles (e.g. the state of the *VAZ* cycle) and proteins (like PsbS activation) to the quenching. This model relates the multiple directly observed timescale components to the overall extent of quenching (as opposed to the biochemical state), in order to

draw conclusions about how multiple regulatory mechanisms combine to result in the overall quenching regulation on the seconds to minutes timescales. Due to this focus, the observed quenching parameter is modeled explicitly, instead of relying on assumptions of an intrinsic rate of quenching or density of quenchers to predict the observable fluorescence yield or fit parameters relating biochemical concentrations to the quenching effect.

The advantage to this framework is that the overall ability of the model to reproduce the observed quenching relies on the ability to experimentally resolve the various time components, instead of predicting the biochemical state. Memory is maintained between periods without explicitly modeling the biochemical state due to the inability of slower components of quenching regulation to relax during the short dark exposure. However, one current limitation of this framework is the inability to account for the effects of transient spikes in ΔpH that occur in the first few seconds after a transition between dark and light, before settling to a light-dependent equilibrium [40, 59]. Although possible to include, incorporating the transient spikes would rely on incorporating extra fit parameters in the model. All the existing parameters are entirely determined from the experimental observations. Therefore, a choice is made to neglect the transient spikes in ΔpH in order to allow the model to highlight coupling of the rapidly reversible regulation to slower timescale regulation via the maximum quenching and maximum recovery envelopes over successive periods, while maintaining minimal complexity.
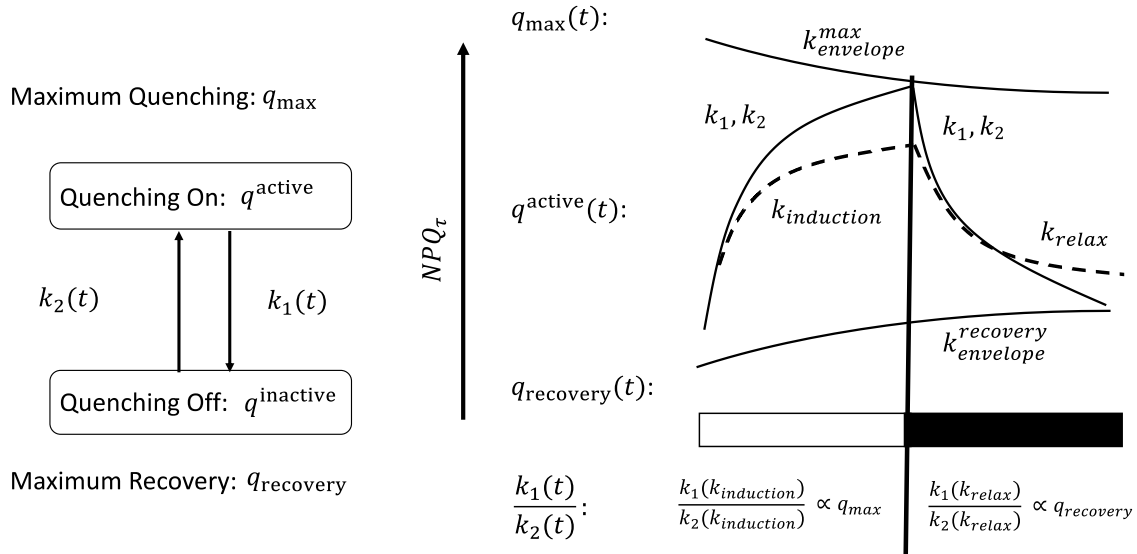
Figure 6. Schematic and diagrammatic representation of the mathematical model of the regulation of quenching. (A) The observed macroscopic quenching is represented as a two-state system that can transition between on and off states, controlled by a pair of time-dependent rate constants. (B) The quenching can move within an envelope created between the time dependent states of maximum quenching, $q_{\max}(t)$, and maximum recovery, $q_{\text{recovery}}(t)$ (*Upper and lower solid lines, unitless*). Time dependences of $q_{\max}(t)$ and $q_{\text{recovery}}(t)$ are determined by separate decay timescales of $k_{envelope}$ corresponding to each decay. The time-dependent rate constants $k_1(t)$ and $k_2(t)$ are piecewise functions of intrinsic, constant rates of rapid response occurring in the light, $k_{induction}$, and the dark, k_{relax}, modified by the time-dependent maximum quenching, $q_{\max}(t)$, in the light, or maximum recovery, $q_{\text{recovery}}(t)$, in the dark. The ratio of the time constants is proportional to $q_{\max}(t)$ in the light and $q_{\text{recovery}}(t)$ in the dark. $k_{induction}$ and k_{relax} are intrinsic rates of rapidly reversible regulation (*dashed lines*). In this formulation, the observed quenching, $q^{\text{on}}(t)$ (*solid line, between envelopes*), is contained in a single variable subject to multiple elements of regulatory control, instead of the sum of separate elements of quenching such as q_E, q_Z, and q_I.

85

Mathematically, the model is constructed using an adiabatic, or slowly varying coefficients, approximation. The piecewise portion tracks whether the light is on or off, and within each portion of the piecewise differential equation, the rate constants are determined by the intrinsic, constant, rate of induction or relaxation of the rapidly reversible quenching and the state of the maximum quenching and maximum recovery envelopes. The state of the maximum quenching and maximum recovery envelopes vary slowly relative to the induction or relaxation of the quenching within periods. Each of the maximum quenching and recovery envelopes are modeled as additional two-state differential equation systems, with constant coefficients. The approximation allows for solutions to the three two-state differential equation systems to be obtained analytically by treating the slowly varying coefficients as constants. The analytical solutions can then be equated to the fit values of the envelope and rapidly reversible induction and decays to relate all the model parameters to previously obtained fit parameters without relying on any additional fitting or free parameters.

The general equation for the conservative two-state differential equation systems is shown in Eqn. 1. Each of the three systems – the rapidly reversible system, the recovery envelope, and the maximum quenching envelope – are represented by a q^{active} describing the active value of quenching and q^{inactive} describing an inactive value of quenching. However, the output – observed quenching, NPQ_τ – is only associated with the value of q^{active} for the rapidly reversible differential equation system. The values of q^{active} for the two auxiliary differential equation systems describing the envelopes describe the bounds within which the rapidly reversible regulation can cause quenching to vary. Values of $k_1(t)$ and $k_2(t)$ are defined for the three systems, in terms of fit values, under the slowly varying coefficients approximation, in Eqns. 2-5. The rate values $k_1(t)$ and $k_2(t)$ for the rapidly reversible system, $k_1^{\text{rapid}}(t)$ and $k_2^{\text{rapid}}(t)$ defined in Eqns. 2 and 3 are piecewise defined as functions of time depending on whether the system is in the light or dark.

All of the model parameters are analytically determined from direct fits of experimental data. There are no free parameters used to fit the model result to the data. $k_{\text{fit}}^{\text{induction}}$ and $k_{\text{fit}}^{\text{relaxation}}$ are the constant best fit values of the time constants of the induction and relaxation of the rapidly reversible regulation of quenching upon the envelopes reaching steady state in the final periods of the experimental data, as shown in Figure 5A and 5B and Table 3. $q_{\text{max}}(t)$ and $q_{\text{recovery}}(t)$ are the time-dependent values of $q^{\text{on}}(t)$ associated with the auxiliary differential equation systems for the maximum quenching and recovery envelope systems, respectively. The $q_{\text{max}}(t)$ and $q_{\text{recovery}}(t)$ values contain the slowly varying time dependence of the coefficients.

For the two auxiliary differential equation systems, k_1^{env} and k_2^{env}, defined in Eqns. 4 and 5, relate the values of $k_1(t)$ and $k_2(t)$ for the maximum quenching and recovery envelope systems and are constant for each envelope. In each case, k_{fit} is defined as the best fit time constant for the exponential decay fit for the envelopes, obtained as previously described and shown in Figures 3A and 3B and Table 1. Similarly, q_{ss} is the best fit additive constant, representing the steady state value, obtained from the corresponding exponential fit.

Initial conditions are determined algebraically from the approximate analytical solutions for the conservative systems and the initial quenching values. With all the model parameters

predetermined from the direct fits of data, the system of differential equations is then solved numerically without subsequent fitting via iterative solutions to obtain the model traces presented in Figure 7.

$$\frac{d}{dt}\begin{bmatrix} q^{\text{active}} \\ q^{\text{inactive}} \end{bmatrix} = \begin{bmatrix} -k_1(t) & k_2(t) \\ k_1(t) & -k_2(t) \end{bmatrix}\begin{bmatrix} q^{\text{active}} \\ q^{\text{inactive}} \end{bmatrix} \quad (11)$$

$$k_1^{\text{rapid}}(t) = \begin{cases} k_{\text{fit}}^{\text{induction}}(1 - q_{\max}\ (t)), \text{light} \\ k_{\text{fit}}^{\text{relaxation}}(1 - q_{\text{recovery}}(t)), \text{dark} \end{cases} \quad (12)$$

$$k_2^{\text{rapid}} = \begin{cases} k_{\text{fit}}^{\text{induction}} q_{\max}(t), \text{light} \\ k_{\text{fit}}^{\text{relaxation}} q_{\text{recovery}}(t), \text{dark} \end{cases} \quad (13)$$

$$k_1^{\text{env}} = k_{\text{fit}}(1 - q_{\text{ss}}) \quad (14)$$

$$k_2^{\text{env}} = k_{\text{fit}} q_{\text{ss}} \quad (15)$$

Calculations based on the model demonstrating the roles of the contributions of both rapidly reversible dynamics and the moderate and long timescale dynamics (including both the maximum quenching and the maximum recovery dynamics) are shown in Figure 7. The model accurately describes the observed behavior of oscillatory quenching and recovery during light and dark periods constrained by multiperiod envelopes. There are discrepancies, especially for the *szl1* mutant, during the beginning of the high light portions of each period, due to the choice to neglect the very-short timescale regulatory response associated with the spike in ΔpH, described previously. However, despite the discrepancies, the simplified mathematical description allows the connection between the rapidly reversible timescale regulation and the slower regulation to be highlighted: the model demonstrates how the initial induction of NPQ depends on both the induction timescale of the rapidly reversible quenching and the dynamics of the slower timescale of the maximum quenching envelope. When comparing the model results for *wt* and *L17*, despite the intra-period dynamics of *L17* displaying a slower timescale of rapidly reversible regulation upon the envelopes reaching steady state than *wt* (cf. Fig. 5), the initial rapid induction of quenching is faster in initial periods for *L17* than *wt* due to the influence of the larger magnitude, and resulting rise, of the maximum quenching envelope. While the magnitude of the rapidly reversible quenching remains larger for *L17* throughout the experiment, it operates on a slower timescale throughout much of the experiment once the initial changes in the maximum quenching envelope decay.
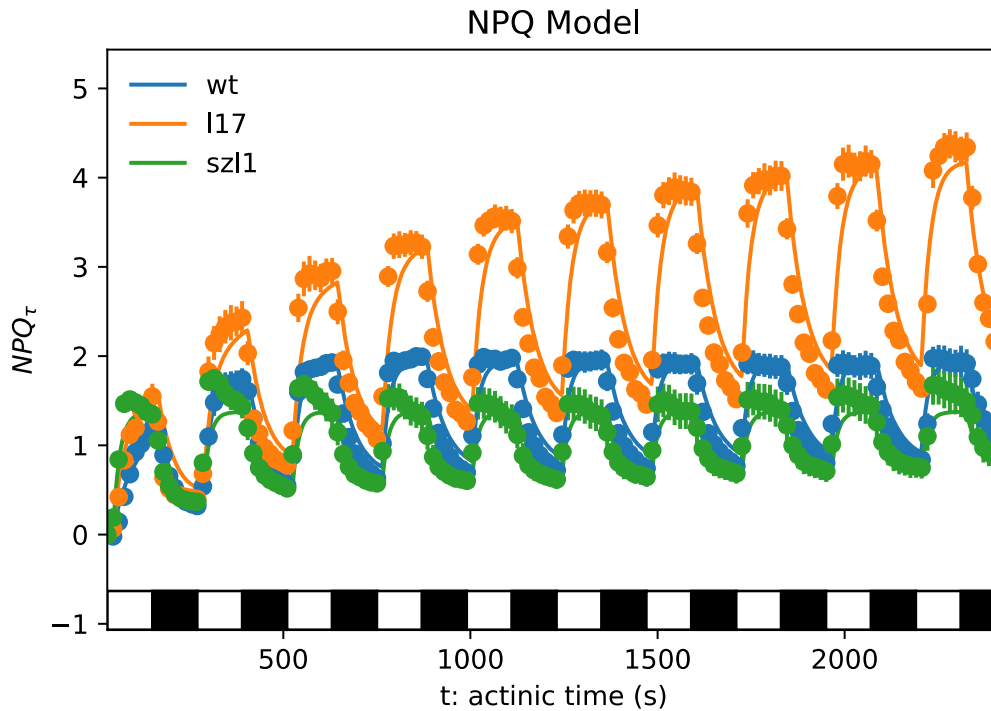
Figure 7. Comparison of modeled NPQ_τ (solid lines) with NPQ_τ values calculated from observed lifetime snapshots (circles with error bars, SD via bootstrap resampling) for the PsbS containing lines: *wt* (blue), *L17* (orange), and *szl1* (green). Model parameters are determined from best fit values of exponential decay fits of the maximum quenching and maximum recovery envelopes and the induction and relaxation of rapidly reversible quenching within a period upon reaching quasi-periodic steady state. The simple model accurately depicts the nature of rapidly reversible quenching induction and relaxation occurring simultaneously with, and coupled to, slower timescale quenching processes.

In addition, the model accurately reproduces the changing magnitude of the rapidly reversible quenching between the maximum quenching and maximum recovery envelopes over successive periods. This would not be the case for a model of rapidly reversible regulation of quenching q$_E$ that is not also coupled to slower regulation of quenching such as q$_Z$ and q$_I$, such as a formulation inferred from single light exposure period measurements where each component operated independently on either unique or shared photochemical mechanisms. This suggests that the components of quenching likely operate to regulate one or more common photochemical mechanisms in different ways, either through modification of the intrinsic quenching rate via rapidly inducible conformational changes within pigment protein complexes, or more slowly modulating the effective density of quenchers via chemical substitutions, with membrane organization changes impacting the connectivity of quenching sites to other areas of the photosynthetic antenna. This formulation could explain how zeaxanthin impacts both multiple quenching components: the substitution of zeaxanthin may influence an intrinsic rate of quenching or density of quenching sites for which zeaxanthin plays a direct role, as well as influence structural properties of pigment-protein complexes that regulate conformational fluctuations and membrane organization that activate additional or alternate quenching mechanisms.

A final conclusion can be drawn from the nature of the mathematical model required to reproduce the observed quenching. Both of the rate values $k_1(t)$ and $k_2(t)$ must be modulated by the light and the dark cycle, instead of a simpler formulation where only a single rate value is modulated by the light or dark, in order to achieve the simultaneous agreement between the observation and the model for the magnitude of the rapidly reversible quenching, and the two observed timescales of induction and relaxation. This is because the ratio of the rate constants in a two-state differential equation system determines the steady-state value (in the case e.g. the maximum quenching or maximum recovery within a period.) For a fixed recovery rate constant, either the induction rate constant or the resulting steady-state value can be accurately reproduced, but not both simultaneously. When considering how PsbS interactions with LHCII might induce quenching, the simplest conceivable mechanism assumes LHCII naturally favors an unquenched state, and when an interaction with protonated PsbS activated by ΔpH occurs, LHCII is forced into a quenched state [34, 35]. When ΔpH relaxes, the simplest assumption is then that the interaction between PsbS and LHCII ceases, the LHCII can relax back to an unquenched state. This would correspond to the description in the model where only a single rate value was modulated by the light and dark, which is unable to reproduce the observed result. Therefore, it suggests that not only do interactions between protonated PsbS and LHCII induce quenching, but also that the interactions between deprotonated PsbS and LHCII must also actively induce the recovery of LHCII from quenching, or at the very least that the protein interactions involved are not well described by such a simple kinetic scheme.

Conclusion

Isolating quenching components using periodic actinic light exposure reveals the complex, overlapping, and coupled nature of the various regulatory processes contributing to observed quenching in *A. thaliana*. Our observations of the fluorescence lifetime response to periodic light exposure suggest that not only is PsbS required for the rapidly reversible quenching, but also longer timescale components likely involving membrane organization or morphology. Dual roles of zeaxanthin are also apparent, distinct from roles observed in single light exposure period experiments. Finally, the multiple regulatory elements appear to be coupled: the magnitude of the rapidly reversible element of quenching depends on the state of slower timescale regulatory elements, but is still well described by a single intrinsic timescale of rapidly reversible quenching. We conclude by briefly summarizing major features of the data and the conclusions we draw based on our understanding of the physical picture of the processes involved.

First, focusing on the wild type, the analysis of our data reveals two clearly distinct pairs of timescales associated with the turning on and off of quenching. When the slower processes have reached steady state, there remains a rapidly reversible component that turns on in 18 s and turns on off in about one minute. We expect the chemical composition (e.g. zeaxanthin concentration) to be constant on this timescale, which also seems too short for significant membrane organization, leading us to suggest that this component arises from local protein interactions and conformational changes due to the formation and relaxation of transmembrane potential gradients. Turning to the slower components for *wt*, maximum quenching is reached in about three minutes, similar to the timescale of zeaxanthin formation by VDE [40, 46]. This is consistent with the result from the *szl1* mutant which lacks zeaxanthin and appears to use lutein instead: no detectable rise of the maximum quenching value is resolved, consistent with the putative lack of the need to replace violaxanthin for zeaxanthin in this mutant for quenching to be initiated. A slower timescale is also evident in the maximum recovery from quenching, which for *wt* is about 8 minutes. It seems likely that these slower timescales also involve changes to the membrane organization or morphology as suggested by biochemical assay and imaging experiments [18, 19].

In order to isolate the roles of the PsbS protein, we subtracted quenching recovery data of the PsbS-lacking mutant *npq4* from the data for the three PsbS-containing plants. For *wt* and *szl1*, this procedure resolves an additional timescale not discernable in the fits of the raw recovery data. *npq4* shows less recovery (e.g. more quenching) relative to *wt* and *szl1*. The discrepancy occurs with a time constant of about 30 min, but only after a transient increase of quenching during recovery in *wt* and *szl1* with about a 5 min risetime. This result is consistent with the idea that PsbS plays a significant role in the ability to recover from quenching due to changes in membrane organization or morphology, as well as in the rapid turning on or off of quenching.

At first glance, the results from the *L17* mutant with excess PsbS do not seem to fit with the picture sketched above. The rapidly reversible component isolated after steady state is reached more slowly than in *wt* or *szl1*, although the magnitude of quenching is larger; the rapid turn off is the same in all three strains. Similar trends are seen in the time required to reach maximum quenching (about four times longer for *L17* than *wt*) and the time to reach steady-state recovery (about twice that of *wt*). When the *npq4* data are subtracted, no additional timescale of recovery

levels relative to *npq4* is detected for *L17*. Instead, *L17* only shows a long-timescale fixed difference with excess quenching during recovery. One possibility is that the excess PsbS leads to some form of regulation of the membrane morphology slowing those processes that depend on changes in, for example, the connectivity of the bulk LHCII antenna. These are especially complicated to interpret given the light-dependent change in the trend of protein mobility relative to PsbS concentration [21]. In addition, PsbS's role in generating quenching sites clearly leads to greater overall maximum NPQ values and smaller recovery values, perhaps overpowering a more subtle effect of changes in membrane morphology or organization brought about by PsbS.

Our lab has recently presented spectroscopic evidence for the involvement of both excitation energy transfer and charge transfer involving chlorophyll-zeaxanthin interactions in the quenching process in *Nannochloropsis* and spinach thylakoids [45, 46, 47]. In the case of *Nannochloropsis*, both the enzyme VDE and the pH sensing protein LHCX1 (which takes the place of the plant protein PsbS) are necessary for the observation of these two pathways. However, neither process is present in the first 10-20 s of light exposure of dark-acclimated thylakoids or algae, and it seems that the rapidly reversible process must not require the conversion of violaxanthin to zeaxanthin. Although only suggestive, the similar observations between *Nannochloropsis* and spinach are consistent with results presented here for *szl1*. On the other hand, in *wt*, zeaxanthin is clearly involved in the slower components of the quenching as suggested by the greater value of maximum quenching reached in *wt* compared to *szl1* after initially being mediated by the rise of the 3 min timescale in *wt*.

Finally, the observation of changes in the magnitude of the rapidly reversible quenching over successive periods strongly suggests that individual regulatory components of quenching do not operate on independent and decoupled mechanisms. Instead, it is likely that the components of quenching – including a combination of intra-protein conformational, chemical composition, and membrane organization changes – are coupled via their operation on shared quenching sites on similar timescales. This formulation lends itself readily to developing extensible kinetic models of the regulation of quenching that can be parameterized based on the character of the fluctuations in light exposure and expression levels of proteins in the biochemical regulatory networks to enable systems models with predictive power for optimizing crop yields and design of biomimetic devices.

However, despite the potential for predictive power, kinetic models derived from fluorescence measurements alone cannot directly connect understandings of dissipative mechanisms and structural processes from steady-state measurements to the observed regulation of fluorescence studies. Snapshot transient absorption measurements have been developed that relate observables of quenching mechanisms to regulatory timescales, incorporating one aspect of quenching [46, 47]. Further development of similar "snapshot" versions of techniques that can relate changes in protein conformation dynamics or membrane organization to these regulatory timescales will be necessary to integrate understanding of physical phenomena with kinetic regulatory models. Possible avenues include combining more rapid freeze-fracture preparation [21] with advances in single-particle analysis, that can already measure changes in protein conformation distributions during enzymatic reactions in solution [61], to measure changes in pigment-protein conformational distributions over regulatory timescales, or high-speed atomic force microscopy [62, 63]. Finally, connection between resulting kinetic or regulatory models to

physical models of the photochemical mechanisms of dissipation [38] will require resolving heterogeneity to address distributions of lifetimes associated with quenching sites in various conformations and protein organizations through techniques like single molecule fluorescence detection and microscopy [64, 65] or time-resolved ultrafast stimulated emission depletion [66].

Author Information

Author Contributions

The manuscript was written through contributions of all authors. All authors have given approval to the final version of the manuscript.

Funding Sources

Acknowledgements

References

[1]   R. E. Blankenship. Molecular Mechanisms of Photosynthesis, Second Edition. Wiley-Blackwell, 2014.

[2]   B. Demmig-Adams, C. M. Cohu, J. J. Stewart, and W. W. Adams III. *Non-photochemical Quenching and Energy Dissipation in Plants, Algae and Cyanobacteria*, Volume 40. Springer Netherlands, 2014.

[3]   J. Kromdijk, K. Głowacka, L. Leonelli, S. T. Gabilly, M. Iwai, K. K. Niyogi, and S. P. Long. Improving photosynthesis and crop productivity by accelerating recovery from photoprotection. *Science*, 354(6314):857-861 (2016).

[4]   L. Tian, P. Xu, V. U. Chukhutsina, A. R. Holzwarth, and R. Croce. Zeaxanthin-dependent nonphotochemical quenching does not occur in photosystem I in the higher plant Arabidopsis thaliana. *Proceedings of the National Academy of Sciences of the United States of America*, *114*(18), 4828-4832 (2017).

[5]   K. K. Niyogi. Photoprotection revisited: genetic and molecular approaches. *Annual Review of Plant Physiology and Plant Molecular Biology*, 50(1):333–359 (1999).

[6]   B. Demmig-Adams and W. W. Adams III. Photoprotection and other responses of plants to high light stress. *Annual Review of Plant Physiology and Plant Molecular Biology*, 43:599–626 (1992).

[7]   Ruban, A. V. Nonphotochemical Chlorophyll Fluorescence Quenching: Mechanism and Effectiveness in Protecting Plants from Photodamage. *Plant Physiology*, *170*(4), 1903–16 (2016).

[8]   X.-G. Zhu, D. R. Ort, J. Whitmarsh, and S. P. Long. The slow reversibility of photosystem II thermal energy dissipation on transfer from high to low light may cause large losses in carbon gain by crop canopies: a theoretical analysis. *Journal of Experimental Botany*, 55(400):1167–1175 (2004).

[9]   Y. Tarazona, G. Kodis, K. Bhushan, J. Zaks, C. Madden, A.L. Moore, T. A. Moore, G.R. Fleming, and D. Gust. Mimicking the Role of the Antenna in Photosynthetic Photoprotection. *Journal of the American Chemical Society*, 133(9):2916-2922 (2011).

[10]   C. A. Wraight and A. R. Crofts. Energy-Dependent Quenching of Chlorophyll a Fluorescence in Isolated Chloroplasts. *European Journal of Biochemistry*, 17(2):319–327 (1970).

[11]   G. H. Krause and E. Weis. Chlorophyll Fluorescence and Photosynthesis: The Basics. *Annual Review of Plant Physiology and Plant Molecular Biology*, 42(1):313–349 (1991).

[12]   J. M. Morris and G. R. Fleming. Quantitative modeling of energy dissipation in Arabidopsis thaliana. *Environmental and Experimental Botany*, 154:99-109 (2018).

[13]   D. I. G. Bennet, K. Amarnath, S. Park, C. J. Steen, J. M. Morris, and G. R. Fleming. Models and mechanism of rapidly reversible regulation of photosynthetic light harvesting. *Open Biology*, 9:190043 (2019).

[14]   A. V. Ruban. Nonphotochemical chlorophyll fluorescence quenching: mechanism and effectiveness in protecting plants from photodamage. *Plant Physiology*, 170(4):1903–16 (2016).

[15]   Verhoeven. Sustained energy dissipation in winter evergreens. *New Phytologist*, 201: 57–65 (2014).

[16]   M. P. Johnson, M. L. Pérez-Bueno, A. Zia, P. Horton, and A. V. Ruban. The zeaxanthin-independent and zeaxanthin-dependent qE components of nonphotochemical quenching involve common conformational changes within the photosystem II antenna in Arabidopsis. *Plant Physiology*, 149(2):1061–1075 (2009).

[17]   A. V. Ruban and P. Horton. An investigation of the sustained component of non-photochemical quenching of chlorophyll fluorescence in isolated chloroplasts and leaves of spinach. *Plant Physiology*, 108(2):721–726 (1995).

[18]   M. A. Ware, V. Giovagnetti, E. Belgio, and A. V. Ruban. PsbS protein modulates non-photochemical chlorophyll fluorescence quenching in membranes depleted of photosystems. *Journal of Photochemistry and Photobiology B*: Biology, 152:301–307 (2015).

[19]   M.P. Johnson, T.K. Goral, C.D.P Duffy, A.P.R. Brain, C.W. Mullineaux, A.V. Ruban. Photoprotective energy dissipation involves the reorganization of photosystem II light harvesting complexes in the grana membrane of spinach chloroplast. *Plant Cell* 23:1468-1479 (2011).

[20]   A.Z. Kiss, A.V. Ruban, P. Horton. The PsbS Protein Controls the Organization of the Photosystem II Antenna in Higher Plant Thylakoid Membranes. *J. Bio. Chem.* 283:3972-3978 (2008).

[21]   T.K. Goral, M.P. Johnson, , C.D.P Duffy, A.P.R. Brain, A.V. Ruban, C.W. Mullineaux. Light-harvesting antenna composition controls the macromolecular organization dynamics of thylakoid membranes in Arabidopsis. *Plant J.* 69:289-301 (2012)

[22]   Brooks, M. D., Sylak-Glassman, E. J., Fleming, G. R., & Niyogi, K. K. A thioredoxin-like/β-propeller protein maintains the efficiency of light harvesting in Arabidopsis. *Proceedings of the National Academy of Sciences of the United States of America*, *110*(29), E2733-40 (2013).

[23]   P. Xu, L. Tian, M. Kloz, and R. Croce. Molecular insights into zeaxanthin-dependent quenching in higher plants. *Scientific Reports*, 5:13679 (2015).

[24]   N. E. Holt, D. Zigmantas, L. Valkunas, X. Li, K. K. Niyogi, and G. R. Fleming. Carotenoid cation formation and the regulation of photosynthetic light harvesting. *Science,* 307(5708):433–436 (2005).

[25]   T. J. Avenson, T. K. Ahn, D. Zigmantas, K. K. Niyogi, Z. Li, M. Ballottari, R. Bassi, and G. R. Fleming. Zeaxanthin radical cation formation in minor light-harvesting complexes of higher plant antenna. *The Journal of Biological Chemistry*, 283(6):3550–3558 (2008).

[26]   T. K. Ahn, T. J. Avenson, M. Ballottari, Y. Cheng, K. K. Niyogi, R. Bassi, and G. R. Fleming. Architecture of a charge-transfer state regulating light harvesting in a plant antenna protein. *Science*, 320(5877):794 (2008).

[27]   S. Bode, C. C. Quentmeier, P. Liao, N. Hafi, T. Barros, L. Wilk, F. Bittner, and P. J. Walla. On the regulation of photosynthesis by excitonic interactions between carotenoids and chlorophylls. *Proceedings of the National Academy of Sciences of the United States of America*, 106(30):12311–6 (2009).

[28]   P. Horton, A.V. Ruban, and M. Wentworth. Allosteric regulation of the light-harvesting system of photosystem II. *Philosophical Transactions of the Royal Society of London B*: *Biological Sciences*, 355:1361–1370 (2000).

[29]   M. Nilkens, E. Kress, P. Lambrev, Y. Miloslavina, M. Müller, A. R. Holzwarth, and P. Jahns. Identification of a slowly inducible zeaxanthin- dependent component of non-photochemical quenching of chlorophyll fluorescence generated under steady-state conditions in Arabidopsis. *Biochimica et Biophysica Acta (BBA) - Bioenergetics*, 1797(4):466–475 (2010).

[30]   G. Noctor, D. Rees, A. Young, P. Horton. The relationship between zeaxanthin, energy-dependent quenching of chlorophyll fluorescence, and trans-thylakoid pH gradient in isolated chloroplasts. *Biochimica et Biophysica Acta*, 1057:320-330 (1991).

[31]   X.-P. Li, A. M. Gilmore, S. Caffarri, R. Bassi, T. Golan, D. Kramer, and K. K. Niyogi. Regulation of photosynthetic light harvesting involves intrathylakoid lumen pH sensing by the PsbS protein. *The Journal of Biological Chemistry*, 279(22):22866–74 (2004).

[32]   X.-P. Li, O. Björkman, C. Shih, A. R. Grossman, M. Rosenquist, S. Jansson, and K. K. Niyogi. A pigment-binding protein essential for regulation of photosynthetic light harvesting. *Nature*, 403(6768):391–395 (2000).

[33]   V. Correa-Galvis, G. Poschmann, M. Melzer, K. Shühler, P. Jahns. PsbS interactions involved in the activation of energy dissipation in Arabidopsis. *Nature Plants* 2:15225 (2016).

[34]   P. Jahns, D. Latowski, and K. Strzalka. Mechanism and regulation of the violaxanthin cycle: The role of antenna proteins and membrane lipids. *Biochimica et Biophysica Acta (BBA) – Bioenergetics*, 1787(1):3-14,(2009).

[35]   J. Sacharz, V. Giovagnetti, P. Ungerer, G. Mastroianni, A. V. Ruban. The xanthophyll cycle affects reversible interactions between PsbS and light-harvesting complex II to control non-photochemcial quenching. *Nature Plants* 3:16225 (2017).

[36]   G.W. Robinson. Excitation Transfer and Trapping in Photosynthesis. Brookhaven Symposia in Biology Number 19: Energy Conversion by the Photosynthetic Apparatus, Report of Symposium Held at Upton June 6–9, 1966, Upton, NY, 1967.

[37]   K. Amarnath, D. I. G. Bennett, A. R. Schneider, and G. R. Fleming. Multiscale modeling of light harvesting by photosystem II in plants. *Proceedings of the National Academy of Sciences of the United States of America*, 113(5):1156–1161 (2015).

[38]   D.I.G Bennett, G.R. Fleming, K. Amarnath. Energy-dependent quenching adjusts the excitation diffusion length to regulate photosynthetic light harvesting. *Proceedings of the National Academy of Sciences of the United States of America* 115:E9523 (2018).

[39]   E. J. Sylak-Glassman, A. Malnoë, E. De Re, M. D. Brooks, A. L. Fischer, K. K Niyogi, and G. R. Fleming. Distinct roles of the photosystem II protein PsbS and zeaxanthin in the regulation of light harvesting in plants revealed by fluorescence lifetime snapshots. *Proceedings of the National Academy of Sciences of the United States of America*, 111(49):17498-503 (2014).

[40]   M. Leuenberger, J. M. Morris, A. M. Chan, L. Leonelli, K. K, Niyogi, and G. R. Fleming. Dissecting and modeling zeaxanthin- and lutein-dependent nonphotochemical quenching in Arabidopsis thaliana. *Proceedings of the National Academy of Sciences of the United States of America*, 114(33):E7009-E7017 (2017).

[41]   P. Horton, M. Wentworth, and A.V. Ruban. Control of the light harvesting function of chloroplast membranes: the LHCII aggregation model for non-photochemical quenching. *Federation of European Biochemical Societies Letters*, 579:4201–4206 (2005).

[42]   A. Dreuw, G.R. Fleming, M. Head-Gordon. Charge-transfer state as a possible signature of a zeaxanthin-chlorophyll dimer in the non-photochemical quenching process in green plants. *J. Phys. Chem. B*, 107:6500-6503 (2003).

[43]   A. Dreuw, G.R. Fleming, M. Head-Gordon. Chlorophyll fluorescence quenching by xanthophylls. *Phys. Chem. Chem. Phys.*, 5:3247 (2003).

[44]   A. Dreuw, G.R. Fleming, M. Head-Gordon. Role of electron-transfer quenching of chlorophyll fluorescence by carotenoids in non-photochemical quenching of green plants. *Biochem. Soc. Trans.*, 33:858-862 (2005).

[45]   S. Park, C.J. Steen, D. Lyska, A.L. Fischer, B. Endelman, M. Iwai, K.K. Niyogi, G.R. Fleming. Chlorophyll-carotenoid excitation energy transfer and charge transfer in *Nannochloroopsis oceanica* for the regulation of photosynthesis. *Proceedings of the National Academy of Sciences of the United States of America*, 116(9):3385-3390 (2019).

[46]   S. Park, A.L. Fischer, C.J. Steen, M. Iwai, J.M. Morris, P.J. Walla, K.K. Niyogi, G.R. Fleming. Chlorophyll-Carotenoid Excitation Energy Transfer in High-Light Exposed Thylakoid Membranes Investigated by Snapshot Transient Absorption Spectroscopy. *J. Am. Chem. Soc.* 140:11965-11973 (2018).

[47]   S. Park, C.J. Steen, A.L. Fischer, G.R. Fleming, Snapshot transient absorption spectroscopy: toward in vivo investigations of nonphotochemical quenching mechanisms. *Photosynthesis Research*, https://doi.org/10.1007/s11120-019-00640-x (2019).

[48]   G.S. Schlau-Cohen, H.-Y. Yang, T.P.J. Krüger, P. Xu, M. Gwizdala, R. van Grondelle, R. Croce, W.E. Moerner. Single-molecule identification of quenched and unquenched states of LHCII. *J. Phys. Chem. Lett.*, 6:860-867 (2015).

[49]   T. Kondo, A. Pinnola, W.J. Chen, L. Dall'Osto, R. Bassi, G.S. Schlau-Cohen. Single-molecule spectroscopy of LHCSR1 protein dynamics identifies two distinct states

responsible for multi-timescale photosynthetic photoprotection. *Nat. Chem.*, 9:772-778 (2017).

[50] Külheim, J. Agren, S. Jansson. Rapid regulation of light harvesting and plant fitness in the field. *Science* 297(5578):91-91 (2002).

[51] Y. Yang, L. Xu, J. A. Cruz, L. J. Savage, D. M. Kramer, J. Chen. PhenoCurve: capturing dynamic phenotype-environment relationships using phenomics data. Bioinformatics, 33(9):1370-1378 (2017).

[52] Y. Tian, J. Sacharz, M. A. Ware, H. Zhang, A. V. Ruban. Effects of periodic photoinhibitory light exposure on physiology and productivity of Arabidopsis plants grown under low light. J. Exp. Botany, 68(15):4249-4262 (2017).

[53] E. J. Sylak-Glassman, J. Zaks, K. Amarnath, M. Leuenberger, and G. R. Fleming. Characterizing non-photochemical quenching in leaves through fluorescence lifetime snapshots. *Photosynthesis Research*, 127(1):69–76, (2016).

[54] Z. Li, T. K. Ahn, T. J. Avenson, M. Ballottari, J. A. Cruz, D. M. Kramer, R. Bassi, G. R. Fleming, J. D. Keasling, and K. K. Niyogi. Lutein accumulation in the absence of zeaxanthin restores nonphotochemical quenching in the Arabidopsis thaliana npq1 mutant. *The Plant Cell*, 21(6):1798–812, (2009).

[55] X-P. Li, P. Müller-Moulé, A. M. Gilmore, and K. K. Niyogi. PsbS-dependent enhancement of feedback de-excitation protects photosystem II from photoinhibition. *Proceedings of the National Academy of Sciences of the United States of America*, 99(23):15222-15227 (2002).

[56] M. Havaux and K. K. Niyogi. The violaxanthin cycle protects plants from photooxidative damage by more than one mechanism. *Proceedings of the National Academy of Sciences of the United States of America*, 96(15):8762-8767 (1999).

[57] G. Schansker, S. Z. Toth, and R. J. Strasser. Dark recovery of the Chl a fluorescence transient (OJIP) after light adaptation: The qT-component of non- photochemical quenching is related to an activated photosystem I acceptor side. *Biochimica et Biophysica Acta (BBA) - Bioenergetics*, 1757(7):787–797, (2006).

[58] K. Takizawa, J. A. Cruz, D. M. Kramer. The thylakoid proton motive force in vivo. Quantitative, non-invasive probes, energetics, and regulatory consequences of light-induced pmf. Biochimica Biophysica Acta 1767:1233-1244 (2007).

[59] J. Zaks, K. Amarnath, D. M. Kramer, K. K. Niyogi, and G. R. Fleming. A kinetic model of rapidly reversible nonphotochemical quenching. *Proceedings of the National Academy of Sciences of the United States of America*, 109(39):15757–62 (2012).

[60] A. Matuszyńska, S. Heidari, P. Jahns, O. Ebenhöh. A mathematical model of non-photochemical quenching to study short-term light memory in plants. *Biochimica et Biophysica Acta (BBA) – Bioenergetics* 1857(12):1860-1869 (2016).

[61] J. Frank. Time-resolved cryo-electron microscopy: Recent progress. *Journal of Structural Biology* 200(3):303-306 (2017).

[62] Onoa, S. Fukuda, M. Iwai, K.K. Niyogi, C. Bustamante. Dynamic Characterization of Photosynthetic Proteins on Thylakoid Membranes by High-Speed AFM. Biophysical Journal 114(3)S1:70a (2018)

[63] Onoa, S. Fukuda, M. Iwai, C. Bustamante, K.K. Niyogi. High-speed atomic force microscopy visualizes the mobility of photosynthetic proteins in grana thylakoid membranes. bioRxiv doi:10.1101/426759 (2018).

[64]   J. Ogren, A. Tong, S. Gordon, A. Chenu, Y. Lu, R. Blankenship, J. Cao, G.S. Schlau-Cohen. Impact of the lipid bilayer on energy transfer kinetics in the photosynthetic protein LH2. *Chem Sci*, 8:3095 (2018).

[65]   M. Tutkus, F. Saccon, J. Chmeliov, O. Venckus, I. Ciplys, A. V. Ruban, L. Valkunas. Single-molecule microscopy studies of LHCII enriched in Vio or Zea. *BBA-Bioenergetics* 1860:499-507 (2019).

[66]   S.B. Penwell, L.D.S. Ginsberg, R. Noriega, N.S. Ginsberg. Resolving ultrafast exciton migration in organic solids at the nanoscale. *Nature Materials* 16:1136-1141 (2017).

Chapter 4: Analysis Methods

Introduction

As discussed throughout, fluorescence measurements of photosynthetic systems are a powerful tool for observing the behavior of protective energy dissipative mechanisms, collectively known as non-photochemical quenching. Upon "closing" reaction centers with saturating light, the productive path for utilizing energy from photons absorbed by chromophores via photochemistry is blocked, leaving a variety of other pathways for energy to dissipate (Brooks 2011). As one of these paths is fluorescence, changes in the fluorescence yield, or equivalently, lifetime, are able to indirectly monitor changes in the ability of excitonic energy to be dissipated through alternative pathways. Because plants and other photosynthetic organisms face highly variable light conditions (Külheim et al. 2002), the ability to rapidly tune the amount of energy that is dissipated through non-photochemical quenching mechanisms to the light conditions is advantageous to both prevent photodamage due to the occurrence of unwanted photochemical reactions and avoid unnecessarily dissipating excess energy in order to ensure efficient conversion of solar energy to chemical energy (Demmig-Adams et al. 2014).

Energy transfer, photochemistry, and dissipation are "ultrafast" processes, occurring on timescales between femtoseconds to picoseconds, long studied with spectroscopic techniques in chemical systems (Morris and Fleming 2018). However, in order to tune the photosynthetic apparatus to changing light conditions, plants regulate these ultrafast processes on timescales as short as a few seconds. In studying the relationship between the ultrafast processes and their regulation, experiments must be able to resolve the ultrafast processes in relatively short averaging times in order to observe changes in the ultrafast processes subject to dynamic regulation on the order of seconds.

For example, as discussed extensively in previous chapters, important questions in the field surround the nature of the component of non-photochemical quenching characterized by rapidly reversible regulation, qE: are the photochemical mechanisms of dissipation that cause qE within a few seconds of a transition from dark to high light the same as mechanisms that would be observed after a long time exposure to high light? Measurements that are able to resolve the ultrafast processes, but require long averaging time (to achieve adequate signal to noise) relative to the plants' ability to regulate the underlying ultrafast processes cannot address such a question. To address questions like those concerning qE, the acquisition of data capable of resolving the ultrafast processes must be faster than the timescales on which the ultrafast processes are regulated.

A common measure of non-photochemical quenching is the NPQ parameter, traditionally defined as

$$NPQ = \frac{(F_m - F'_m)}{F'_m}$$

with F_m defined as the maximum fluorescence (upon closing reaction centers) after dark acclimation and F'_m as the variable fluorescence (upon closing reaction centers) upon exposure to actinic light (Blankenship 2014). The variability of F'_m can occur in timescales of as fast as a few

seconds – rapid, but still well separated from the timescales of the underlying ultrafast photochemical processes. Traditionally these fluorescence values are measured as yield, e.g. the ratio of emitted fluorescence to absorbed light, via a ubiquitous technique called pulse-amplitude modulated (PAM) fluorometry (Brooks and Niyogi 2011). However, because PAM measures fluorescence yield, it is subject to problems that make extended measurements of NPQ over longer exposure periods difficult.

The experimental determination of yield is sensitive to the absorption cross section. Plants have been documented to regulate their absorption cross section on timescales similar to that of NPQ using processes such as chloroplast avoidance (Sylak-Glassman et al. 2014a, Cazzaniga et al. 2013). Therefore, in order to measure timescales of processes impacting fluorescence yields, that may be similar to timescales impacting the absorption cross section, either the changes in absorption cross section must be accounted for or a measurement insensitive to such changes devised.

A measurement of fluorescence lifetime is one such method that is insensitive to changes in the absorption cross section, and obtains all the information obtained in a fluorescence yield measurement. Following the notation in Lakowicz (Lakowicz 2006), the fluorescence yield can be defined as

$$\Phi_f = \frac{k_f}{k_f + \sum k_{other}}$$

where Φ_f denotes the fluorescence yield, k_f denotes the rate of fluorescence, and k_{other} denotes the rates of other, non-fluorescence processes. The fluorescence lifetime is similarly defined as

$$\tau_f = \frac{1}{k_f + \sum k_{other}}$$

where τ_f. Thus,

$$\Phi_f = k_f \tau_f$$

and therefore a measurement of the fluorescence lifetime is equivalent to a measure of the fluorescence yield, up to an (assumed) constant rate of fluorescence that cancels out in the definition of the measure NPQ.

In addition to obtaining information equivalent to fluorescence yield, a measurement of fluorescence lifetime can, in principle, also observe simultaneous changes in separate lifetime components. However, in complicated systems like the photosynthetic apparatus, the observed lifetimes are an average of the distribution of many lifetimes. (In principle, each chromophore may have a unique and fluctuating lifetime.)

One experimental technique to monitor changes in fluorescence is time correlated single photon counting (TCSPC). TCSPC measures the arrival time of photons relative to a reference photon. Over successive laser pulses, a histogram of the arrival times is created enabling the

measurement of fluorescence lifetimes upon fitting the characteristic decay timescale(s) of the histogram. Removing the influence of chloroplast avoidance allows for longer measurements to be performed, in turn facilitating multiple actinic light exposure periods to be performed to measure repeated induction and relaxation of quenching. Using periodic actinic light schemes allows for simultaneously observing fast and slow regulatory dynamics.

Practical considerations for obtaining, processing, analyzing, and interpreting snapshot fluorescence measurements are numerous. For discussion of practical considerations of obtaining and the initial processing of TCSPC data on whole leaves suitable for further analysis, the reader is referred to previous journal publications and dissertations (Sylak-Glassman 2014a, Sylak-Glassmann 2014b, Sylak-Glassmann 2016, Leuenberger 2017a, Leuenberger 2017b). These include the design and setup and configuration of the laser apparatus, fitting numerous fluorescence decays and determining that reaction centers are "closed" to obtain data analogous to PAM traces, and organizing data into forms suitable for further analysis and interpretation. Despite utilizing more complex actinic light exposure patterns, many of these practical considerations are largely the same as in TCSPC snapshot experiments with simpler actinic exposure patterns, apart from requiring updated processing scripting to organize raw data into convenient data structures for subsequent analyses. This scripting depends heavily on the specifics of a particular experiment and the desired analyses.

The remainder of this chapter focuses on aspects of analyzing and interpreting snapshot fluorescence lifetime data obtained using complex actinic exposure patterns to probe and quantify aspects of the regulatory response of quenching. First, a technique involving interleaving data from measurements on separate leaves to achieve increased actinic timescale resolution is discussed, including the application of filters to remove artifacts of leaf-to-leave systematic variability that introduce high frequency oscillation in the data. Second, the application of singular value decomposition on complex data sets for validation and filtering is discussed.

Filtering

Measurement of NPQ using TCSPC snapshots has been validated at 30 s resolution against PAM traces without damage to the leaf sample ((Sylak-Glassman et al. 2014a, Sylak-Glassmann 2014b, Sylak-Glassmann et al. 2016, Leuenberger et al. 2017a, Leuenberger 2017b). However, the induction of quenching occurs on similar timescales. At 30 s resolution, much of the turn on has occurred within the first 30 s, making it difficult to resolve the actual induction timescale. Therefore, in order to achieve 15 s resolution, measurements can be performed on two leaves, each at 30 s resolution, but with a 15 s offset. In the case of periodic measurement at constant time separation, this 15 s offset can be referred to as a phase offset. Upon obtaining 30 s resolution measurements on two leaves, the two data series can be combined in order to achieve a 15 s resolution data series. These data series are then averaged to obtain characteristic fluorescence traces that can be further analyzed to obtain measures of NPQ via the process outlined above.

However, combining these measurements introduces the effects of leaf-to-leaf variability in fluorescence lifetime within a single data series that is not present in a data series obtained from a single leaf, as discussed in Chapter 3. In the case that the leaf-to-leaf variability is small relative to measurement-to-measurement variability within a leaf, this could be ignored. However, this is not the case – the leaf-to-leaf variability is larger than measurement-to-measurement variability introducing a high frequency oscillation in the observed fluorescence lifetimes within a single two-leaf sample trace. Simply averaging over numerous samples would require large numbers of leaf samples – double that of a measurement using single-leaf samples to obtain similar resolutions. However, because the period of experimental artifacts is known (15 s, in this case), a filtering process can be applied to remove the oscillations arising due to the interleaving of data series collected from multiple leaf samples without requiring a large increase in the total number of leaf samples required to impractical levels.

The process of filtering must be undertaken carefully, as filtering can introduce additional artifacts in the data that interfere with important properties of the data set. Selection or design of a filter often requires balancing contradictory requirements (Antoniou 2018). In the case of the periodic actinic light measurement, the fundamental oscillation frequency is determined by the driving frequency of the actinic light. (In the case considered in the previous chapter, the actinic light had a 2 minute half-period, or a 240 s period.) Therefore, a 15s period artifact is much shorter in period (equivalently, higher in frequency) than the data, suggesting a low-pass filter is appropriate. In the case of a low pass filter, high frequencies are attenuated and lower frequencies are preserved.

However, despite the low fundamental frequencies involved, the transitions from light-to-dark and dark-to-light are rapid, and thus the observed data set is essentially a repeated observation of the step response of the quenching system. This results in rapid decay (or rise) to the resulting quenching levels. When rapid decays (and rises) such as those observed are Fourier analyzed, the ability to rapidly tune the quenching levels in response to a step in the light are observed as relatively high frequencies. Removing high frequency components of a step response can introducing "ringing" to a signal, where the filtered signal overshoots the actual response at first, then recovers excessively before settling to the actual response. Care must be taken to ensure that further analysis of the signal is not impacted by ringing, or that uncertainty introduced by ringing is considered and accounted for.

Here, a low-pass Butterworth filter is chosen, due to the characteristics of a flat frequency response below the cutoff frequency, that therefore will minimally impact moderate timescale signals of interest for further analysis of the period-to-period changes in the data set (Butterworth 1930). However, the Butterworth filter is susceptible to ringing, that can impact further analysis of rapid step responses, but in this case, the measurement-to-measurement variability is still large enough that significant ringing is not readily apparent. A Bode plot, displaying the complex transfer function (e.g. the effect of the filter on the amplitude and phase of an input signal at various frequencies) of a Butterworth filter is provided in Figure 1. The cutoff frequency in the example Bode plot is 1 rad/s. Frequencies below the cutoff frequency (in the passband) have a nearly flat amplitude gain of zero, indicating that they are well preserved. Frequencies above the cutoff frequency (in the stopband) have amplitudes attenuated. The phase response is also relatively flat in the passband, compared to many other filter choices.
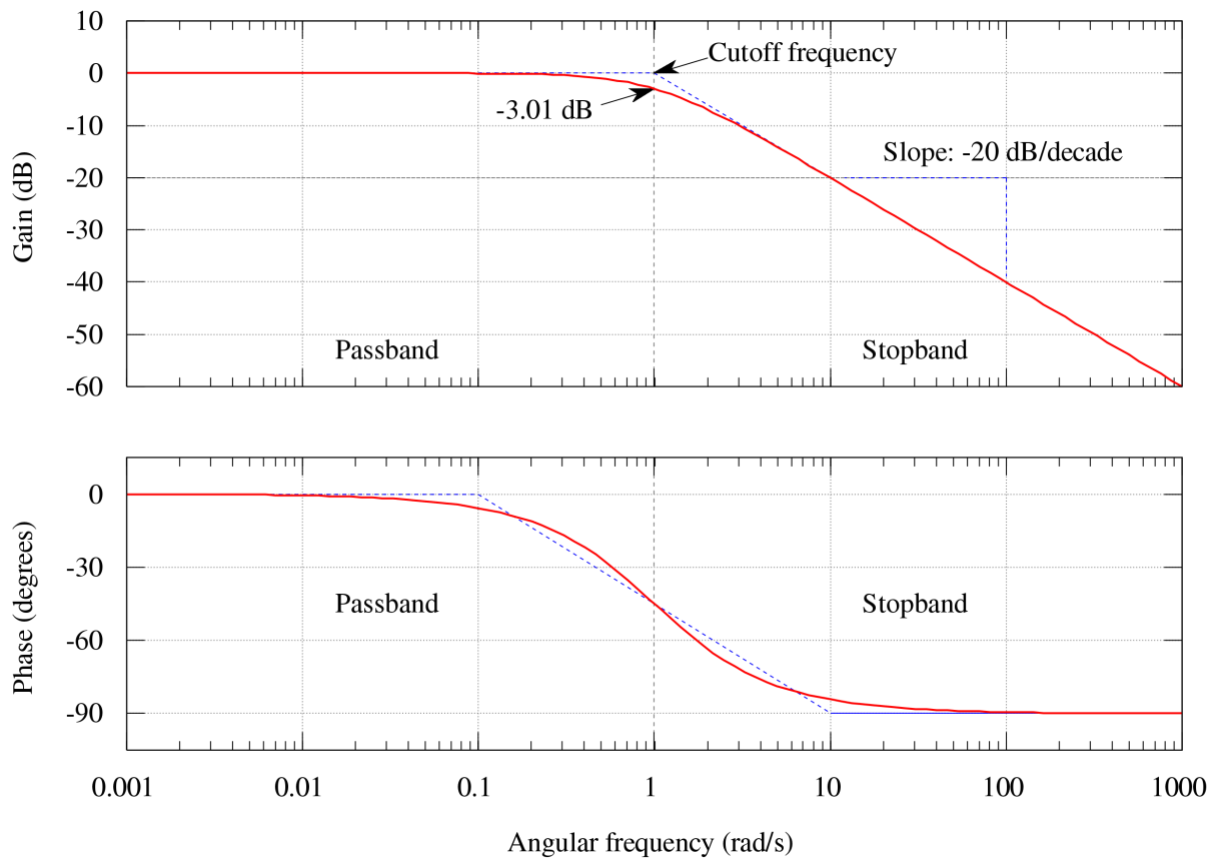

Figure 1. Bode Plot of an example Butterworth Filter with cutoff frequency of 1, with annotations demonstrating the low frequency passband and high frequency stopband, the location of the cutoff frequency, and the attenuation at the cutoff frequency. Original image generated by Alessio Damato for use on Wikipedia's entry on the Butterworth Filter under a CC BY-SA 3.0 license.

In order to apply the first order Butterworth filter to the interleaved data, the cutoff frequency is selected as half the Nyquist frequency of the interleaved data. The Nyquist frequency is the one half of the sampling rate; therefore, the highest frequency components the experiment can resolve without introducing aliasing are 30^{-1} s^{-1} For the interleaved data, the sampling rate is 15^{-1} s^{-1}; therefore, the cutoff frequency is 60^{-1} s^{-1}; so the 15^{-1} s^{-1} frequency oscillation is attenuated by 12dB. The filter is applied numerically using an infinite impulse response discretization of the analog Butterworth filter using second-order sections, implemented in SciPy signal processing package (Jones et al. 2001).

Because each leaf sample is independent, any individual combination of 0 s and 15 s phase offset pairings is equally valid. Therefore, in order to estimate the error in the filtered traces, a bootstrapping method is applied. Each pairwise combination of interleaved 0 s and 15 s data series are treated independently, and the filter applied. This method generates a set of filtered traces with a mean and standard deviation at each time index or time point, allowing an estimate of the uncertainty after filtering to be applied.

Figures 2-4 visualize the process for an example data set of lifetimes. In Figure 2, an example set of pairwise combinations are plotted, with each combination shown in a different color. The high frequency oscillation is apparent in each trace. Figure 3 shows the results of applying the filter to each pairwise combination. Upon applying the filter, the high frequency oscillation in each pairing is removed. There is still significant variance between individual combinations, resulting from leaf-to-leaf variation that is much larger than the variance between successive snapshots on an individual leaf sample. Figure 4 shows the trace of the mean and standard deviation of the filtered combinations overlaid with a scatter plot of the original data points.
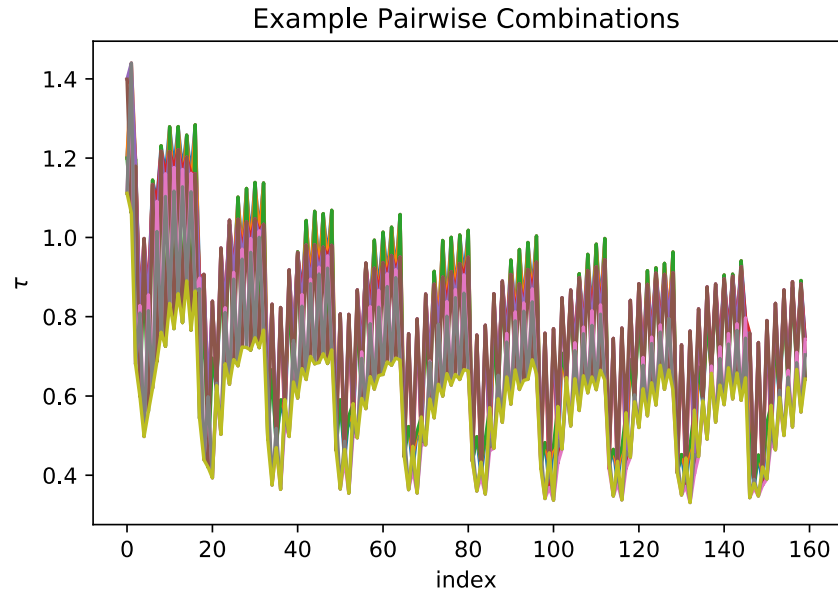
Figure 2. Example pairwise combinations of 0 s and 15 s phase offset TCPSC snapshot fluorescence lifetime traces at 30 s resolution. Fluorescence lifetime values in ns (y-axis) from TCPSC snapshots are plotted by the index of the timepoint (x-axis), for convenience of the subsequent application of the Butterworth filter that is parameterized by a cutoff frequency that is normalized by the Nyquist frequency. The resolution between each index unit is 15 s. Each color represents a unique combination of an individual 0 s and 15 s phase offset trace. Oscillations between successive timepoints are apparent that are much larger than the variance between successive snapshot measurements performed upon a single leave generated at 30s resolution (even and odd indices within a combination.)
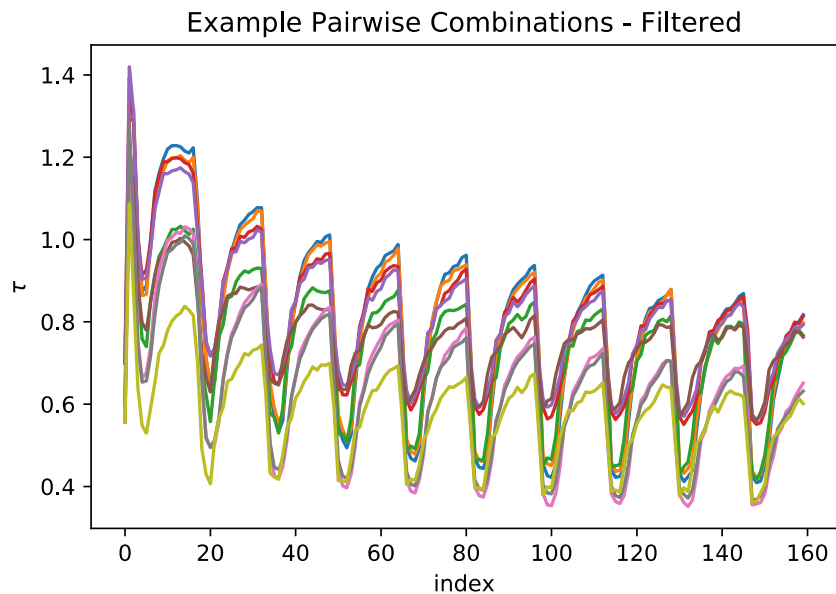
Figure 3. Results of application of a 1st order Butterworth filter with a cutoff frequency of half the Nyquist frequency to the pairwise combinations shown in Figure 2. Each colored trace represents the results of the application of the filter to an individual pairwise combination. Filtered fluorescence lifetime values in ns (y-axis) are plotted by the index of the timepoint (x-axis), for convenience of the application of the Butterworth filter that is parameterized by a cutoff frequency that is normalized by the Nyquist frequency. The resolution between each index unit is 15 s. The large oscillations between successive timepoints introduced by interleaving the 30 s resolution data series are removed.
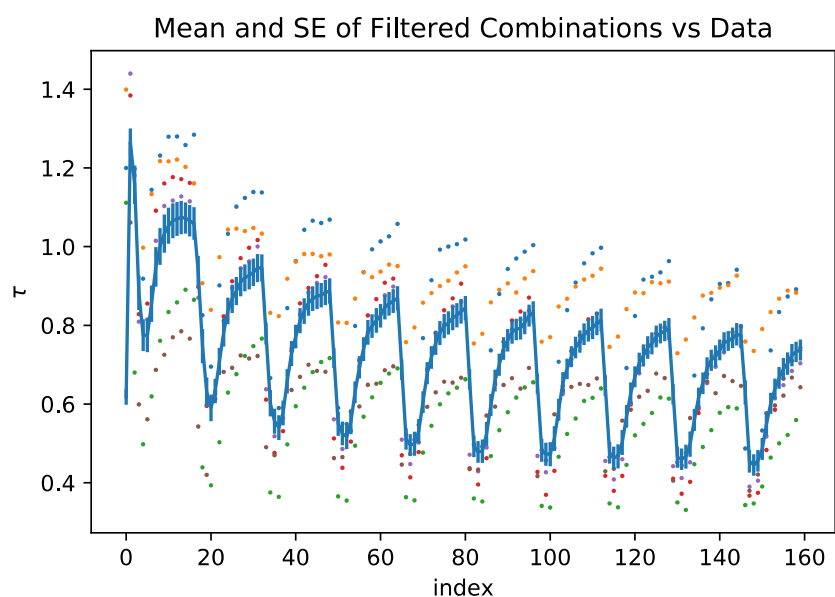
Figure 4. Mean and standard deviation of filtered combinations (blue line and error bars) overlaid on a scatter plot of individual TCSPC snapshot fluorescence lifetime measurements (points, multiple colors representing snapshots obtained from a single leaf sample). Fluorescence lifetime values and the resulting filtered mean in ns (y-axis) from TCPSC snapshots are plotted by the index of the timepoint (x-axis), for convenience of the subsequent application of the Butterworth filter that is parameterized by a cutoff frequency is normalized by the Nyquist frequency. The resolution between each index unit is 15 s.

In order to validate the resulting filtered data series means and uncertainties, the mean and standard deviation of the filtered pairwise combinations are plotted for comparison overlaying a plot of the naïve mean and standard deviation of the individual traces in Figure 5. The naïve mean, in blue, shows considerable high frequency oscillation, relative to the snapshot-to-snapshot variance. Alternating time points, arising from the 0 s and 15 s phase offset samples at 30 s resolution, form a pair of smooth traces, but upon interleaving, the resulting 15 s resolution data oscillates with a magnitude similar to the uncertainty of each individual 30 s resolution trace. In comparison, the filtered data plotted in orange appears to average out the oscillation, tracing a path intuitively similar the average of successive timepoints from the two 30 s resolution data series. The uncertainty generated from the standard deviation is similar to the magnitude of the oscillation, effectively capturing an estimate of the variance between the two combined data series.
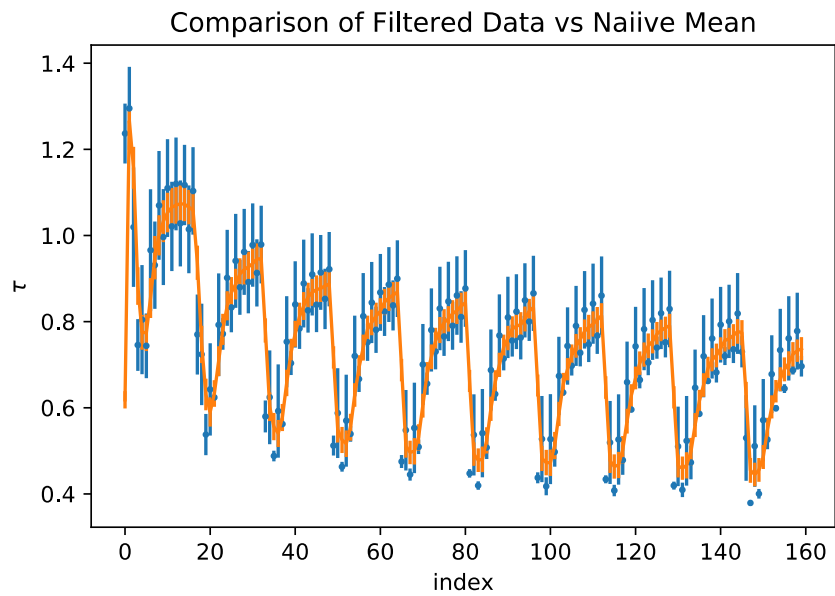
Figure 5. Mean and standard deviation of filtered combinations (orange line and error bars) overlaid with the naïve mean and standard deviation of TCSPC snapshot fluorescence lifetime measurements (blue line and error bars). The filtered values trace out smooth curves that eliminate the oscillatory behavior that arises from interleaving data from pairs of individual leaf samples, with error estimates that are similar in magnitude to the variance between mean traces obtained from individual leaves. Mean fluorescence lifetime values and the associated filtered mean in ns (y-axis) from TCPSC snapshots are plotted by the index of the timepoint (x-axis), for convenience of the subsequent application of the Butterworth filter that is parameterized by a cutoff frequency is normalized by the Nyquist frequency. The resolution between each index unit is 15 s.

The comparison between the filtered means and the naïve means and associated uncertainties also allows for an evaluation of whether the potential for "ringing" characteristic of the Butterworth filter's application to step responses is significant. The filtered traces faithfully remain within the variability between the two 30 s resolution traces, suggestive that the filtering of the high frequency components does not generate ringing that would impact subsequent analysis. This is likely due to the particular choice of the cutoff frequency in relation to the sampling rate and the Nyquist frequency, that limits the resolution of the underlying data.

Singular Value Decomposition

Rich and complex data sets are difficult to interpret. Often, in spectroscopic measurements of *in vivo* systems, many processes can impact the results of a measurement. Therefore, an ability to isolate the contributions of various dynamical processes is an important aspect of any measurement. This is often the case in the study of photosynthesis and NPQ, where many aspects of the complex biological system influence the ability of photosynthetic organisms to adapt to their environments. As discussed throughout much of this work, one challenge involves distinguishing the effects on the observed fluorescence lifetimes that arise from the simultaneous induction of

quenching processes that are regulated independently or on separate timescales. Two examples this can occur in are the multiple decay exponential decay components of a fluorescence lifetime on ultrafast timescales or features of the regulation of quenching during a snapshot lifetime trace in response to actinic light over seconds to minutes timescales.

Singular value decomposition (SVD) provides one analysis method to determine independent features of these data sets. SVD is often used in signal processing and statistics for methods such as principle component analysis (Jackson 1980, 1981), relevant to the analysis of spectroscopic measurements for filtering such as in two-dimensional electronic vibrational (2DEV) spectroscopy that must deal with highly congested spectra (Lewis 2016). Mathematically, SVD is a generalization of eigen decomposition, a factorization of a matrix into eigenvalues and linearly independent eigenvectors, that is a common tool in the physical sciences and familiar to physical chemists from quantum mechanics. The SVD of a matrix, X, involves the factorization of X into three matrices

$$X = U\Sigma V^*$$

that describe two sets of singular vectors (contained in U and V^*) that are similar to eigenvectors and a set of singular values (contained in Σ) that are similar to eigenvalues. Imprecisely (to avoid technical mathematical jargon), it generalizes the eigen decomposition from a subset of square matrices that have special properties (including the Hermitian matrices of quantum mechanics) to a more general non-square matrix, as might arise when measuring a relatively small number of items (such as the lifetime components of a fluorescence decay, or the response of quenching to a light-to-dark transition) repeatedly over time.

The utility and interpretation of the singular vectors and singular values depends on the structure of the matrix X. In the analysis of TCSPC snapshot experiments, the structure of X involves structuring the data into rows and columns based on separation of timescales. In the analysis used in Chapter 2, the separation of timescales is the separation between the ultrafast timescales of decay components of individual fluorescence lifetime snapshots and the regulatory timescales in response to actinic light. The analysis is also possible for periodic actinic light measurements such as those in Chapter 3 based on the separation of between intra-period and inter-period behavior. In either case, successive rows of the matrix X are formed by tiling the repeated measurement (either the ultrafast fluorescence decays themselves, the amplitudes & lifetimes, in the case of the analysis of Chapter 2 or the amplitude weighted average lifetime). This process is similar to the analysis of more complicated multi-dimensional spectra such as 2DEV by encoding successive 2DEV spectra at different waiting times into successive rows (Lewis 2016).

The subsequent example analysis utilizes SVD to separate long timescale dynamics from short timescale components, and is similar to Alter et al.'s application of SVD to genomics data (Alter et al. 2000). As an example, consider the TCSPC snapshot data collected using periodic actinic light presented in Figure 6. The dynamics of fluorescence lifetimes of *A. thaliana* leaves are plotted over 40 minutes of exposure to periodic actinic light with a 2 minute half-period, showing repeated induction and relaxation of quenching for two mutant lines. Over successive periods, the recovery or quenching decreases, showing moderate-to-long timescale dynamics that co-occur with fast regulatory dynamics of induction and recovery within each period. In this case,

the separation of timescales used to construct the matrix X are the repeated intra-period measurements over successive periods. Considering only a single trace, e.g. from the WT data series, the data forms a vector of average lifetime values, ordered as the measurements during repeated periods of high light and dark. This vector can be split into the values of the average lifetimes during each period, and reshaped into a matrix where each row is subset of the vector from each period. A visualization is shown in Figure 7, with the resulting matrix X obtained from this tiling procedure visualized as a heat map shown in Figure 8.
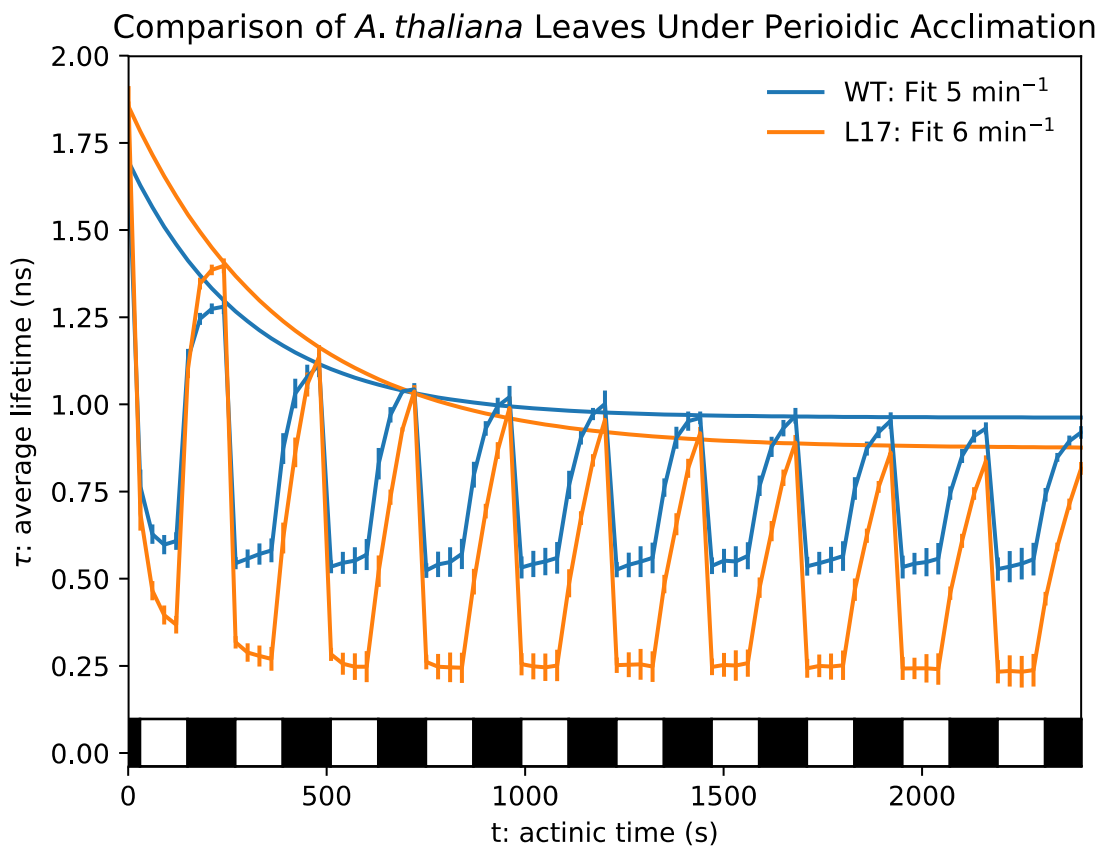

Figure 6. Example periodic actinic light TCSPC snapshot traces for SVD analysis. Average fluorescence lifetimes (y-axis) are plotted against the exposure time to periodic actinic light with a two-minute half-period represented by the dark and light bars for two mutant lines. A simple fit of the recovery envelope is plotted and the timescales shown in the legend.
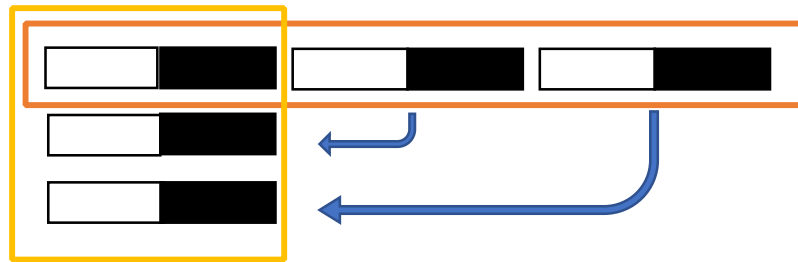
Figure 7. Visualization of the formation of the matrix X from a vector of average fluorescence lifetime values over successive periods. The vector shown in the top row (bounded by the red rectangle) containing data from multiple periods is reshaped into a matrix (bounded by the yellow rectangle) by tiling data from successive periods into rows containing just one period.
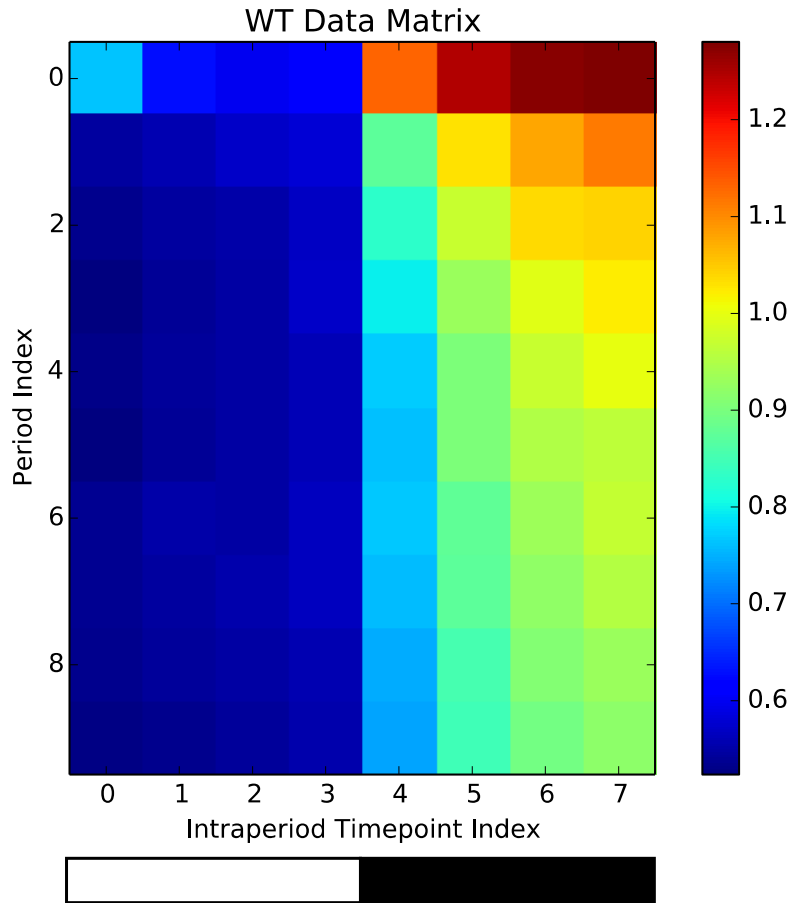
Figure 8. Heat map visualization of the matrix *X* obtained from tiling the WT data series shown in Figure 6 via the process shown in Figure 7. Each row contains the average lifetime values obtained by a single period of high and dark light exposure. Successive rows hold data from successive periods. The left half of columns contain high light quenching induction; the right half of columns contain dark quenching recovery.

Upon performing the SVD, visualized in Figure 9, the *U* and *V** matricies contain pairs of linearly independent singular vectors, each associated with a singular value in Σ, similar to the linearly independent eigenvectors and eigenvalues obtained from performing an eigen decomposition on a suitable matrix. The columns of *U* contain singular vectors corresponding to multi-period dynamics. Each column of *U* corresponds to a row of *V** containing a singular vector describing intra-period behavior. The singular values, contained in the diagonal matrix Σ in monotonically decreasing order are the singular values that weight each pair of singular vectors' contribution to the overall signal contained in *X*.

Therefore, the largest components of the dynamics are contained in the pair of singular vectors present in the first column of U and the first row of V^* associated with the first and largest singular value. Subsequent pairs of singular vectors and their associated singular values describe additional dynamics associated with successive singular values. Due to the properties of matrix multiplication, the product of the three matrices is also equal to the sum of the outer products of successive pairs of singular vectors, each weighted by the singular value. In many applications, this allows for filtering of the data by retaining only components with clear dynamical structure above a noise floor (Hendler and Shrager 1994). In the example shown in Figure 9, the first three pairs of singular vectors show discernable structure, suggesting the experiment can resolve three linearly independent dynamical processes affecting dynamics. Subsequent singular vectors, that make up only a small fraction of the overall dynamics due to their associated singular values, show no discernable structure, suggesting they contain noise.
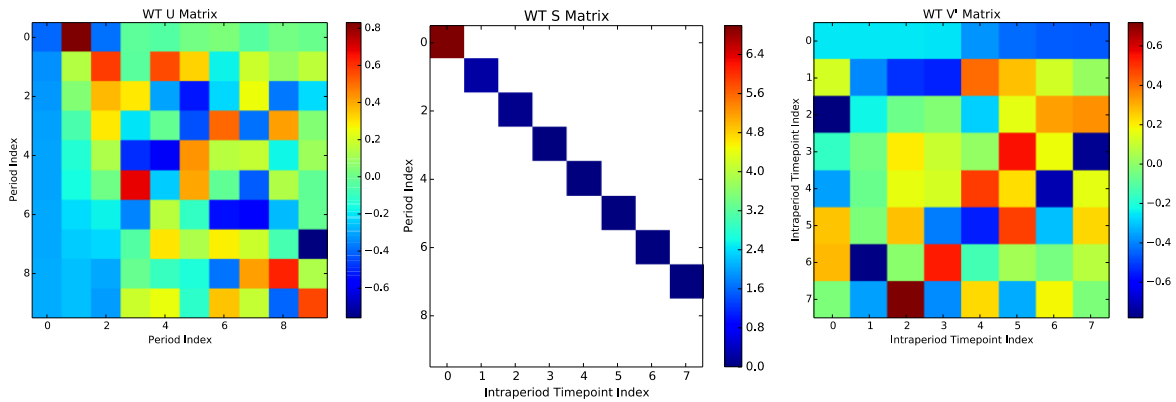

Figure 9. Results of performing SVD on the matrix X visualized in Figure 8 via the tiling procedure shown in Figure 7 from the TCSPC fluorescence lifetime snapshot data series obtained under periodic actinic light exposure shown in Figure 6. Columns of the matrix U contain singular vectors describing components of inter-period dynamics. Rows of the matrix V^* contain singular vectors describing components of intra-period dynamics. Singular values are contained in the diagonal matrix Σ and occur in monotomically decreasing order. Therefore, the first column of U and the first row of V^* describe the largest components of the dynamics contained in the matrix X. In this example, the first three pairs of singular vectors show discernable structure, suggesting the data resolves three independent components of dynamics. Subsequent pairs of singular vectors show no discernable structure, suggesting they describe noise.

In addition to simply encoding a single data series into the matrix X, multiple data series can be encoded in a similar manner in order to obtain common dynamics shared between the multiple data series. The choice of encoding determines whether either the multi-period dynamics or the intra-period dynamics are shared between the encoded data sets. In order to obtain shared multi-period dynamics, the periodic behavior from each data series is included in a row corresponding to each period. For the example in Figure 6 containing data from WT and L17

mutant lines, for example, data at common time points can be encoded in pairs, resulting in a vector with data from WT at even indices and L17 at odd indices. The paired data is then tiled in rows for each successive period in the same way shown in Figure 7. Upon obtaining the singular vector pairs, the resulting data can be de-coded from the tiled matrix vectors and plotted against time to obtain time series traces for the multi-period and intra-period dynamics. For the multi-period dynamics, singular vectors with the length equal to the number of periods are obtained describing the common multi-period dynamics shared by both data series. A single value in a particular left singular vector describes a multiplicative factor for the set of intra-period dynamics values contained in the corresponding right singular vector. Using the encoding procedure described above, the values at even indices in the right singular vectors contain the intra-period dynamics of the WT data series and values at odd indices in the right singular vectors contain the intra-period dynamics of the L17 data series.

This is particularly useful when some knowledge of the underlying physical processes are involved – in this case, the L17 mutant overexpresses the PsbS protein that plays a large role in the rapid sensing of Delta pH and activation of quenching. By analyzing the dynamics utilizing shared multi-period dynamics, the role of PsbS overexpression in the rapid regulation of quenching can be isolated independent of long timescale dynamics that may differ slightly due to complicated network feedback effects. An example of the first singular value pair obtained by encoding the WT and L17 data series shown in Figure 6 using the procedure described above, upon subsequent decoding of the intra-period behavior, is shown in Figure 10. The common multi-period dynamics, contained in the left singular vector, is plotted with the corresponding light and dark bars showing the light and dark actinic light corresponding to each period and the axis is labeled by the index of the period. The decoded intra-period dynamics are for WT (blue) and L17 (green) show that much of the difference between the WT and L17 data series can be expressed in the differing right singular vector, isolating the contribution of just the difference in the rapid regulation of quenching attributable to the excess PsbS in the L17 mutant.
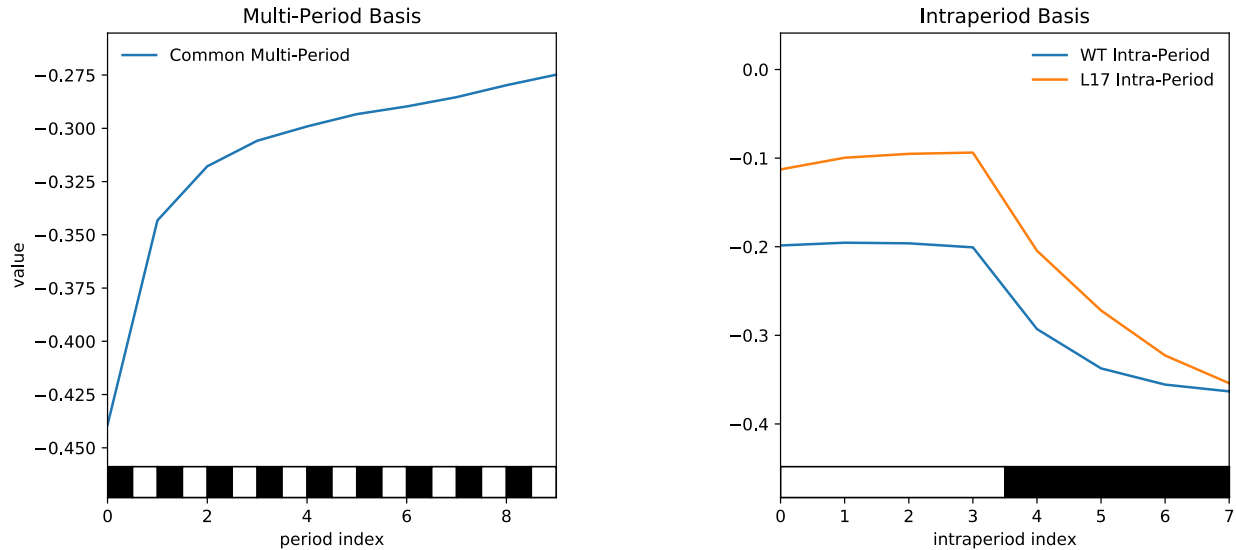
Figure 10. First pair of singular vectors for the WT and L17 TCPSC fluorescence lifetime snapshot data series obtained under periodic actinic light exposure, encoded into a matrix to extract common multi-period dynamics and independent intra-period dynamics. In the multi-period basis, the vector of singular values are plotted against an index corresponding to each period, shown using the repeated dark and light bars. In the intra-period basis, the indices of the right singular vector correspond to successive data points obtained within an actinic light exposure period.

The full data series can, conceptually, be reconstructed by computing the outer product of the multi-period vector with the intra-period vectors. The scalar product of the first value of the intra-period vector (at index = 0), the intra-period vector, and the first singular value recovers a vector of the filtered values of the first period of the data series. The vector obtained from the scalar product of the second value in the multi-period basis (at index = 1), the intra-period vector, and the second singular value, can then be appended to the first period vector to obtain a vector of the first two periods. Subsequent periods are obtained similarly and appended to obtain the full filtered data series. In practice, the same values are more easily obtained by masking the matrix Σ and computing the matrix product of U, Σ and V^*, and then decoding the filtered approximation of the matrix X.

In the case that both the rapid regulation and the longer time scale regulation are impacted by a change between the data sets, independent SVDs can be computed, although care must be taken to ensure that the singular vectors are comparable. In principle, the singular vectors are unique up to a sign: either both are "positive," both are "negative," or the pair are of opposite "signs." As a vector, individual values may be both positive or negative and the overall sign of the vector can be determined from some overall measure, at the simplest, even the first value. Negating each value in a pair of singular vectors has no impact upon computing the outer product: the signs cancel. Depending on stability concerns in actually computing the vectors, an algorithm may generate singular vectors that differ by a sign from the same matrix X. Either a simple parity check and choice of convention to assign vectors with the same sign as positive or negative and one of the pair of vectors with opposing signs as the negative vector, or more complicated

114

algorithms can be utilized to resolve the sign ambiguity and ensure that direct comparisons between independent SVD components can be undertaken (Bro and Kolda 2007).

Upon obtaining the filtered multi-period and intra-period dynamics, additional analysis can be performed to extract timescales that are not as easily extracted directly from the raw time series data. An example utilizing the encoded SVD of the data series that results in shared multi-period left singular vectors follows. First, for the multi-period data, an additional time component is able to be resolved in addition to the simple recovery envelope fit. Instead of simply evaluating the final time point of each period by selecting the maximum recovery value at the dark-to-light transition, the left singular vector accounts for the scaling of the entire intra-period dynamics during each period, therefore including some aspect of both the changes to the induction dynamics and the recovery dynamics. In addition, a clear set of rapid regulatory dynamics common across all the periods is obtained from the intra-period singular vector. Examples of the fit values obtained for both the multi-period singular vector and the intra period singular vectors are shown in Figure 11.
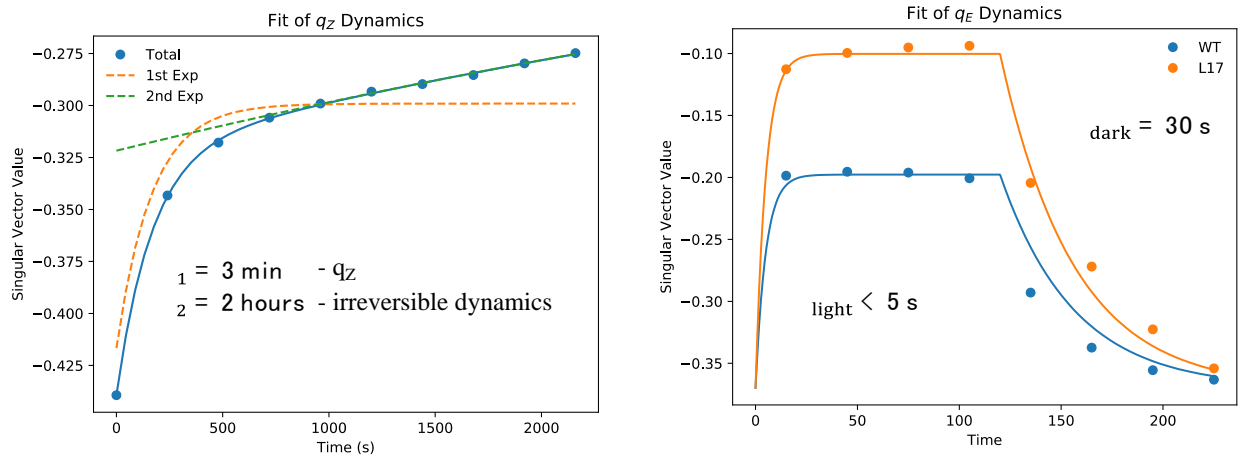

Figure 11. Fitting analysis of the first component singular vectors obtained from SVD analysis of the WT and L17 TCSPC snapshot average lifetime data series shown in Figure 6. The first component of the multi-period dynamics displays two timescales, a 3 minute and a 2 hour decay. The first component of the intra-period dynamics shows distinct induction and relaxation timescales, although the induction timescale cannot be reliably determined due to the limited resolution of the trial data set.

For the multi-period basis, two timescales are able to be resolved. One timescale is approximately 3 minutes; a second is approximately 2 hours. These are not resolvable from a simple fit of the envelopes themselves. In the intra-period dynamics, a common timescale of induction and recovery across all the periods is obtained, without requiring free parameters or greybox fitting of model equations to account for the discrepancies between successive periods to the effects of longer timescale dynamics. The fits indicate that the timescales for induction and recovery are similar between the two mutant lines, with much of the discrepancy solely due to the

amplitude of the induction and decays, suggesting that modulating the amplitude of the rapid regulation of quenching is a primary effect of the PsbS protein, and the multi-period basis dynamics are the result of other regulatory processes such as zeaxanthin accumulation.

A final caveat of SVD to discuss is the distinction between components of the SVD analysis and the underlying physical processes. SVD components are mathematical representations inforumed purely by co-variance of data set, and are not directly connected to the underlying physical processes that give rise to a signal. Although the first component describes the largest extent of the data that can be represented by a single pair of singular vectors, the second and third components of additional singular vectors essential apply corrections to the first order component. It is easily the case that the first component describes not "the most important physical process" but rather a linear combination of the behavior of multiple underlying processes, followed by secondary components that describe another linear combination of the the same processes to achieve the overall dynamics. While a firm conclusion can be drawn from the presence of multiple components apparent relative to noise in the SVD that the dynamics must be described by some number of multiple linearly independent processes, there is no guarantee that the particular singular vectors form a basis directly from distinct physical processes and not linear combinations of the effects of the processes.

Conclusion

The study of NPQ in *in vivo* systems whole leaves using TCPSC fluorescence lifetime snapshots generates rich and complex data sets. Due to the robust systems in plants, it is difficult to distinguish the effects of a single process despite the convenient probe of chlorophyll fluorescence. The two tools discussed in this chapter are important for analysis of quenching: together, they make it practical to obtain data with high time resolution and clear distinction between separate elements of the response of the change in fluorescence and quenching behavior in response to actinic light. These two factors are necessary for the development of understanding of the quenching process suitable to generate predictive models that can be incorporated into systems level models necessary for the engineering of quenching systems to optimize desired characteristics.

To reach an ability to engineer the quenching processes to optimize crop yields, predictive models that are valid over a realistic light conditions are necessary. These models will require a multivariate description of the quenching response that relate controllable variables, such as varying protein concentrations and expression levels of the regulatory proteins involved, to the quenching response in the range of realistic light conditions that vary not only in intensity, but in characteristic timescales of fluctuations. The range of timescales – from the rapid fluctuations of light specking in a canopy, to the diurnal fluctuations of light over the course of a day, to the seasonal fluctuations over a growth period, may all impact what determines an optimal quenching system for a desired result, such as yield.

Therefore, it is foreseeable that a model must account for the response of the many quenching processes over the range of environmental conditions, resulting in large data sets that span a multivariate range of conditions. Filtering allows for the combination of measurements of multiple leaf samples at different timepoints into single data series without introducing additional

high frequency oscillations that would require repeated measurements on an impractical number of samples to achieve similar results, thereby extending the practical length scales of TCSPC snapshot measurements and the number of conditions that can be varied. SVD allows for important exploratory analysis of data sets to determine the ability of an experiment to determine distinct components, and provides important clues as to the importance of various conditions on different elements of the regulatory response. While both have important caveats that must be considered to ensure that results are rooted in physical understanding, they make the rich data sets tractable and identify the sensitivity of elements of the response to a particular variable condition.

References

Alter, O., Brown, P. O., and Botstein, D. Singular value decomposition for genome-wide expression data processing and modeling. *Proc. Natl. Acad. Sci. USA* 18:10101-10106 (2000).

Antoniou, A. *Digital Filters: Analysis, Design, and Signal Processing Applications*. McGraw-Hill Education, 2018.

Blankenship, R. E.. Molecular Mechanisms of Photosynthesis, Second Edition. Wiley-Blackwell, 2014.

Bro R., Acar E., and Kolda, T. *Resolve the Sign Ambiguity in Singular Value Decomposition*. Sandia Report SAND2007-6422 (2007).

Brooks, M. D. and Niyogi, K. K. *Use of a Pulse-Amplitude Modulated Chlorophyll Fluorometer to Study the Efficiency of Photosynthesis in Arabidopsis Plants. Chloroplast Research in Arabidopsis Plants*. In: Jarvis R. (eds) *Chloroplast Research in Arabidopsis*. Methods in Molecular Biology (Methods and Protocols), vol 775. Humana Press, Totowa, NJ

Butterworth, S. On the Theory of Filter Amplifiers. *Experimental Wireless and the Wireless Engineer*, 7:536–541 (1930).

Cazzaniga, S., Dall'Osto, L., Kong, S. G. , Wada, M., and Bassi, R. Interaction between avoidance of photon absorption, excess energy dissipation and zeaxanthin synthesis against photooxidative stress in Arabidopsis. *Plant J*. 76(4):568–579 (2013).

Demmig-Adams, B., Cohu, C. M., Stewart, J. J., and Adams III, W. W. *Non-photochemical Quenching and Energy Dissipation in Plants, Algae and Cyanobacteria*, Volume 40. Springer Netherlands, 2014.

Hendler, R. W. and Shrager, R. I.. Deconvolutions based on singular value decomposition and the pseudoinverse: a guide for beginners. *J. Biochem. Biophys. Methods* 28:1−33 (1994).

Jackson, J.E. Principal components and factor analysis: part I - principal components, *Journal of Quality Technology*, 12:201-213 (1980).

Jackson, J.E. Principal components and factor analysis: part II - additional topics related to principal components, *Journal of Quality Technology*, 13:46-58 (1981).

Jones E, Oliphant E, Peterson P, et al. SciPy: Open Source Scientific Tools for Python, 2001-, http://www.scipy.org/ [Online; accessed 2019-06-25].

Külheim, C., Agren, J., and Jansson, S. Rapid regulation of light harvesting and plant fitness in the field. Science 297(5578):91-91 (2002).

Lakowicz, J. R. *Principles of Fluorescence Spectroscopy*, Third Edition. Springer, 2006.

Leuenberger, M. L, Morris, J. M., Chan, A. M., Leonelli, L., Niyogi, K. K., and Fleming, G. R. Dissecting and modeling zeaxanthin- and lutein-dependent nonphotochemical quenching in Arabidopsis thaliana. Proceedings of the National Academy of Sciences of the United States of America, 114(33):E7009-E7017 (2017a).

Leuenberger, M. L. Exploration of Nonphotochemical Quenching Mechanisms in *A. thaliana* via Time Correlated Single Photon Counting Snapshots (Doctoral dissertation). (2017b). Retreived https://escholarship.org/uc/item/52w4j6z3

Morris, J. M. and Fleming, G. R. Quantitative modeling of energy dissipation in Arabidopsis thaliana. Environmental and Experimental Botany, 154:99-109 (2018).

Sylak-Glassman, E. J., Malnoë, A., De Re, E., Brooks, M. D., Fischer, A. L., Niyogi, K. K., and Fleming, G. R. Distinct roles of the photosystem II protein PsbS and zeaxanthin in the regulation of light harvesting in plants revealed by fluorescence lifetime snapshots. *Proc. Natl. Acad. Sci. USA*, 111(49):17498 (2014a).

Sylak-Glassman, E. J. Development of Time-Resolved Spectroscopic Tools to Study the Dynamics of Photoprotective Quenching in Plants (Doctoral dissertation). (2014b). Retreived https://escholarship.org/uc/item/56h682nc

Sylak-Glassman, E. J., Zaks, J., Amarnath, K., Leuenberger, M., and Fleming, G. R. Characterizing non-photochemical quenching in leaves through fluorescence lifetime snapshots. Photosynthesis Research, 127(1):69–76, Jan 2016.

Chapter 5: Conclusion and Outlook

This work describes several advancements in the development of quantitative models of NPQ regulatory dynamics that arise due to the utilization of measurements employing multi-period actinic light exposure.

TCSPC snapshot measurements described in Chapters 2 and 3 both employ multi-period actinic light to distinguish elements of the regulatory processes that occur simultaneously upon the initial exposure of a photosynthetic system to high light after dark acclimation. In Chapter 2, the use of a second period of actinic light shows that the accumulation of zeaxanthin influences the observed timescale of the induction of quenching upon initial exposure to high light, and that the recovery of quenching is reduced upon the accumulation of zeaxanthin, in agreement with single period measurements that examine relaxation kinetics. In Chapter 3, this is extended to a periodic actinic light exposure sequence that allows for multiple timescales of quenching induction to be resolved, that have not previously been measured independently. The relaxation kinetics are only able to identify relative magnitudes of various components, and cannot resolve different induction timescales. However, despite the use of multiperiod actinic light schemes, it still remains difficult to distinguish the effects of a single process. The two tools discussed in Chapter 4 demonstrate that sophisticated signal processing and statistical analysis techniques are necessary elements of analyzing periodic acclimation snapshot measurements.

The results described in Chapter 3 indicate that there is an intrinsic timescale to the rapidly reversible regulation of quenching of about 15 s in *Arabidopsis*, for wild type levels concentrations of the protein PsbS, and independent of whether the rapidly reversible quenching arises due to lutein or zeaxanthin. The dependence on PsbS concentration is nonlinear: in the absence of PsbS, the rapidly reversible quenching does not occur, but at high concentrations, the timescale is increased, requiring additional time to transition, but over a greater magnitude of quenching values. Upon dark recovery, the rapidly reversible quenching in the wild type recovers on a timescale of about 50 s, but the recovery timescale depends on whether the lutein or zeaxanthin dependence gives rise to the rapidly reversible quenching: lutein dependent quenching recovers more quickly, despite similar magnitudes (upon overexpression of lutein) and similar induction timescales. Based on results in Chapter 2, upon normalization for concentration, it seems that lutein dependent and zeaxanthin dependent rapidly reversible quenching both contribute to the overall quenching, but that when operating simultaneously, the overall quenching is greater, suggesting that although multiple xanthophylls can dissipate excess excitation energy, specific sites are perform optimally with different xanthophylls, both in terms of the ability to quench and in regulatory response.

Results in Chapter 3 also resolve longer timescale regulatory processes that correspond to distinct maximum quenching and maximum recovery envelopes upon periodic actinic light exposure. This requires some form of coupling between the rapidly reversible quenching and longer timescale quenching processes to occur, suggesting that the different regulatory components operate on common quenching sites. When viewed in light of evidence of the various quenching states of LHCII and membrane organization, the various timescales appear to arise due to the difference in length scales of reorganization of proteins and membranes. In addition, the longer timescale quenching is found to depend on the PsbS concentration. This suggests that PsbS

influences membrane reorganization ability in addition to its primary function activating rapidly reversible quenching. Isolating quenching components using multi-period actinic light exposure reveals the complex, overlapping, and coupled nature of the various regulatory processes contributing to observed quenching in *A. thaliana*, that cannot be distinguished by genetic modification alone due to the overlapping roles of different biochemical regulators of quenching that include not only zeaxanthin, as commonly understood, but also PsbS.

Finally, two different constructions of mathematical models demonstrate how kinetic schemes can be constructed for various purposes to describe how the regulatory processes determine the observed quenching. The first formulation, described in Chapter 2, allows for different isolated contributions from two xanthophylls that play a direct role in quenching can be combined to generate an overall quenching response. The second formulation, described in Chapter 3, demonstrates how rapidly reversible quenching processes and longer timescale quenching processes that occur simultaneously combine to produce the overall quenching response.

Despite the advances made in this work, to reach an ability to quantitatively engineer the quenching processes to optimize crop yields, predictive models that are valid over a realistic light conditions are necessary. These models will require a multivariate description of the quenching response that relate controllable variables, such as varying protein concentrations and expression levels of the regulatory proteins involved, to the quenching response in the range of realistic light conditions that vary not only in intensity, but in characteristic timescales of fluctuations. The mathematical models described in this work here are simple enough to parameterize over a range of these conditions; especially the model employed in Chapter 3. Extracting the parameter dependence over a range of light intensities, timescale of light fluctuations, and protein concentrations is a key next step in developing models of crop yield that refine the contributions of quenching from a purely heuristic model to a quantitatively informed model. On the other hand, a model like that described in Chapter 2 may be useful as an experimental validation of first principles models of energy transfer in the photosynthetic membrane that include the presence of multiple quenching mechanisms.

However, despite the potential for predictive power, these types of kinetic models derived from TCSPC snapshot fluorescence measurements alone are not sufficient to develop a complete understanding of the photosynthetic quenching system. One example is the recently developed snapshot transient absorption measurements that relate observables of quenching mechanisms to regulatory timescales. As of yet, TA snapshots only use simple two exposure period actinic light schemes, but with further development, periodic actinic light may provide additional insight. In turn, further development of similar "snapshot" versions of techniques that can relate changes in protein conformation dynamics or membrane organization to these regulatory timescales will be necessary to fully integrate mechanistic and physical understanding of the regulatory processes with kinetic regulatory models.